ABSTRACT

Title of Document: EXPERIMENTAL CHARACTERIZATION OF VASCULAR TISSUE VISCOELASTICITY WITH EMPHASIS ON ELASTIN'S ROLE

Danial Shahmirzadi
MSc, Texas A&M University, 2005
BSc, University of Tehran, 2002

Directed By: Assistant Professor Adam Hsieh
The Fischell Department of Bioengineering

Elucidating how cardiovascular biomechanics is regulated during health and disease is critical for developing diagnostic and therapeutic methods. The extracellular matrix of cardiovascular tissue is composed of multiple fibrillar networks embedded in an amorphous ground substance and has been found to reveal time-dependent mechanical behavior. Given the multiscale nature of tissue biomechanics, an accurate description of cardiovascular biomechanics can be obtained only when microstructural morphology is characterized and put together in correlation with tissue-scale mechanics. This study constitutes the initial steps toward a full description of cardiovascular tissue biomechanics by examining two fundamental questions: How does the elastin microstructure change with tissue-level

deformations? And how does the extracellular matrix composition affect tissue biomechanics? The outcome of this dissertation is believed to contribute to the field of cardiovascular tissue biomechanics by addressing some of the fundamental existing questions therein.

Assessing alterations in microstructural morphology requires quantified measures which can be challenging given the complex, local and interconnected conformations of tissue structural components embedded in the extracellular matrix. In this study, new image-based methods for quantification of tissue microstructure were developed and examined on aortic tissue under different deformation states. Although in their infancy stages of development, the methods yielded encouraging results consistent with existing perceptions of tissue deformation. Changes in microstructure were investigated by examining histological images of deformed and undeformed tissues. The observations shed light on roles of elastin network in regulating tissue deformation.

The viscoelastic behavior of specimens was studied using native, collagen-denatured, and elastin-isolated aortic tissues. The stress-relaxation responses of specimens provide insight into the significance of extracellular matrix composition on tissue biomechanics and how the tissue hydration affects the relaxation behavior. The responses were approximated by traditional spring-dashpot models and the results were interpreted in regards to microstructural composition.

EXPERIMENTAL CHARACTERIZATION OF VASCULAR TISSUE VISCOELASTICITY WITH EMPHASIS ON ELASTIN'S ROLE

By

DANIAL SHAHMIRZADI

Dissertation submitted to the Faculty of the Graduate School of the
University of Maryland, College Park, in partial fulfillment
of the requirements for the degree of

Doctoral of Philosophy
2010

Advisory Committee:
Assistant Professor Adam Hsieh, Chair
Associate Professor Hugh Bruck, Member
Assistant Professor Teng Li, Member
Assistant Professor Santiago Solares, Member
Professor Mohamad Al-Sheikhly, Dean's Representative

Preface

This dissertation is the outcome of four and half years of struggle in the pursuit of building the foundations of my career in bioengineering. Given my former background in the fields barely relevant to bioengineering and with purely theoretical nature, my transition to bioengineering and working on a project that dealt with all kinds of experimental challenges were adventurous and bold as well as procrastinating and unsteady. In my sometimes-nostalgic assessment of my previous career options, it was common for me to rethink making the decision of shifting my research field, but now that this dissertation is complete, I can feel that I am very delighted of each and every move.

Having experienced working in theoretical and experimental fields, I can realize pros and cons inherent to each and if I am going to summarize my findings, I would say, “what really matters are the experimental observations”; theory is only a tool toward improving experimentation correctness. Though it might be already known, but I am specifically focusing on the importance of the relation between theory and experiment out of my personal experience. As an individual formerly working with theoretical techniques, I used to think theoretical observations are what really matters and experimentalists would be desperately happy if they produce results just close to theoretical ones. Now I think just the other way.

In summary, what should be kept in mind throughout reading this dissertation is that any minor result therein has taken good amount of time to obtain. Though it might look similar, an experimental data point is considerably different from a theoretical data point. The former is real and the latter is imaginary.

I will end my little note by referring to a quote that I heard from a friend of mine who took it from the notes of another friend who had it anonymously. So without knowing the name of the original narrator, I will copy the following quote which puts the story in a beautiful and simple manner:

"In theory, theory and practice are the same; in practice they are not."

-unknown

Foreword

As far back as I remember from my elementary school era throughout the high school years and later on during the university times, there has always been the question of "Whether knowledge is better or wealth?". The simple answer to that question that we have been convinced was "Knowledge" as it brings morals to the life, unlike fading "Wealth". This question has always been on my mind in shaping up my future life but simultaneously inherent was the at-the-time-paradoxical feeling that "Wealth could be moral too".

I don't ask the question of "knowledge OR wealth" from myself anymore since there is a way for happy coexistence of "knowledge AND wealth". However, this distinction might not be easy for everybody to realize and more importantly to take it into practice in daily life. The delicacy of the discussion is in the fact that knowledge brings power and power can be extremely advantageous or dangerous. The same knowledge that makes nuclear energy also makes nuclear bombs.

I will finish my brief thought on this with a nicely-put quote by C. S. Lewis:

"Education without values,

as useful as it is,

seems rather to make man a more clever devil."

-C. S. Lewis (1898-1963)

Dedication

To the most passionate mother ever

FARAHNAZ

&

to my father

EBRAHIM

who has constantly been providing that great inspiration for higher education

Acknowledgements

First of all, I would like to thank the research advisor and the chairman of my dissertation committee, Dr Adam Hsieh, for all his inspiration and patience during the course of this research. Without his charming and positive attitude as well as his scientific expertise and insightful guidance, it would have been impossible for me to complete this dissertation. I would also like to thank all of the permanent and temporary members of the Orthopaedic Mechanobiology Laboratory for all the help, collaboration and inputs.

I would also like to thank all the faculty members who taught me so much in the classrooms and even more outside the classrooms: Dr Adam Hsieh, Dr Henry Haslach, Jr., Dr Abhijit Dasgupta, Dr Teng Li, Dr Sheryl Ehrman, Dr Steve Marcus and Dr Rama Chellappa.

I would like to extend my gratitude to all the current and former members of my advisory committee, some of which considerably helped me at the proposal presentation but had to leave the committee because of other commitments: Dr Adam Hsieh, Dr Hugh Bruck, Dr Teng Li, Dr Santiago Solares, Dr Mohamad Ak-Sheikhly, Dr Abhijit Dasgupta, Dr Henry Haslach, Jr. and Dr Keith Herold. In particular, a very special thanks goes to Dr Solares for his dedication in detailed editing of this dissertation.

Furthermore, I also wish to gratefully thank Dr Balakumar Balachandran, director of graduate studies, for his incredible and thoughtful guidance to maintain my good academic standing during the entire program, and Mr Amarildo DaMata, graduate studies coordinator, for his kind efforts in timely conducting various

departmental and university procedures. A very special thank is going to Dr Sami Ainane, director of students affairs, who gratefully helped me to obtain my extensive teaching experience and to maintain the source of financial support during a very large part of my PhD program.

Finally, and most importantly, I truly owe my parents and close relatives who have always been my constant inspiration and motivation, even from miles and miles away, to handle the academic and non-academic challenges of my life. I am dedicating this success to them and will be always thankful to them.

Table of Contents

List of Tables

List of Figures

I. INTRODUCTION

I.1. Overview

None of the existing models for mechanics of biological soft tissues is capable of universally characterizing soft tissue viscoelastic behavior in the sense that they are not able to describe tissue behavior under a variety of test conditions and within a wide range of loading/deformation.

Studying the structural and mechanical properties of biological tissues in general, and cardiovascular tissue specifically, is significant mainly because: (1)Diagnostic/therapeutic tools for pathological conditions- During the pathological conditions in the cardiovascular system, the structural composition and mechanical properties of the cardiovascular tissues and the ECM alter and therefore impair the functionality of the system. Based on the difference between the structural and mechanical properties of the tissue under normal and pathological conditions, criteria can be developed for diagnosis of different disorders. For example, one of the roles of ECM is to act as the auxiliary pump to the heart to facilitate blood circulation. Understanding this is relevant in diseases like atherosclerosis which causes accumulation of macrophages and lipids inside the arterial vessel, prompted by low density lipoproteins [Maton 1993]. Atherosclerosis reduces the ECM's compliance to pulsatile flow, i.e., it increases the stiffness [Horvath 2003]. Therefore, a change in compliance of the ECM of cardiovascular tissue could be a measure to predict developing atherosclerosis. Another example of a fatal cardiovascular disease is the

local abnormal dilation of the arterial wall, known as aneurysm [Humphery 2002]. It is found that aneurysms initiate mainly at areas with abnormal elastin content, e.g., low concentration or structural alteration of elastin [He 1994; Sacks 1999]; however, the concentration of other components, like vascular smooth muscle (VSM) and glycosaminoglycan (GAG) also decreases [He 1994; Sobolewski 1995]. In addition to alterations in structural composition of the tissue, the pathological conditions can also occur due to changes in the normal configuration of the tissue. For example, the disorder of high frequency poststenosis vibrations of the arterial wall, e.g $f = 200 - 600Hz$ (compared to exciting frequency of heart beat of $f = 1 - 8Hz$), which is accompanied by a noise referred to as bruit, occurs beyond the areas where the arterial vessel narrows down [Lillie 1986]. (2)Replacement for artificial tissue- Due to the compositional and structural alterations in the tissue, the tissue fails to function properly. If the level of alterations in the tissue is higher than what could be recovered physiologically, then the tissue can be substituted by transplant operation with a donated biological tissue or artificial one, which is in the area of tissue engineering. In order to generate the artificial substitute, which accurately mimics the original tissue, the first step is to characterize the mechanical and structural properties of the biological tissue [Buttafoco 2006; Cox 2006]. Arterial tissue engineering in particular has been the subject of numerous studies [Sarraf 2003].

The essential reason which limits predictability of exiting models in describing tissue behavior is that none of the models incorporates the fundamental basis of tissue viscoelasticity which is root-caused by tissue structural components and their interactions through extracellular matrix. Instead, majority of the models are

simply developed by parameter fitting to tissue behavior under certain conditions. Given the viscoelastic and highly nonlinear behavior of tissue biomechanics, models obtained by such approaches are not able to describe tissue behavior under new arbitrary conditions. Even in more biologically-inspired models, which include spring and damper components to mimic some of tissue structural features, predictability is limited to a narrow range of loading/deformation, because tissue viscoelastic properties vary under load and deformation, and therefore they can not be captured through constant elastic and viscous parameters.

Any approach to accurately model tissue viscoelastic behavior under arbitrary conditions should capture the fundamental causes of tissue viscoelasticity which arise from its composite-like structure. Considering tissue composite structure, overall tissue biomechanics can be attributed to two different sources: (1)Mechanics of individual structural components, (2)Effects of interaction between different structural components through extracellular matrix. This research focuses on particular problems related to the roles of the elastin network in cardiovascular tissue viscoelasticity, as well as effects of interaction of elastin with the rest of the extracellular matrix. The global hypothesis for this research study can be summarized as: Elastin network biomechanics is correlated to vascular tissue biomechanics through the extracellular matrix composition.

I.2. Background

The level of sophistication in developing constitutive formulation for a material depends on the material property in question and the assumptions applicable to the

material. When developing the constitutive law for arterial tissue (and most of the biological soft tissues), it should be noted that the material is not elastic(e.g. hookean) [Fung 2003], but nonlinear, viscoelastic, anisotropic [Young 1977; Zhou 1997; Bischoff 2004; Fonck 2006] and more controversially, compressible [Humphrey 2002]. Furthermore, there is another characteristic of soft biological tissues that makes modeling the material behavior more complicated and it is that the properties emerge as the result of interaction of different structural components. Therefore, the overall behavior of the tissue in whole, as a composite material, is different from that predicted by individual components. This effect is more dominant in properties of the tissue in vivo; however, depending on the test conditions in vitro, the biomechanics of the tissue could still be affected. Besides the aforementioned assumptions on the material properties of the arterial tissue, another geometrical approximation is to assume the blood vessel as a thin-wall vessel [Fung 1993]. This assumption facilitates the development of the constitutive formulation by simplifying the stress state of the arterial vessel to two components of circumferential and longitudinal stress and without a radial stress component[1].

Various approaches were applied to model cardiovascular mechanics where each makes certain assumptions in terms of material properties and mechanical behavior to simplify the modeling procedure. Some primitive studies on modeling arterial tissue assume that the material is homogenous and cylindrically orthotropic [Patel 1969; Choung 1986]. However, it is known that due to non-uniform and

[1] A pressure vessel with thickness t and radius r is treated as a thin-wall pressure vessel if $t < 0.2r$ which gives rise to wall stress state with circumferential stress component $\sigma_c = pr/t$ and longitudinal stress component $\sigma_l = 0.5pr/t$, where p is the internal pressure [Timoshenko 1956, Shigley 2004].

directional distribution of different components of the wall, the artery wall is extremely heterogeneous and anisotropic, respectively [Matsumoto 2004; Fonck 2006]. In fact, the heterogeneity of the arterial wall material due to its fibrilar structure is to the extent that a great deal of research is performed to model the arterial tissue as fiber-reinforced composite material [Shadwick 1998; Holzapfel 2000(b); Demjancukova 2006; Gundiah 2007].

Clinical and experimental observations on the behavior of arterial tissue indicate that the arterial tissue is viscoelastic which means that the mechanical behavior of the tissue is changing over time, i.e., it is in a state of non-equilibrium [Apter 1964; Gow 1968; Fung 1972(a)]. Indeed, the viscoelasticity of the cardiovascular tissue is vital for proper functioning of the cardiovascular system. Amongst many others, one example which shows the necessity of the tissue to be viscoelastic is the timely gradual contraction and dilation of pulmonary and systemic artery tissues, respectively, during hypoxic[2] conditions that facilitate the proper oxygen circulation [Tsai 2004]. The time-variation of the arterial mechanics is one of the challenges in many existing modeling techniques.

Based on the observations from loading the tissue with monotonically-increasing and monotonically-decreasing loads, the behavior of the tissue is approximated to be time-independent, which motivates developing nonlinear (hyper)elastic models for arteries [Skalak 1975; Fung 1993]. Though capable of capturing the behavior of the tissue under simple loading or unloading experiments, the elastic models are unable to reproduce the time-dependent behavior of the tissue, e.g. stress relaxation, creep and cycling loading.

[2] Hypoxia is the condition of deficiency of oxygen of the tissue.

To deal with the inelastic behavior of the arterial tissue, the concept of pseudo-elasticity was introduced by Fung [Fung 1972(a)] and reported in other studies [Chuong 1986; Zhou 1997]. Observing the hysteresis in strain-stress behavior during loading and unloading of the arterial tissue, though small, was the main basis for Fung's development. The material behavior is modeled as two simultaneous, yet different, elastic models, one for the loading region and one for the unloading region. Fung realizes that instead of looking at nonlinear data of stress, e.g. $\underset{\sim}{P}$, 1st Piola-Kirchhoff, versus stretch, λ, the data can be re-plotted as, what he called stiffness, $d\underset{\sim}{P}/d\lambda$, versus $\underset{\sim}{P}$ which surprisingly demonstrates a linear behavior [Fung 1967]. Therefore starting from the linear relation between $\frac{d\underset{\sim}{P}}{d\lambda}$ and $\underset{\sim}{P}$:

$$\frac{d\underset{\sim}{P}}{d\lambda} = c_1 \underset{\sim}{P} + c_2 \tag{1}$$

with c_1 and c_2 as the material parameters, stress could be derived as:

$$\underset{\sim}{P} = ce^{c_1\lambda} - \frac{c_2}{c_1} \tag{2}$$

where the constant c is determined from the initial stress value at $\lambda = 1$, e.g. $\underset{\sim}{P} = 0$ for the unloaded tissue with no residual stress. However, for strain energy derivation, W, the 2nd Piola-Kirchhoff stress, $\underset{\sim}{S}$, is used instead of $\underset{\sim}{P}$. Since the correspondent strain tensor to $\underset{\sim}{S}$ is the Green-Lagrange strain tensor, $\underset{\sim}{E}$, the strain energy formulation gives the following relation:

$$\underset{\sim}{S} = \frac{\partial W(\underset{\sim}{E})}{\partial \underset{\sim}{E}} \tag{3}$$

Motivated by the exponential form of the 1st Piola-Kirchhoff stress, strain energy function is also chosen to be exponential in terms of Green-Lagrange strain and therefore the resulting 2nd Piola-Kirchhoff stress also gets the exponential form. Choosing the strain energy function as:

$$W = c\left[e^{Q(\underset{\sim}{E})} - 1\right] \tag{4}$$

results in a stress form of:

$$\underset{\sim}{S} = ce^{Q(\underset{\sim}{E})}\frac{\partial Q(\underset{\sim}{E})}{\partial \underset{\sim}{E}} \tag{5}$$

where Q is an arbitrary function of Green strain tensor, $\underset{\sim}{E}$. After fitting different functional forms $Q(\underset{\sim}{E})$, it is realized that the following quadratic form gives the best result for a linearly elastic behavior [Fung 1993]:

$$Q(\underset{\sim}{E}) = \frac{1}{2}c_{IJKL}E_{IJ}E_{KL} \tag{6}$$

Fung proposed the idea of pseudoelasticity to merely account for the hysteresis phenomenon in loading and unloading of the arterial tissue with the idea that each of the loading and unloading parts could be modeled as separate elastic behaviors. On the other hand, the Fung exponential model was based on data from a uniaxial test and therefore it does not account for anisotropy of the tissue. Indeed, the Fung model is a phenomenological model mainly motivated by the behavior of the tissue under cyclic loading and it does not capture any tissue structural contributions nor the effects of tissue components on the viscoelastic behavior of the tissue [Humphrey 2002]. It should be noted that the material modeled by this formulation is still an elastic material, sometimes called Fung elastic, and thus inappropriate for

modeling a viscoelastic material such as arterial tissue. However, the pseudo-elasticity model might appreciate the fact that the behavior of the tissue is not purely elastic, although it does not accurately predict the viscoelastic behavior of the tissue, particularly under different dynamic and high strain-rate loading experiments [Humphrey 2002]. Fung's constitutive model of the stress-strain behavior of most soft tissues is nonlinear and so it is not that straightforward to develop a universal model fitting different data. After all, because of its unique handling of the nonlinearity, Fung's model is still among the common models used to model soft tissue behavior.

Aiming to capture the behavior of the tissue in certain experiments, nonlinear empirical models were also proposed, such as the rubber-based model proposed by Fung [Fung 1972(b)]. It has been known for long time that biological tissues are not practically Hookean [Roy 1880]. Indeed, the pure Hooke's law is of no practical application to describe any material behavior and even metals follow the Hooke's law only up to very small strain level, e.g. $\varepsilon = 0.2\%$ [Timoshenko 1956]. Biological soft tissues are no exception in this matter where they do not follow the Hooke's law as well [Fung 1993], and the most evident observation to prove this is the nonlinearity of the behavior of the tissue. If the behavior of biological soft tissues is desired to be compared with that of any nonliving material, the closest material is an elastomer, e.g. rubber [Humphrey 2002]. Therefore, there have been studies to model the biological soft tissues as rubber-like material which go under the field of finite elasticity. Since, the stress, which is used in the following formulations, is the Cauchy stress tensor, $\underset{\sim}{\sigma}$, the corresponding strain tensor is the right Cauchy-Green strain tensor, $\underset{\sim}{C}$. The finite elasticity is essentially part of the hyperelasticity theory, which

means that the stress derivation is based on the strain energy function. The goal here is to appropriately define strain energy as a function of the right Cauchy-Green strain tensor, $W(\underset{\sim}{C})$ [Humphrey 2002]. More specifically, the strain energy function is preferred to be formulated not as an explicit function of strain, $\underset{\sim}{C}$, but as a function of its invariants, $I_{\underset{\sim}{C}}$, $II_{\underset{\sim}{C}}$ and $III_{\underset{\sim}{C}}$:

$$W(\underset{\sim}{C}) = W(I_{\underset{\sim}{C}}, II_{\underset{\sim}{C}}, III_{\underset{\sim}{C}}) \tag{7}$$

where $I_{\underset{\sim}{C}} = tr\,\underset{\sim}{C}$, $II_{\underset{\sim}{C}} = \frac{1}{2}\left[(tr\,\underset{\sim}{C})^2 - tr\,\underset{\sim}{C}^2 \right]$ and $III_{\underset{\sim}{C}} = \det \underset{\sim}{C}$. Adopting finite elasticity with an isothermal approach for rubber (and presumably for a rubber-like material) which is isotropic and incompressible, the strain energy function takes the form of:

$$W(\underset{\sim}{C}) = W(I_{\underset{\sim}{C}}, II_{\underset{\sim}{C}}) - \tilde{l}(III_{\underset{\sim}{C}} - 1) \tag{8}$$

Note that the incompressibility condition gives the third invariant as $III_{\underset{\sim}{C}} = \det \underset{\sim}{C} = [\det \underset{\sim}{F}]^2 = J^2 = 1$, and so the additional term in Eq. 8 serves as a constraint with Lagrangian multiplier of $\tilde{l}$. Similar to Eq. 3, the Cauchy stress tensor can be obtained by the following differentiation of strain energy function:

$$\underset{\sim}{\sigma} = \frac{\partial W(\underset{\sim}{C})}{\partial \underset{\sim}{C}} \tag{9}$$

Substituting Eq. 8 into Eq. 9, transforming the right Cauchy-Green strain tensor, $\underset{\sim}{C}$, into the left Cauchy-Green strain tensor, $\underset{\sim}{b}$, and simplifying the relations gives the Cauchy stress tensor in the form:

$$\underset{\sim}{\sigma} = -2\left(\tilde{l} - II_{\underset{\sim}{b}} \frac{\partial W(\underset{\sim}{C})}{\partial II_{\underset{\sim}{C}}} \right) \underset{\sim}{I} + 2\frac{\partial W(\underset{\sim}{C})}{\partial I_{\underset{\sim}{C}}} \underset{\sim}{b} - 2\frac{\partial W(\underset{\sim}{C})}{\partial II_{\underset{\sim}{C}}} \underset{\sim}{b}^{-1} \tag{10}$$

where $\underset{\sim}{I}$ is the identity tensor with the proper dimension. Now, the exact form of the strain energy function, W, should be specified in order to determine the stress-strain relation. Numerous different forms for the strain energy function of Eq. 8 or other forms have been proposed in the literature [Mooney 1940; Rivlin 1951; Carmichael 1961; Hart-Smith 1967; Valanis 1967; Treloar 1975; Ogden 1984]. Based on the same form of strain energy function, $W(\underset{\sim}{C})$, as given in Eq. 8, two of the most common models developed are the Neo-Hookean and Mooney-Rivlin models.

Motivated by the polymeric structure of elastomers and based on statistical mechanical models of long-chain molecular structures with various idealizations for molecule-to-molecule interactions, Treloar proposed his strain energy function from a purely entropic model as [Treloar 1975]:

$$W(\underset{\sim}{C}) = \alpha(I_{\underset{\sim}{C}} - 3) \tag{11}$$

with the coefficient as $\alpha = nkT$, where n is the number of polymeric chains per unit volume, k is Boltzman's constant and T is the absolute temperature, and so it is immediately realized that in isothermal problems, α is constant. The resulting Cauchy stress from this strain energy function can be shown as:

$$\underset{\sim}{\sigma} = -2\left(\underset{\sim}{l} - II_{\underset{\sim}{b}} \frac{\partial W(\underset{\sim}{C})}{\partial II_{\underset{\sim}{C}}}\right)\underset{\sim}{I} + 2\alpha \underset{\sim}{b} \tag{12}$$

Partly due to the linear relationship between the Cauchy stress tensor and the left Cauchy-Green strain tensor which exist in Eq. 12, this formulation is called the Neo-Hookean constitutive law. Despite the accuracy of the Hookean relation in modeling rubber behavior only to a very limited strain level, the Neo-Hookean model captures the behavior of rubber up to a strain level of $\varepsilon = 30\%$ [Humphrey 2002].

Motivated by experimental observations to find a strain energy function which yields a stress relation with nonlinear strain-stress behavior in extension but linear in shear, Mooney proposed his strain energy function, $W(\underset{\sim}{C})$, as [Mooney 1984]:

$$W(\underset{\sim}{C}) = \alpha(I_{\underset{\sim}{C}} - 3) + \beta(II_{\underset{\sim}{C}} - 3) \tag{13}$$

where α and β are material constants with units of stress. Due to contributions of Rivlin, this model is well-known as the Mooney-Rivlin constitutive law. It should be mentioned that the form of the strain energy in Eq. 13 has no physical interpretation and it is mostly a mathematical postulation, however, it extends the benefits of the Neo-Hookean model in some applications. For example, it gives a better description for the behavior of elastomers in higher strain ranges.

In addition to those models which are based on the strain energy as a function of tensor-invariants, $I_{\underset{\sim}{C}}$, $II_{\underset{\sim}{C}}$ and $III_{\underset{\sim}{C}}$, there are other models which are developed from the strain energy function written directly in terms of eigenvalues of the right stretch tensor, $\underset{\sim}{U}$, i.e. principal stretches, λ_i with $i = 1,2,3$. Among these models, the most well-known is the one introduced by Ogden [Ogden 1984], which proposed the strain energy function as:

$$W(\lambda_1, \lambda_2, \lambda_3) = \sum_{k=1}^{N} \frac{\beta_k}{\alpha_k} (\lambda_1^{\alpha_k} + \lambda_2^{\alpha_k} + \lambda_3^{\alpha_k} - 3) \tag{14}$$

where α_k and β_k are material parameters. Stress calculations based on this strain energy function lead to constitutive relations known as Ogden constitutive law. For certain values of material parameters, the Ogden and Mooney-Rivlin models are interchangeable.

When trying to apply the rubber-based material models, e.g. Fung, Neo-Hookean, Mooney-Rivlin, Ogden, etc., to soft biological tissue, it should be noted that none of these model characterizes the true behavior of the tissues and that is because of the essential assumptions which have been made in developing these models. For example, the energy formulation used in these models has no dissipative term to account for the viscosity of the tissue. Therefore, these models do not describe the behavior of a viscoelastic material such as arterial tissue. In addition, since these models are developed primarily to model rubber, it is reasonable to assume the material to be incompressible and isotropic. However, when applied to soft tissues with fibrous structure and porous walls, these assumptions are not valid anymore. Most of the rubber-based models even fail to capture the thermal variation in the material -which is inherent to biological soft tissues- and are valid only for isothermal processes [Humphrey 2002]. Another assumption, that further undermines the application of rubber-based models for arterial tissue, is material incompressibility [Humphrey 2002]. The Fung empirical model has been particularly shown incapable to capture the behavior of soft tissues, except in a very small range of frequency [Decraemer 1980].

The next step toward incorporating the viscoelastic features of the arterial mechanics has been taken by building a tissue mechanical model composed of viscous and elastic components, i.e. spring and dashpot, respectively. This component-based approach is a subset of the more general methods to characterize energy dissipation in non-equilibrium behavior of viscoelastic materials, through models that incorporate internal variables to account for non-equilibration processes

[Holzapfel 2000(b); Haslach 2005]. The constitutive law for individual elastic and viscous components is given by:

$$F_c = c\dot{u} \tag{15}$$

$$F_k = ku \tag{16}$$

where F_k and F_c are the force through the elastic and viscous components, respectively, k and c are the elasticity and viscosity constants, respectively, and u is the uniaxial deformation of the component. By utilizing a different number of elastic and viscous components attached together in different configurations, various viscoelastic constitutive laws could be obtained. Two of the linear viscoelastic models composed of different arrangements of elastic and viscous components are the Maxwell and Kelvin-Voigt models, Figs. 1(a) and 1(b), which were proposed to describe the non-equilibrium processes of stress relaxation and creep, respectively [Holzapfel 2000(b)]. The Maxwell model describes stress relaxation as:

$$\sigma(t) = \varepsilon_0 k e^{-kt/c} \tag{17}$$

where ε_0 is the constant strain under which stress relaxation occurs. As far as stress relaxation modeling concerns, the Kelvin-Voigt model is not capable of describing the stress relaxation behavior -only the creep behavior. These constitutive laws produced by these models are linear viscoelastic with limited applicability. However, a more general viscoelastic model has been developed to describe the behavior of viscoelastic materials during different non-equilibrium processes. Based on the standard linear solid model, Fig. 1(c), the stress relaxation is described as [Holzapfel 2000(b)]:

$$\sigma(t) = \varepsilon_0 \left[k_2 + k_1 e^{-k_1 t/c} \right] \tag{18}$$

It is shown that the standard linear solid model was able to describe some dynamic behavior of the arterial tissue, though in a limited loading rate [Staverman 1956] and its modified version was also used to model the viscoelastic behavior of strain-controlled loading of the arterial tissue [Apter 1964]. Although, there exist studies which attempt to correlate viscoelastic behavior of the arterial tissue to its microstructure [Apter 1966; Apter 1968], the component-based models do not essentially incorporate the physiology of the tissue. They are also not capable of describing the nonlinear, viscoelastic, anisotropic and non-isothermal behavior of the arterial tissue under non-equilibrium processes.

A modified configuration of the linear standard model has been applied to arterial tissue under strain-control loading mode [Apter 1964]. Modified Kelvin-Voigt model with a sequence of different-length spring elements was also adapted to model arterial tissue specifically to account for stiffening of the tissue under stretch [Viidik 1968]. A combination of spring-dashpot models based on the properties of each of the elastin and collagen components with corresponding probability density functions for each, was adapted by Lanir to model the structural elastin-collagen network [Lanir 1983]. However, the complexity of determining the parameters of the model as well as the fact that the interaction of individual components is not taken into account in such models, limit the usefulness of this model.

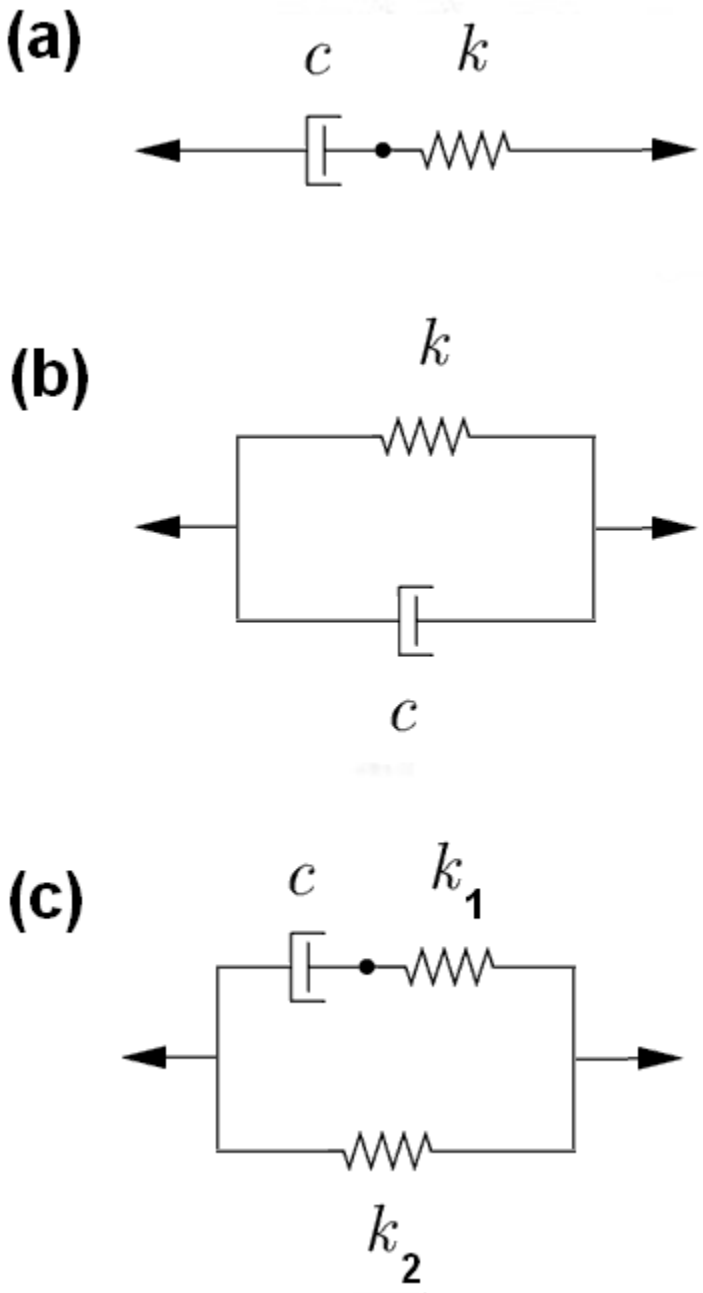

Figure 1- Most commonly used spring-dashpot structures to model viscoelastic behavior: (a)Maxwell, (b)Kelvin-Voigt, (c)Standard linear solid.

All the modeling approaches considered so far require making some type of assumption to simplify the artery tissue material and developing methods to determine a set of model parameters. This usually encompasses performing numerous —often long-term— experiments which is a major drawback for many of these types

of models [Haslach 2005]. To avoid dealing with such drawbacks, another approach is to use the strain energy functions to develop appropriate constitutive formulations for arterial tissue. For example, constitutive relations for arterial tissue have been derived from strain energy functions. However, the arterial tissue has been assumed to be (nonlinear) elastic and incompressible, which impairs the accuracy of the model and does not capture the time-variation of the tissue's behavior [Chuong 1983; Hayashi 1993; Humphrey 1999; Holzapfel 2000(a)]. On the other hand, many studies have been based on the elastic strain energy function (or elastic complementary strain energy function) which leads to hyperelastic (or hypoelastic) constitutive relations, respectively, which do not capture the time dependence of the tissue mechanics.

To extend the energy-based derivation for viscoelastic modeling, dissipative energy components have been added in the energy function to account for the viscoelastic features of the behavior. Recent developments in modeling the viscoelastic behavior of arterial tissue have used the concepts of elastic and viscous properties of each of the main arterial components to develop appropriate strain energy functions [Zulliger 2004]. For example, the Helmholtz energy function is written as a sum of a long-term hyperelastic component and a viscous component [Holzapfel 2000(a), Bonet 2001]. This formulation leads to stress with elastic and viscous terms, which could describe the viscoelastic behavior of the tissue more accurately. Incorporating the effects of the tissue's structural components in the process of developing the (viscoelastic) model is the least considered approach.

An entire category of modeling techniques is based on taking more direct approaches in describing the soft tissue as a composite material. A wide range of

studies on the modeling of soft tissues as fiber-reinforced composite materials has been carried out mainly to account for the roles of microstructural components within the tissue extracellular matrix [Kunzelman 1992; Huijing 1999; Wu 2002; Basciano 2009; Karami 2009; Tang 2009].

The Cosserat constitutive theory (also known as micropolar theory) has initially been developed to improve the modeling of composites with fibers or particles by enriching the classical elasticity with rotation degree of freedoms on the particles and had been further developed to model more complicate materials [Spillmann 2009]. Models based on Cosserat elasticity have been applied to predict different characteristics of biological tissues [Park 1986; Lakes 1990; Ivancevic 2009; Banerje 2009], specifically deformation of blood vessel tissues [Li 2009].

I.3. Research Objective

The following section reports the research objective for this study. The two specific aims that will be pursued along with the corresponding initiating hypotheses are explained.

I.3.1. Specific Aim 1: Multiscale Deformation Correlation

Understanding the correlation between microscale and macroscale deformation mechanisms is critical in characterizing vascular tissue biomechanics. During tissue deformation, individual microstructural components deform under different mechanisms while interacting with each other and with the extracellular matrix.

Studying the relation between tissue microstructural configuration and macroscale mechanical behavior helps in understanding the contribution of individual components to the overall tissue biomechanics. Given the significant role of elastin in regulating tissue deformation, the first specific aim is:

- Determine how elastin fibrillar networks reconfigure during tissue deformation.

Hypothesis 1: The elastin network conformations within the tissue are regulated by and correlate with tissue-scale deformations. Methodology: Specimens from native and elastin-isolated aortic tissue were tested at different loadings. Histological sections were characterized for elastin network conformations.

I.3.2. Specific Aim 2: Factors Affecting Viscoelasticity

Another relevant problem is to understand the effects of elastin microstructural interactions with the matrix on tissue viscoelastic behavior. Elastin mechanical behavior is shown to shift from crystallized-like to rubbery-like materials at the extremes, and vice-versa, depending on different factors, most importantly hydration. Common causes of change in elastin hydration can be a change in tissue water content, which directly correlates with elastin hydration, and alteration in extracellular matrix composition, which indirectly limits the amount of water available to elastin molecules. Given the importance of extracellular matrix composition on elastin hydration, we set the second specific aim as:

- Determine how extracellular matrix alterations affect tissue viscoelastic behavior.

Hypothesis 2: The amount of water in the extracellular matrix is an important factor in regulating the viscoelastic behavior of tissues. Methodology: A two-stage humidifying method was used to prepare specimens with controlled water content. Specimens were tested under stress relaxation and the mechanical behavior was characterized under different conditions.

Hypothesis 3: Alterations in composition of the extracellular matrix change the tissue viscoelastic behavior. Methodology: Specimens from native, matrix-degraded, and elastin-isolated tissues were tested under stress relaxation and the mechanical behavior was characterized under different conditions.

I.4. Research Approach

The following tables provide a snapshot of the research steps involved in accomplishing each of the specific aims set previously.

Correlation of Elastin Deformation with Macroscale Deformation: To study macro-scale deformation and histological changes under different values of tissue stretch, a custom-made device was used to maintain tissue specimens at certain deformation states. Histological examinations were performed on the tested specimens in order to study the microstructural changes for each of the loading cases. Initial histological studies were performed on specimens under no loading whose results provide the tissue undeformed microstructure. The second set of histological studies was performed on specimens under constant stretch. The final set of

specimens was studied after these have been released from stretch. Histological sections were extracted from the specimens under each of the loading protocols and were stained for highlighting elastin microstructure. Elastin configuration was quantified for their directionality. Evaluating elastin microstructural changes during tissue deformation sheds light on its correlation with tissue deformation. Table 1 shows a summary of the steps.

Table 1- Summary of test procedures and observations involved in investigating the correlation between microstructural- and tissue-scale deformations.

Category I		**Category II**		**Category III**	
Procedure	**Observation**	**Procedure**	**Observation**	**Procedure**	**Observation**
Circumferential specimens were extracted from intact tissue.		Circumferential specimens were extracted from intact tissue.	Specimen dimensions were characterized.	Circumferential specimens were extracted from intact tissue.	
Specimens were kept unstretched.		Different specimens were stretched up to 1.4 and 2.0.		Different specimens were stretched up to 1.4 and 2.0.	
		Specimens were kept at fixed stretch.	Specimen dimensions were characterized.	Specimens were kept at fixed stretch.	
				Samples were unloaded to recover back into free state.	Specimen dimensions were characterized.
Microstructure was fixed.	Histology was quantified.	Microstructure was fixed.	Histology was quantified.	Microstructure was fixed.	Histology was quantified.

Mechanical Testing of Matrix-Degraded and Elastin-Isolated Specimens: Tissue specimens were processed through a two-step chemical treatment. The first step yielded matrix-degraded specimens (collagen-denatured) while the second step resulted in elastin-isolated specimens embedded in an aqueous matrix. Separately, a customized hydration method was used to prepare specimens with a specific water content during storage and mechanical testing. Direct effects of tissue hydration on its viscoelasticity were characterized through comparing stress-relaxation of variably-hydrated tissue specimens. Furthermore, swelling and stress-relaxation of native, matrix-degraded and elastin-isolated specimens were used to understand the effects of alteration in matrix composition on tissue viscoelasticity, for instance, indirect effects of hydration through blockage of available water molecules to elastin. Table 2 shows a summary of the steps.

Table 2- Summary of test procedures and observations involved in investigating the viscoelastic behavior of native and matrix-degraded tissue specimens.

Category I		**Category II**		**Category III**	
Procedure	**Observation**	**Procedure**	**Observation**	**Procedure**	**Observation**
Circumferential specimens were extracted from intact tissue.		Circumferential specimens were extracted from intact tissue.		Circumferential specimens were extracted from intact tissue.	
Specimens were prepared with different hydration values.	Sorption characteristic curves were developed.	**Specimens were autoclaved to get matrix-degraded tissue specimens.**		Specimens were autoclaved to get matrix-degraded tissue specimens.	
		Specimens were prepared with different hydration values.	Sorption characteristic curves were developed.	**Specimens were NaOH-treated to get elastin-isolated tissue specimens.**	
				Specimens were prepared with different hydration values.	Sorption characteristic curves were developed.
Stress-relaxation test was performed.	Stress was measured and the behavior was quantified.	Stress-relaxation test was performed.	Stress was measured and the behavior was quantified.	Stress-relaxation test was performed.	Stress was measured and the behavior was quantified.

II. FUNDAMENTALS OF CARDIOVASCULAR SYSTEM

This section aims to review some of the basic terminology and fundamental concepts on the cardiovascular system which set the background for the rest of the dissertation.

II.2. Vascular Tissue

The entire system of blood circulation within the body is known as the cardiovascular system, which includes the heart and associated valves –cardiac system– as well as the hierarchy of blood vessels including arteries, arterioles, capillaries, venules and veins –vascular system [Humphrey 2002]. Since the focus of this study is on the mechanics of arterial tissue, the main part of the vascular system, the rest of this section is dedicated mainly to the composition and structure of the arterial tissue.

The extracellular matrix (ECM) constitutes a major component of biological soft tissues, including vascular tissue. The major constituents of ECM are different types of proteins with the most prevalent ones being collagen, elastin, proteoglycan, actin, myosin, fibroblast, fibronectin and chaperon. The existence of specific proteins with different density and orientation, as well as the interaction between them, is necessary to provide different tissues with specific properties and functioning [Alberts 1998]. The major ECM proteins in vascular tissue are collagen and elastin [Humphrey 2002].

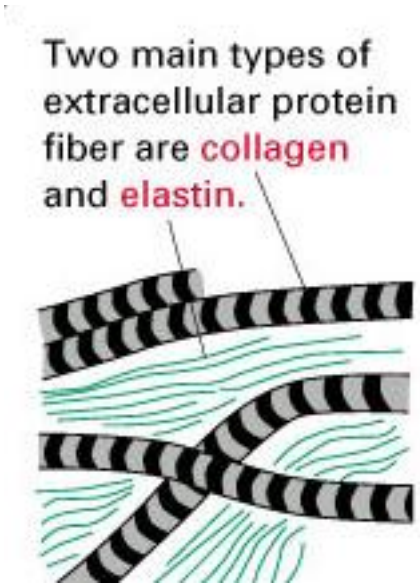

Figure 2- Schematic illustration of elastin-collagen structure in tissue extracellular matrix (Currey 2005).

II.2.1. Main Constituents

Though varying in configuration and concentration, the main components of the arterial tissue are Elastin, Collagen, Smooth Muscle Cell and Proteoglycans [Humphrey 2002], Fig. 2.

- Elastin- The elastin protein is one of the major constituents of most of the biological connective tissues [Fung 1993]. The mature, cross-linked elastin molecule is inert and so stable that, in normal circumstances, it lasts in the body for the entire life of the organism [Fung 1993]. The importance of elastin in arterial tissue is indicated by its prevalence in the tissue, e.g. constituting about 60% by weight of the pig thoracic aorta [Minns 1978]. The elastin within the tissue is hydrated with interstitial fluid, but considering the pure dry elastin, it has a density of approximately

$\rho_e = 1.23\times10^{-3}\, gr/mL$ ($\rho_e = 1.23\times10^{-3}\, gr/mm^3$) [Scandola 1980]. The main role of the elastin in connective tissues is to provide the tissue with the required (visco)elastic properties [Fung 1993; Humphrey 2002]. Elastin is mainly responsible for recovering the deformation of the tissue to its original configuration. Elastin's physiological stretch range is $\lambda = 1.2 - 1.7$ [Apter 1967; Lillie 1996] and can tolerate stretch up to $\lambda_u = 2.50$ before failure [Humphrey 2002].

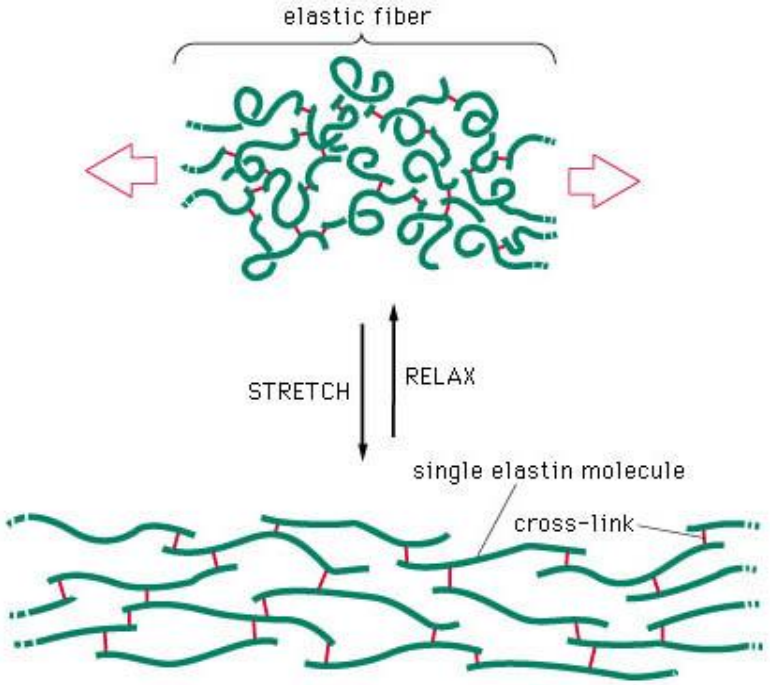

Figure 3- Schematic illustration of deformation mechanisms of elastin fibers under stretch (Alberts 2002)

Elastin recovers the deformation by storing energy in the systole and returning it to the blood vessel in the diastole, which also smoothes the intra-arterial pressure fluctuations to protect tissue against high blood pressure [Lillie 1990]. There exist a lot of speculations in the deformation mechanisms of the elastin network and how they relate to tissue deformation. As it is schematically shown in Fig. 3, it is believed

that elastin fibers are cross-linked to each other and to the extracellular matrix and they start to straighten under tissue stretch. The cycling loading of elastin fibers indicates the existence of a hysteresis loop due to energy dissipation, which indicates that elastin is a viscoelastic material [Fung 1993].

- Collagen- Collectively, collagen is the most abundant protein within different tissues of the body (approximately $25\% - 30\%$ of all proteins) including the cardiovascular tissues which posses mostly collagen types I, III, IV as well as types V, VI and VIII [Mayne 1986]. The collagen molecules consist of three polypeptide α chains, each containing 1300 to 1700 amino acid residues which are primarily organized in a central triple-helix motif [Ayad 1994], which is in the order of $285nm$ in length and $1.4nm$ in diameter. The cross-linking of collagen molecules forms collagen micro-fibrils and further engaging of micro-fibrils leads to collagen fibers with $1 - 500\mu m$ in diameter, which constitute the tissue, Fig. 4. On average, collagen fibers are orienting approximately along the circumferential direction. The angle between collagen fibers and the circumferential direction is almost 0° for collagen fibers in medial regions and about 40° in adventitial regions [Holzapfel 2007]. Collagen fibers have high tensile strength, e.g. $100MPa$ for type I collagen in tendons [Humphrey 2002], which is significant given that the tensile strength of cast iron is only twice that amount. Therefore, collagen fiber is a strong load-bearing component and thus, the main role of the collagen is to provide the tissue with the required mechanical integrity and strength [Fung 1993]. Due to their undulated configuration in the physiological range of deformation (and loading), the collagen fibers do not affect the mechanics of the tissue except at tissue stretch levels beyond $\lambda = 1.7 - 1.9$

[Hoeve 1958; Apter 1967]. Unlike the elastin fibers, the straightened collagen fibers show very little flexibility before failure, having an ultimate stretch of $\lambda_u = 1.10$, measured from initial length of straighten fibers [Humphrey 2002].

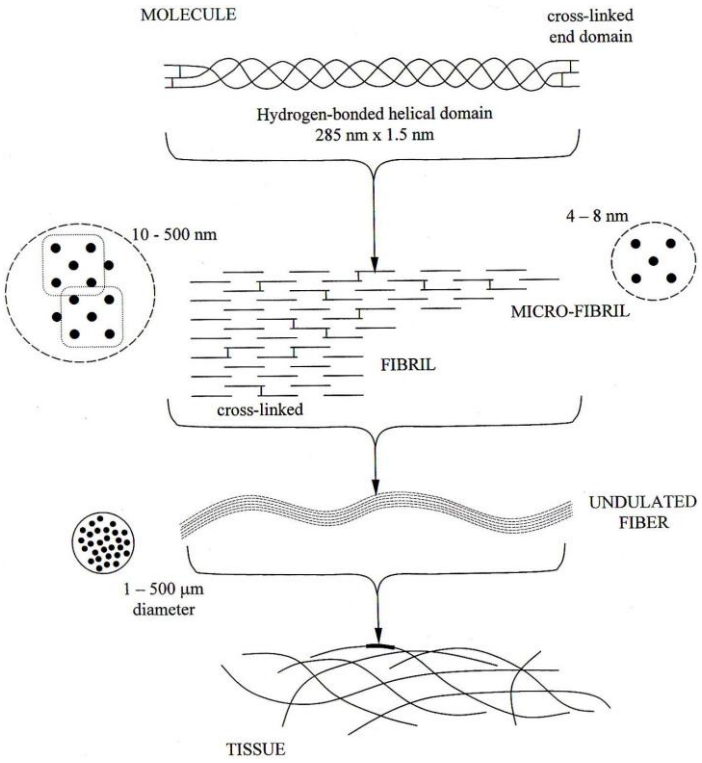

Figure 4- Schematic illustration of hierarchical levels of the collagen structure (Humphrey 2002).

- Smooth Muscle Cell- Smooth muscles are the muscles whose striations are not visible and those available in vascular tissue are called vascular smooth muscles (VSM) [Fung 1993], which comprise about $25\% - 60\%$ of the arterial tissue [Milnor 1990]. The size of the VSM cells is much smaller than that of many skeletal and heart muscle cells [Burnstock 1970] and it varies around $100\mu m$ in length and $5\mu m$ in diameter [Humphrey 2002]. This component is typically embedded in an extracellular plexus of elastin and collagen as well as an aqueous ground substance

matrix containing proteoglycans. Though variant in concentration and structure in different regions of cardiovascular tissue, the VSM is mainly responsible for regulating the local strain and stress distribution within the tissue and to eventually regulate blood flow [Humphrey 2002]. This is primarily due to capability of the VSM cells to change their contractile tone, i.e. to be in contraction, normal configuration or dilation. It is found that there exists a correlation between the tone of the VSM and its stress state [Wang 1995]. In the other word, the VSM change its tone if it experiences certain level of stress, e.g. shear stress, and that, in turn, regulates the stress state. Compared to that of striated muscle cells, the response time of VSM is longer and it normally takes $t = 1 - 10s$ for a VSM to reach its maximum tone [Somlyo 1992]. Most of the unique properties of the VSM are associated with specific interaction mechanisms and configurations of actin and myosin –two other important ECM proteins [Horowitz 1996].

- Proteoglycans- A small portion of the ECM is composed of proteoglycans, molecules with a core protein and attached multiple chains of glycosaminoglycan(GAG), Fig. 5. The proteoglycans are distributed heterogeneously in the ECM [Radhakrishnamurthy 1977] with no preferred structural organization. However, due to their high negative charge and low-density chains, proteoglycans play important roles in absorbing water into the ECM [Humphrey 2002] as well as in maintaining the integrity of the ECM [Berenson 1971]. Through cross-linking to collagen and elastin, proteoglycan contributes significantly to the mechanics of the tissue [Mathews 1965; Sajdera 1969; Radhakrishnamurthy 1977].

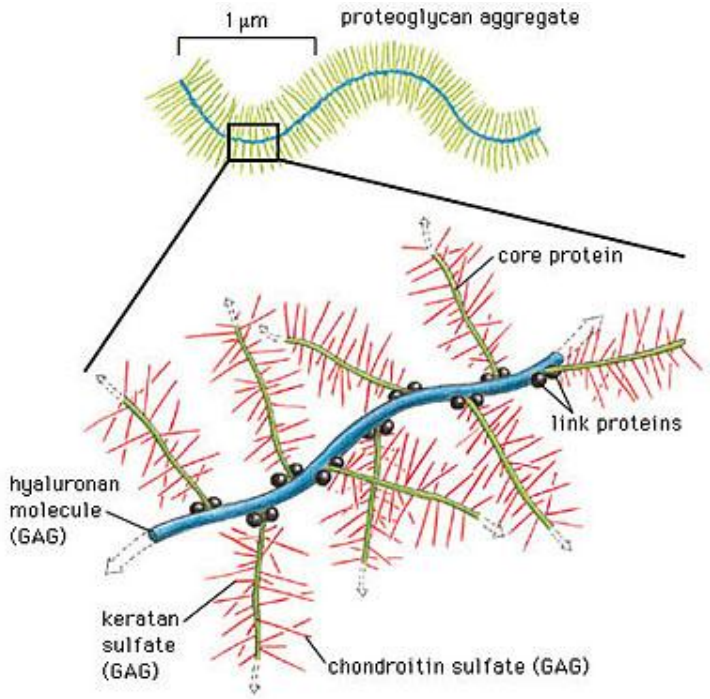

Figure 5- Schematic illustration of proteoglycan molecules and attached GAG chains (Currey 2005)

II.2.2. Wall Layers

Figure 6 shows the wall of arterial tissue which consists of 3 different layers of Intima, Media and Adventitia varying in the density and orientation of structural constituents.

- Tunica Intima: Very thin inner-most layer of the wall which is composed of: (a)Monolayer of endothelial cells which are usually flat and elongated in the direction of the blood flow, $0.2-0.5\mu m$ thick, $10-15\mu m$ wide, $25-50\mu m$ long, (b)Underlying basal lamina with $80nm$ thickness which is largely composed of net-like type IV collagen, the adhesion molecules laminin, fibronectin, and some

proteoglycans, (c)Subendothelial layer of connective tissue & axially oriented smooth muscle cells (in Aorta and Coronary).

- Tunica Media: The middle layer of the artery wall which consists of: (a)Spindle-shaped smooth muscle cells with length of $100\mu m$ and diameter of $5\mu m$, (b)Fenestrated layers of elastic lamina, (c)Fibrils of Collagens of types I and types III, V, (e)Aqueous ground substance matrix containing proteoglycans.

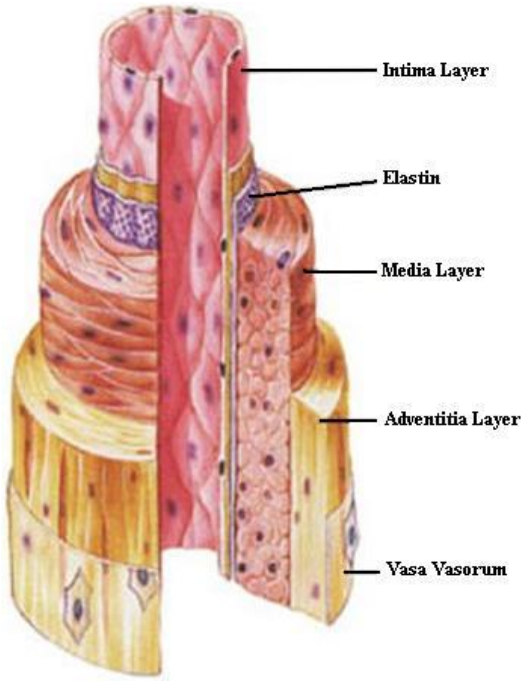

Figure 6- Arterial wall with three different layers of Intima, Media and Adventitia (Fox 2008).

- Tunica Adventitia: The outer-most layer of the arterial wall which is composed of: (a)Dense network of type I collagen fibers which tend to orient axially and undulated and limit high dilations of the artery wall, (b)Admixed elastin, nerves, fibroblasts and vasa vasorum (intramural network of arterioles, capillaries, etc).

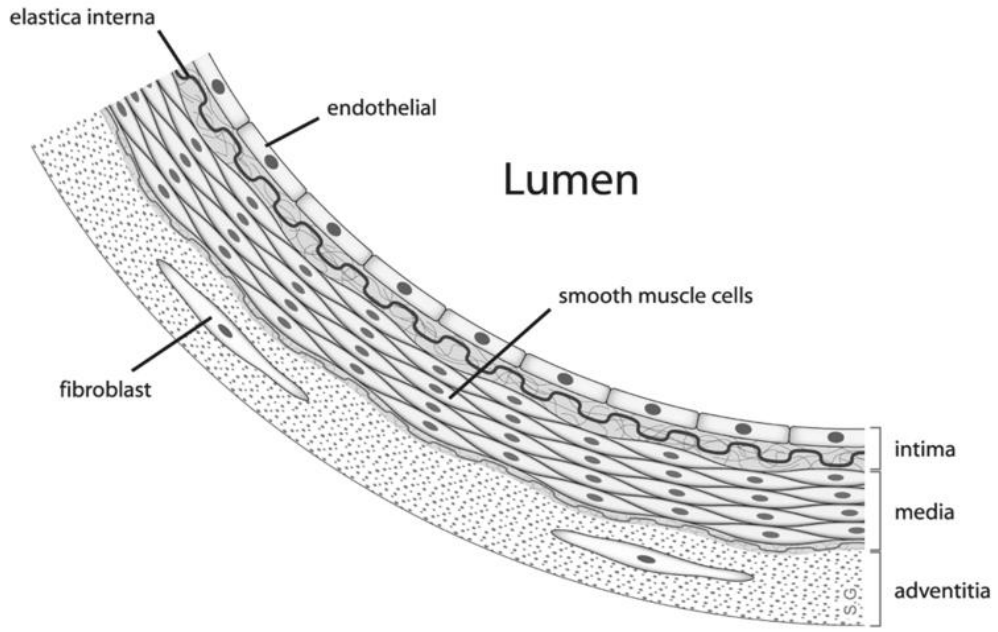

Figure 7- Schema of arterial wall with three different layers as well as endothelial layer (Stjin 2005).

II.3. Blood-Wall Interaction

The circulating blood throughout the vascular system is in contact with the wall of the blood vessels at the inner surface of the blood vessels, which is part of the most-inner layer, the tunica Intima, Fig. 7. As described above, the Intima is partly composed of specialized cells which are called endothelial cells [Holzapfel 2000(c)]. Endothelium cells form a very thin endothelial layer which is responsible for solid-fluid interaction in the vascular system. In fact, these cells experience the main part of the loading on the vascular tissue, which is due to blood pressure, and regulate the vascular tissue's response accordingly [Humphrey 2002].

II.4. Regional Variation

The geometrical properties and mechanical behavior of the artery tissue vary regionally depending on the anatomical and physiological specifications. Specifically, the following factors are decisive in determining the mechanical properties of the tissue:

- Elastic vs. Muscular: The elastic regions are those in the artery which are closer to heart, e.g. upstream aorta or main pulmonary artery, whereas the muscular regions are those that are closer to arterioles, e.g. coronaries, cerebrals. The main difference between the elastic and muscular arteries is in the configuration of smooth muscle cells, Fig. 8. In elastic artery tissues, the medial smooth muscle is organized into $5-15\mu m$-thick concentric layers that are separated by $3\mu m$-thick fenestrated sheets of elastin. In contrast, the smooth muscle cells in muscular arteries are arranged in one thick single layer, which is separated from the Intima and Adventitia layers by two thick internal and external elastic laminas.

- Pulmonic vs. Systemic: The pulmonic vascular system includes those vessels from the heart to the lungs which carry oxygen-poor blood for reabsorbing oxygen at the lungs, whereas the systemic vascular system consists of those feeding vessels which carry oxygen-rich blood from the heart to the tissues in the rest of the body. The important difference between these two types of vessels in testing mechanical properties is the noticeable difference in their blood pressures. The range of blood pressure in the pulmonic vessels is from $1.07-3.33kPa$ $(8-25mmHg)$ with $5kPa$ as the injury threshold pressure, whereas that of the systemic vessels is around $10.67-16kPa$ $(80-120mmHg)$.

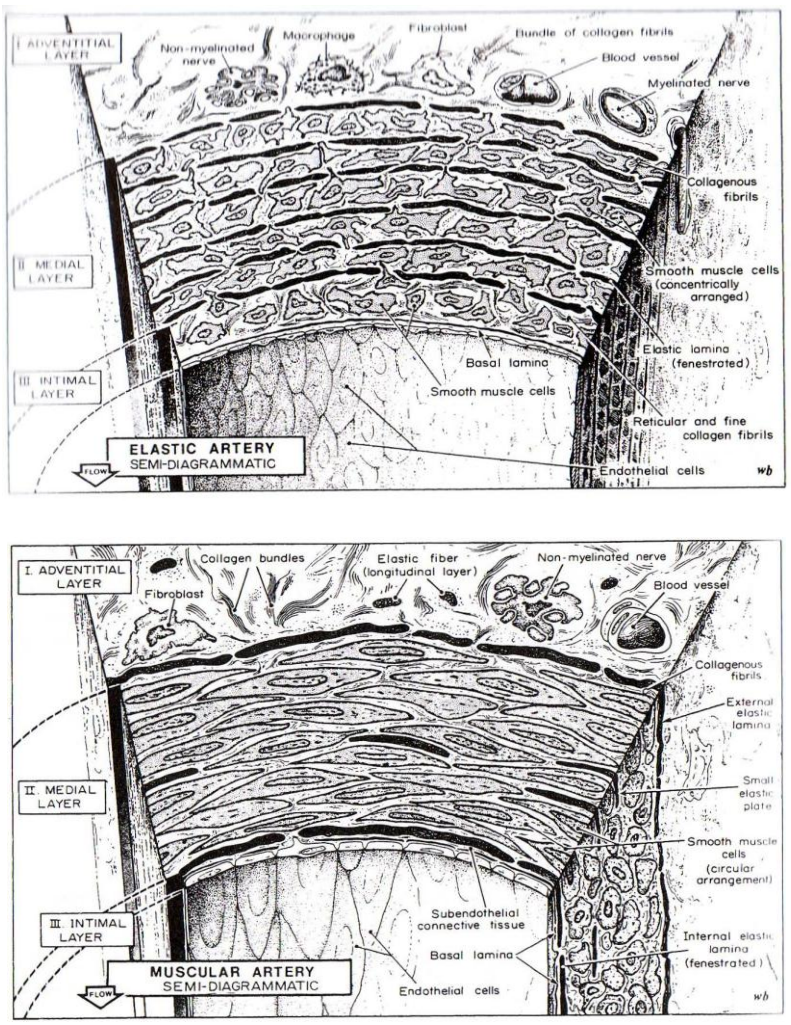

Figure 8- Microstructure of arterial wall: (TOP) elastic, (BOTTOM) Muscular (Rhodin 1979).

II.5. Physiological Conditions

Physiological conditions refer to the loading and deformation states of the cardiovascular tissue during the normal range of operation. The aortic blood pressure typically changes between $p = 0 - 13.7 KPa$ at time of diastole and systole, respectively, which causes a stretch ratio of about $\lambda = 1.3$ in the tissue [Lillie 1990]. Elastin's lower end of physiological range is $\lambda = 1.25$ [Lillie 1996]. Non-physiological

conditions refer to the tissue's loading patterns and associated deformations due to the blood pressure being higher than the physiological range.

III. DEFORMATION CHARACTERIZATION

III.1. Background

A large portion of the biological soft tissues exhibit multiscale biomechanics in which the mechanical behavior of the tissue has characteristics deriving from microstructural components [Lillie 1986; He 1994; Weinberg *in press*]. Characteristic changes in tissue fibrillar structure can potentially serve as an early diagnostic marker in various pathological processes which, in turn, necessitates establishing more precise measures of quantifying the tissue microstructure [Weibel 1989; Roberts 2000; Erikson 2007]. Unlike at tissue-scale, where measuring a specimen's dimensions can provide a sufficient description of tissue deformation, quantification of microstructural deformations is a challenge [Avolio 1998] and has been one of the principal areas of advancement in experimental biology over the past decade [Bolender 1992].

Most of the traditional methods for assessing tissue microstructure have been limited to providing qualitative or semi-numerical assessments of the microstructure [Knodell 1981; Ishak 1995; Brunt 2000; Dahab 2004], rather than fully quantitative measures. The outcome of a qualitative assessment of the microstructural configuration is prone to subjective interpretations by different individuals [Soloway 1971; Bedossa 1994; Masseroli 2000], and it has been found that there could be high discrepancy in the results when the experiments are repeated [Bedossa 1994; Ishak 1995; Brunt 2000]. It is difficult to develop highly reproducible and standardized qualitative measures for assessing microstructural configuration [Kage 1997]. To

overcome the drawbacks of the qualitative assessment, digital morphometric image analysis has been attempted to develop quantitative measures [Masseroli 2000; Zipfel 2003; Dahab 2004; Hui 2004]. Nonlinear optical microscopy, such as excited fluorescence and multiharmonic generation, has been becoming common practice in tissue imaging [Freund 1986; Denk 1990; Maiti 1997; Chu 2001]. Second harmonic generation has been used to measure highly ordered structures such as type I collagen [Brown 2003; Theodossiou 2006; Strupler 2007]. Sun *et al.* has applied second-harmonic generation and two-photon excited fluorescence to quantify the alterations in fibrillar collagen in liver tissue during chronic liver diseases [Sun 2008]. However, these methods can be costly and only effective when applied on subjects with a highly crystalline triplehelix structure that is not centrosymmetric, and the molecules are organized on the scale of the wavelength of light, such as collagen [Erikson 2007]. An entire technique of digital image correlation (DIC) has been developed to investigate microscale deformation measurements through registering sequences of digital images at multiple times [Bruck 1989; Robert 2007; Lord 2008], and the method has recently been used for soft tissues [Sutton 2008; Moerman 2009]. The effectiveness of the DIC method is limited to applications where multiple images can be extracted from the phenomenon. However, the in vitro procedures adapted in the current study are invasive such that histological images can be generated from tissue specimens only at one point in time and therefore the DIC technique is not suitable for this work. Another approach to studying the microstructural morphology in soft issues is through analyzing the histology images obtained under the microscope [Castleman 1996; Amenabar 2006]. Conventional methods of quantifying histology

images, such as linear integration, counting points or the use of a polar planimeter, are manual methods that can be carried out by an operator. Except for a few studies that reported comparable results of manual analysis to those of semi-automated methods [Amenabar 2003; Amenabar 2006], it has been found that manual quantification of histology images is not able to provide repeatable, non-biased and descriptive measures of the morphological state [Manderim-de-lacerda 1995; Avolio 1998; Dickson 2003]; primarily due to the complexity of the tissue microstructural conformations. It has been reported that factors such as size, shape, orientation and area can affect the outcome of the image analysis when qualitative assessment is used [Hamilton 1995], all of which are prevalently seen with large variability in soft tissues. Extra care must be paid when producing digital images from light microscopy, as it has been shown that even small variations in focus and illumination of the images has led to inaccurate measurements [Castleman 1996; Sims 2002].

The majority of the studies relevant to the identification of changes in tissue histology during different healthy and diseased conditions, however, have focused on characterizing the quantity and density of certain tissue components but not so much on their orientation. The collagen fibrillar content in liver tissue, regardless of its orientation, has been quantified for studying chronic liver diseases [Sun 2008]. Besides the content and density of tissue structural components, a key factor in determining tissue biomechanics is the orientation of fibrillar networks. Few studies exist whose goal was to characterize the fibrillar orientation in tissue microstructure. Rubbens *et al.* quantified collagen orientation in engineered cardiovascular tissue

images using an innovative eigen-value based analysis [Tonar 2003; Daniels 2006; Rubbens 2009].

As previously discussed, the primary obstacle in quantifying fibrillar microstructure in the tissue arises from the complex patterns of individual fibers and regional variations throughout the microstructure. Here, the Fourier and Hough transformations were applied to the histological images to extract features which can collectively determine the average state of the microstructural configuration. Fourier transformation is a relatively well accepted method in the field of image analysis to identify properties of the images such as directionality and compactness [Bracewell 1965; Tonar 2003]. In this study, we enriched the interpretations from the Fourier method with those obtained based on the outcome of the Hough method.

III.2. Materials and Methods

This section describes the main experimental setups and laboratory procedures involved in the course of microstructural examination.

III.2.1. Specimen Preparation

Aortas of 291±23 mm length were obtained from Angus male cattle (average age of 20-24 months) at a local abattoir. Each aorta was cut proximally near the heart and distally above the abdominal bifurcation, and was immersed in cold phosphate buffered saline (PBS) while transferred to the laboratory. The tissue was carefully cleaned of large remnants of fat and attached connective tissues, Fig. 9. Only one

third of the tissue at the proximal end was used in order to minimize potential region-dependent discrepancies in tissue properties. Areas of the aorta containing vascular branch points and abnormalities were discarded.

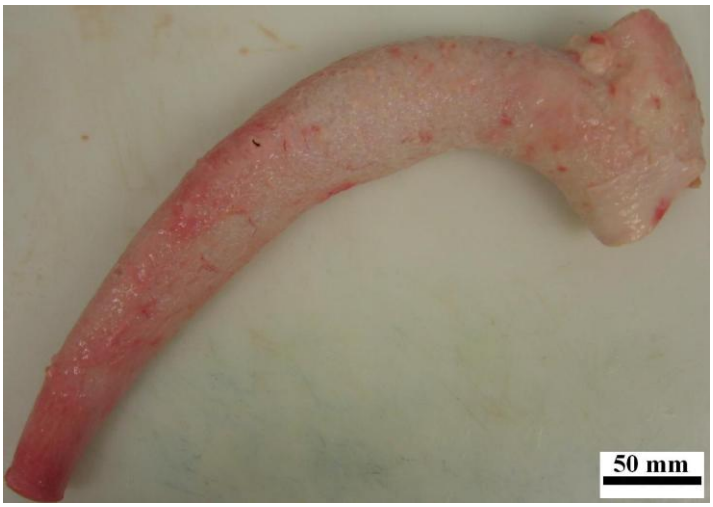

Figure 9- Picture of the aorta after being cleaned from attached lipids and connective tissues.

Given the focus of this study on the deformation and biomechanics of the elastin network and knowing that the structural networks run around the circumferential direction, rectangular specimens were cut from the aorta in the circumferential direction. The aorta was idealistically considered to be a cylinder with the cylindrical polar coordinate system, $r-\theta-z$, set as shown in Fig. 10, which leads to the circumferential specimens cut from the aorta oriented as shown in the figure. Conceptually, the main steps in cutting the specimens out of the aorta are also represented in the figure, however, practically, we used a customized cutting fixture to make the specimens out of a wide cut aortic ring, Fig. 11. The template was set to give specimens with $30\text{mm}\times 10\text{mm}$ length by width dimensions, and the thicknesses

naturally varying in the 3-8mm range, Fig. 12. Extra care was paid to excise specimens in the circumferential direction in order to be able to identify the circumferential direction throughout the later stages under the microscope and the histological examinations. The excised specimens were preserved in PBS solution with protease-inhibitor additives (per 1 Liter of PBS: 1mM of EDTA-Disodium salt, 1mM of EDTA-Tetrasodium salt, 5mM of Benzamadine, 10mM of NEM, 1mM of PMSF) until being used.

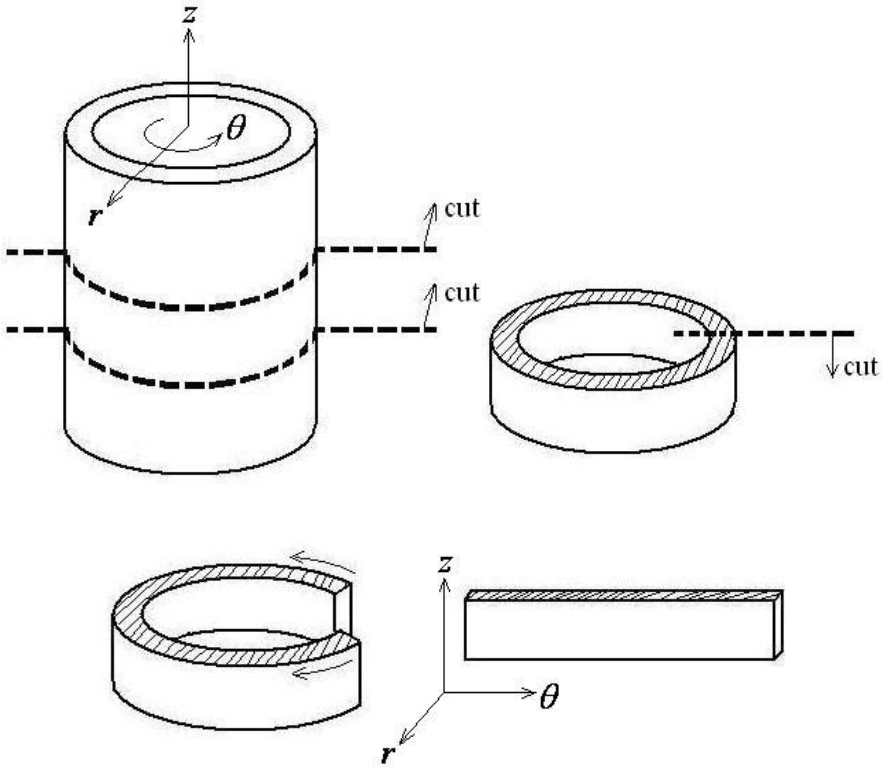

Figure 10- Representation of coordinate systems on the aorta and cut specimens as well as the schematic steps involved in cutting the specimens.

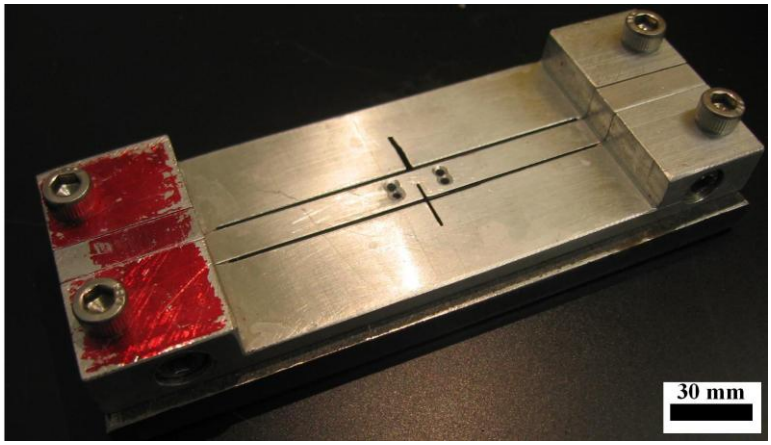

Figure 11- Pictures of the customized cutting device used to extract 30mm × 10mm rectangular specimens from aortic tissue. The apparatus is designated to create side notch and pairs of markers on the specimens in other applications, when necessary, although these were not used in this application.

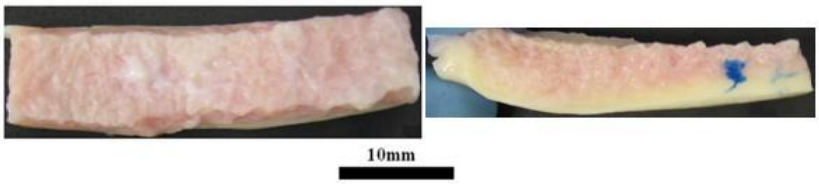

Figure 12- Pictures of cut circumferential specimen: right-top view, left-side view. On the side view, the blue dot shows the mark of tissue dye used to measure thickness on the image.

III.2.2. Degrading the Extracellular Matrix

A group of extracted specimens was treated in order to fragment the main structural component of the tissue, collagen, and other proteins in the extracellular matrix, leaving the elastin intact. These specimens were prepared to examine the effects of

extracellular matrix integrity on the tissue mechanical behavior. Specimens from native tissue were autoclaved for 1 hour under chamber pressure of $p = 15 psi (\approx 103 KPa)$ [Pezzin 1976; Weinberg 1995; Lillie 1996]. The autoclave process was performed using a Consolidated® sterilization system available in the Chemical and Nuclear Engineering building, Fig. 13.

Figure 13- Consolidated® autoclave system available in chemical and nuclear engineering building.

The autoclaving pressure of $15 psi$ was associated with the corresponding superheated temperature of $T = 115^{\circ} C$. Superheating the tissue proteins causes them to denature. However, because the denaturation temperature for collagen is about $T_d \approx 40^{\circ} C - 63^{\circ} C$ [Fung 1993; Samouillan 2000], compared to $T_d \approx 200^{\circ} C$ for elastin [Pezzin 1976], heating the tissue up to around $T = 115^{\circ} C$ only causes collagen denaturation but not elastin. Since denaturation is an irreversible process [Wright

2002], by cooling down the tissue, the collagen proteins do not bond back. It has also been found that the mechanical properties of elastin do not markedly change during the heating and cooling processes [Fung 1993; Lillie 1994]. Superheating the tissue also kills the smooth muscle cells [Humphrey 2002]. Figure 14 shows top and side images of a matrix-degraded specimen.

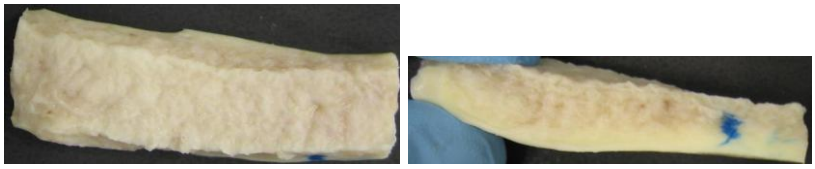

Figure 14- Pictures of matrix-degraded specimen: right-top view, left-side view.

III.2.3. Isolation of Elastin

A group of matrix-degraded specimens were further treated to fully isolate elastin. Elastin is believed to play a major role in giving the arterial tissue its viscoelastic properties [Fung 1993; Humphrey 2002]. Therefore, along with the native tissue, some of the experiments were performed on tissue with mostly isolated-elastin content.

The matrix-degraded specimens were further processed by extraction in $0.1M$ NaOH for 1 hour under temperature of $T = 98^{\circ}C$ to remove proteoglycans from the autoclaved specimens [Pezzin 1976] and to further eliminate pieces of denatured collagen [Samouillan 2000; Brzezinski 2007]. At this point, the treated tissue is essentially composed of elastin embedded in intrafibrillar water of the extracellular matrix. Figure 15 shows top and side images of an elastin-isolated specimen.

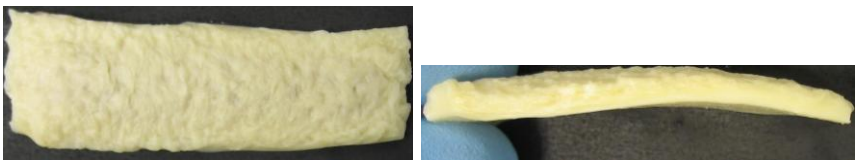

Figure 15- Pictures of elastin-isolated specimen: right-top view, left-side view.

III.2.4. Stretch and Recovery Device

A customized apparatus was designed and manufactured in order to retain tissue specimens under a controlled deformation state over time. The apparatus consists of one stand and two movable jigs which can be screw-secured on the stand. The stand contains a set of holes at measured locations which allow adjustment of the jigs on the stand with a specific distance between them, Fig. 16. To load the specimen on the apparatus, the jigs were first secured on the stand at 1.0 inch apart from each other. The specimen was placed in between the two wings of each jig and the wings were screwed close until they applied enough force to tightly grab the ends of the specimen, but not too tight to squeeze the specimen and damage the tissue integrity. After the specimen was secured between jigs, one jig was unscrewed from the stand and screwed to the new position of interest, i.e. 2.0 inch, if $\lambda = 2$ is needed. For specimens to be examined under stretch, the apparatus and the specimen -under stretch- were left in a 500ml beaker containing tissue fixative for 24 hours. For specimens to be examined after deformation recovery, the apparatus and the specimen –under stretch- were first placed in PBS for 45 minutes in order for stress relaxation to take place in the tissue. One end of the specimen was then released from the jig so

it could retract to the new unloaded state. Specimens were finally left in fixative solution for 24 hours to fix the microstructure.

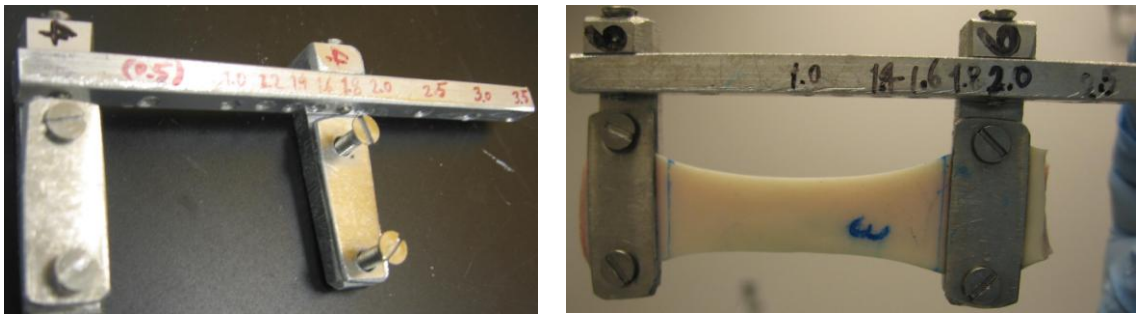

(a) (b)

Figure 16- Customized apparatus used to retain aortic samples under a certain deformation over a long period of time. The apparatus is capable of applying stretch ranging between 1.2 and 7.0; aortic tissue specimens were stretched to 1.4 and 2.0 in this study.

III.2.5. Dimension Measurement

To examine the macroscale changes in the tissue, the dimensions of the specimens were obtained at each of the loading steps of release, extension and recovery. Given the extraction of the samples along the circumferential direction of the aorta, comparing the change in specimen width and thickness during sample elongation can be a partial indicator for different mechanisms of, respectively, in-layer versus cross-layer fibrillar deformations in the tissue. The width and thickness of tissue specimens were measured on the calibrated images taken from top and side views of the specimens, Fig. 17.

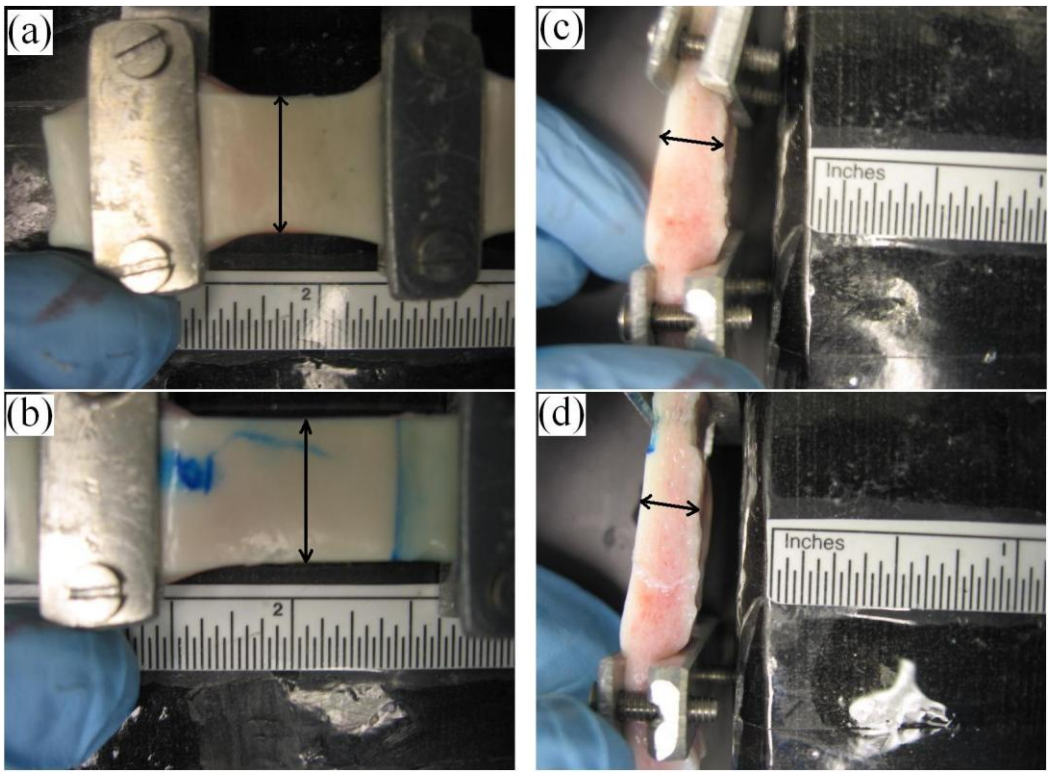

Figure 17- Quantifying dimensional changes during tissue deformation measurements through standardized images taken from the specimens before and after deformation. Images (a) and (b) were used to measure width before and after loading, respectively, and images (c) and (d) were used to make thickness measurements before and after loading, respectively.

III.2.6. Analysis of Statistical Significance

When dealing with experimental data measurements on features that can potentially be compared amongst different groups, there is always the question of whether the measurements and the conclusions drawn are statistically-significant. This question becomes more important when dealing with measurements on samples with large variation such as those taken from soft biological tissues. One of the common methods to investigate the variation in sample measurements and evaluate their statistical significance is the ANOVA (Analysis of Variance) method, initially

introduced in the 1970s (Eisenhart 1947; Lewontin 1974). The two most common problems are usually stated as: 1. How many sample measurements are needed to reach a certain level of statistical significance? and 2. How does a given set of measurements statistically-significant?

To address the first problem, the ANOVA has been particularly formulated to determine how many samples are needed before certain level of statistical significance is reached (Sokal and Rohlf 2000; Pearson and Hartley 1958; Thomson 1951). In parts of this study, it is initially sought to get an estimate of the number of required measurements for reaching reasonable statistical significance, and for this purpose, the ANOVA method is used as follow:

$$n \geq 2\left(\frac{\sigma}{\delta}\right)^2 \left\{t_{\alpha[\nu]} + t_{2(1-P\nu)[\nu]}\right\}^2 \tag{19}$$

$$\nu = a(n-1) \tag{20}$$

where $n =$ number of replications, $\sigma =$ true standard deviation, $\delta =$ the smallest true difference to be detected, $\nu =$ degrees of freedom of the sample standard deviation, $\alpha =$ significance level, $a =$ number of groups. $P =$ desired probability that a difference will be found to be significant (intended power of the test), $t_s =$ values from a two tailed t-table with ν as one tail and both α and $2(1-P)$ as the other tail (Rohlf and Sokal, 2002). To use this method, a few initial measurements are needed so as to provide an approximate picture of the statistical features. The rest of the procedure is a trial and error process where a random number of required samples, n, is initially

chosen to start with, and by substituting back the newly-calculated number n from the formula for the initial random value, it converges toward the actual value.

To address the second type of problems where sets of measurements already exist, and it is sough to know the statistical significance when comparisons are made between different sets, the statistical software SPSS (*IBM, Armonk, NY*) was used to do the analysis. The single-way ANOVA test was used and the groups with $p < 0.05$ were considered to be statistically-significant and were marked with brackets on the bar graph of the data plots, whenever needed.

III.2.7. Histological Examinations

Histological examinations are those to study the microstructure of the tissue for which the first step is to chemically fix the tissue microstructure. A modified fixative solution consisting of 10% Clorox® and 15% Formaldehyde in deionized water was used in this study for this purpose. It has been reported that Clorox® and Formaldehyade show better fixation properties for certain tissue components, primarily elastin and collagen, respectively [Hopwood 1967; Lillie 1996]. After fixing the microstructure, specimens must be subjected to proper procedures before histology slides can be prepared. First, a Leica® TP 1020 tissue processing machine was used to prepare the tissue for paraffin embedding, Fig. 18. Tissue processing consists of dehydration of the tissue by ethanol, removing the ethanol by Xylene and infiltrating the paraffin into the microstructure of the tissue. Then a Leica® EG1160 machine was used to produce a clear-cut block of paraffin enclosing the paraffin-infiltrated specimen, Fig. 19.

Figure 18- Leica® TP 1020 tissue processing machine available in the Orthopaedic Mechanobiology Lab.

Figure 19- Leica® EG1160 paraffin embedding machine available in the Orthopaedic Mechanobiology Lab.

Blocks of paraffin encompassing the tissue specimens were sectioned with a Microm® HM355S apparatus, Fig. 20, to extract sections of $6\mu m - 10\mu m$ thickness. The fibrillar microstructure of aortic tissue is organized into lamellas laid tilted around the circumferential orientation, shown as θ in the cylindrical coordinate system. In this coordinate system, histology sections in $r-\theta$ plane are found to be the most descriptive of fibrillar orientation. Slides of tissue microstructure were stained using a protocol which was a customized modification of Masson's trichrome with Verhoeff's hematoxylin [Sheehan 1980; Gravey 1991]. In this protocol, the elastin is stained with dark blue, the collagen is stained with light blue, and proteoglycans are stained with red, Fig. 21. Stained sections of tissue histology were studied under the Olympus® IX81 microscope, Fig. 22, capable of taking images under $40\times, 100\times, 400\times$ magnification.

Figure 20- Microm® HM 355 S sectioning apparatus available in Orthopaedic Mechanobiology Lab.

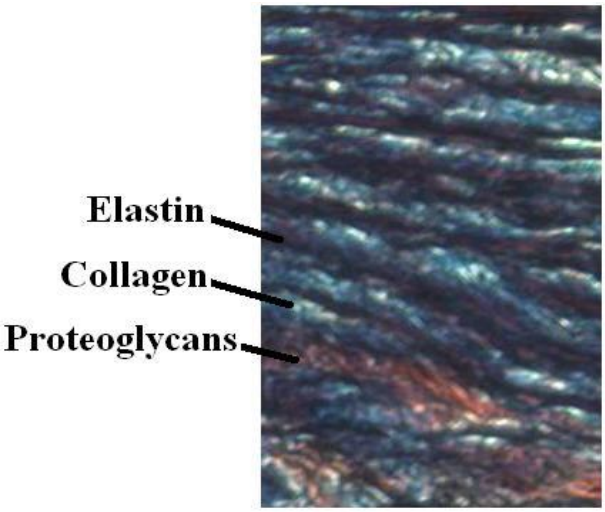

Figure 21- Histological examinations stained with modified Masson's trichrome protocol with Verhoeff's hematoxylin (elastin in dark blue, collagen in light blue and proteoglycans in red).

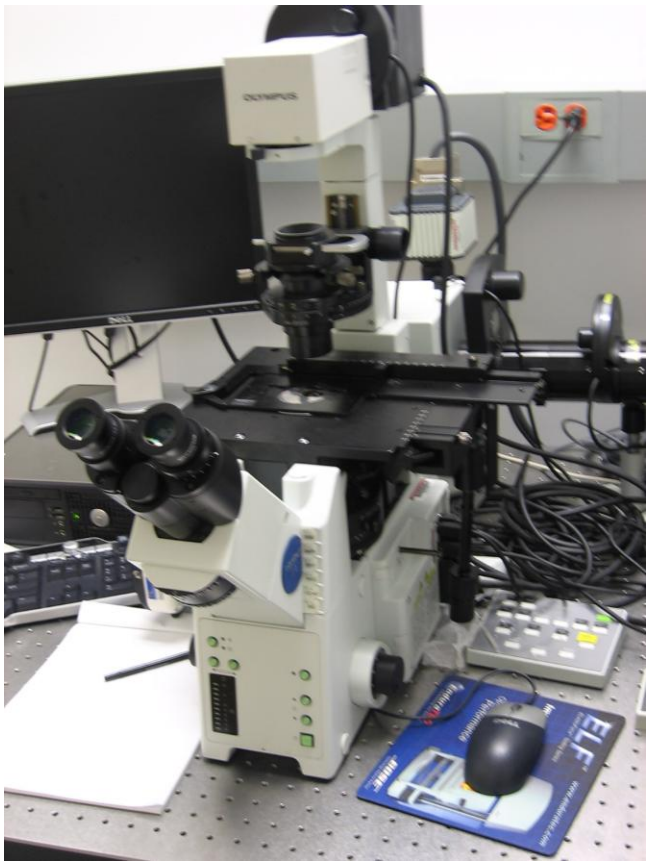

Figure 22- Olympus® IX81 microscope available in the Orthopaedic Mechanobiology Lab.

III.2.8. Microstructural Quantification

Fourier and Hough transformations were separately applied in order to analyze the images captured from histological sections in the $r-\theta$ plane. The Fourier and Hough methods analyze the images in frequency and spatial domains, respectively. Given the preferred direction of fibrillar structure around the aortic circumference, we consistently aligned the circumferential direction along the horizontal axis of all the extracted images. This allows gathering comparable image-processed results from multiple histology images which can then be averaged in order to obtain statistically-meaningful descriptors of the microstructural configurations.

Images of $750\times750\,pixel^2$ size were extracted from histology sections. Maintaining the same size for different images is required in order to ensure that the resulting Fourier- and Hough-transformed images are of the same size and can be averaged. Original color images were transformed into black and white images in order to highlight the elastin microstructure as dark fibrils within bright background. Computational software Matlab® *(The MathWorks Inc, Natick, MA)* was used to perform 2-dimensional (2D) Fourier transformation as well as Hough transformation on the images.

The result of applying 2D Fourier transformation to the image was an image of same size in which, the pixel intensity correlates to the variation in frequency along the relevant directions within the original image [Ballard 1982]. Figure 23 illustrates a sample histology image along with the corresponding Fourier image. On the Fourier image exemplified here, a higher intensity in the vertical direction indicates a higher frequency of variation in the original image, which could interchangeably be

interpreted as if the fibrillar structure is oriented more along the horizontal direction. The Fourier images were quantified by measuring the aspect ratio of the diameters (d_1 / d_2). The software ImageJ *(NIH, Bethesda, MD)* was used to estimate the length of each of the diameters. The higher the value of the aspect ratio, the more oriented the average fibrillar structure. The aspect ratio can nominally take values between 1 and infinity, which represents structures with no preferred direction and perfectly-oriented direction, respectively.

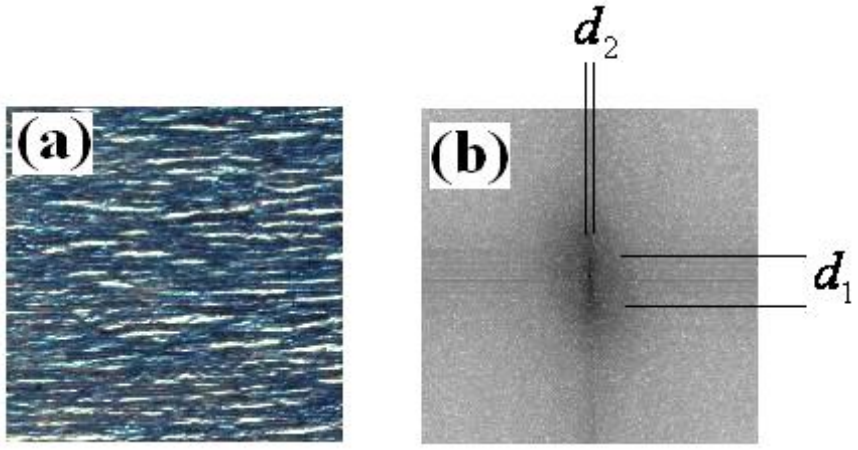

Figure 23- (a) Sample histology image, (b) Fourier transformation image. The diameter aspect ratio (d_1 / d_2) is measured on the Fourier image to quantify the directionality of histology microstructure.

The result of applying the Hough transformation to the histology image was an image in which, the pixel intensity shows whether a line segment can be detected at the corresponding spots in the histology image which is mapped with a polar coordinate system via a Hough transformation [Duda 1972; Shapiro 2001]. Figure 24(a) shows the Hough image of the histology sample in Fig. 23(a). To be computationally effective in estimating the average microstructural orientation, we sought to identify the most evident and observable line segments.

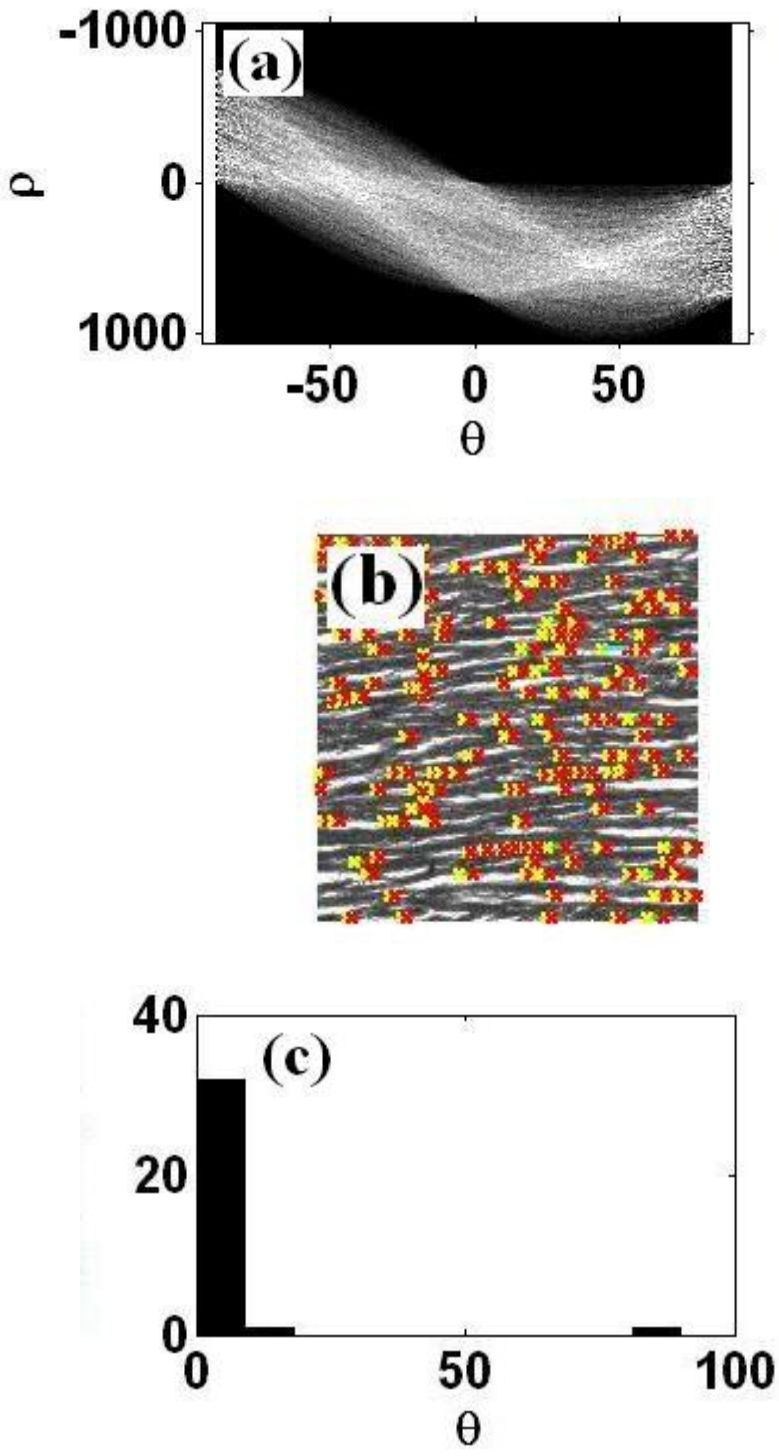

Figure 24- (a) Hough transformation of the histology image in Fig. 23(a), (b) Identification of line segments with highest intensity in Hough image, (c) Histogram of the orientation angle for identified line segments.

The MATLAB® software was used to detect the highest intensity points on the Hough image, and Fig. 24(b) illustrates the detected line segments on the histology image. In order to obtain a quantified measure of the structural orientation from the Hough method, we extracted the histogram of the angles which is shown in Fig. 24(c).

III.3. Results

III.3.1. Changes in Specimen Dimensions

Table 3 shows the average of the measurements on width and thickness of specimens from both native and elastin—isolated tissue when extended to stretches of 1.4 and 2.0 as well as after being recovered from each of the stretch levels. Width and thickness data are represented in Figs. 25 and 26, sorted for loading state and tissue type, respectively. Bars for data sets that are statistically different are connected with brackets.

Table 3- Measurements on width and thickness of tissue specimens at different states of loading.

		Unstretched	**Stretched** $\lambda = 1.4$	**Stretched** $\lambda = 2.0$	**Recovered** $\lambda = 1.4$	**Recovered** $\lambda = 2.0$
Native	**Width**	15.31	14.21	12.70	14.75	12.82
	Thickness	6.30	4.62	4.06	5.80	4.91
Elastin-	**Width**	14.83	12.97	--	13.60	--
Isolated	**Thickness**	3.58	2.98	--	3.32	--

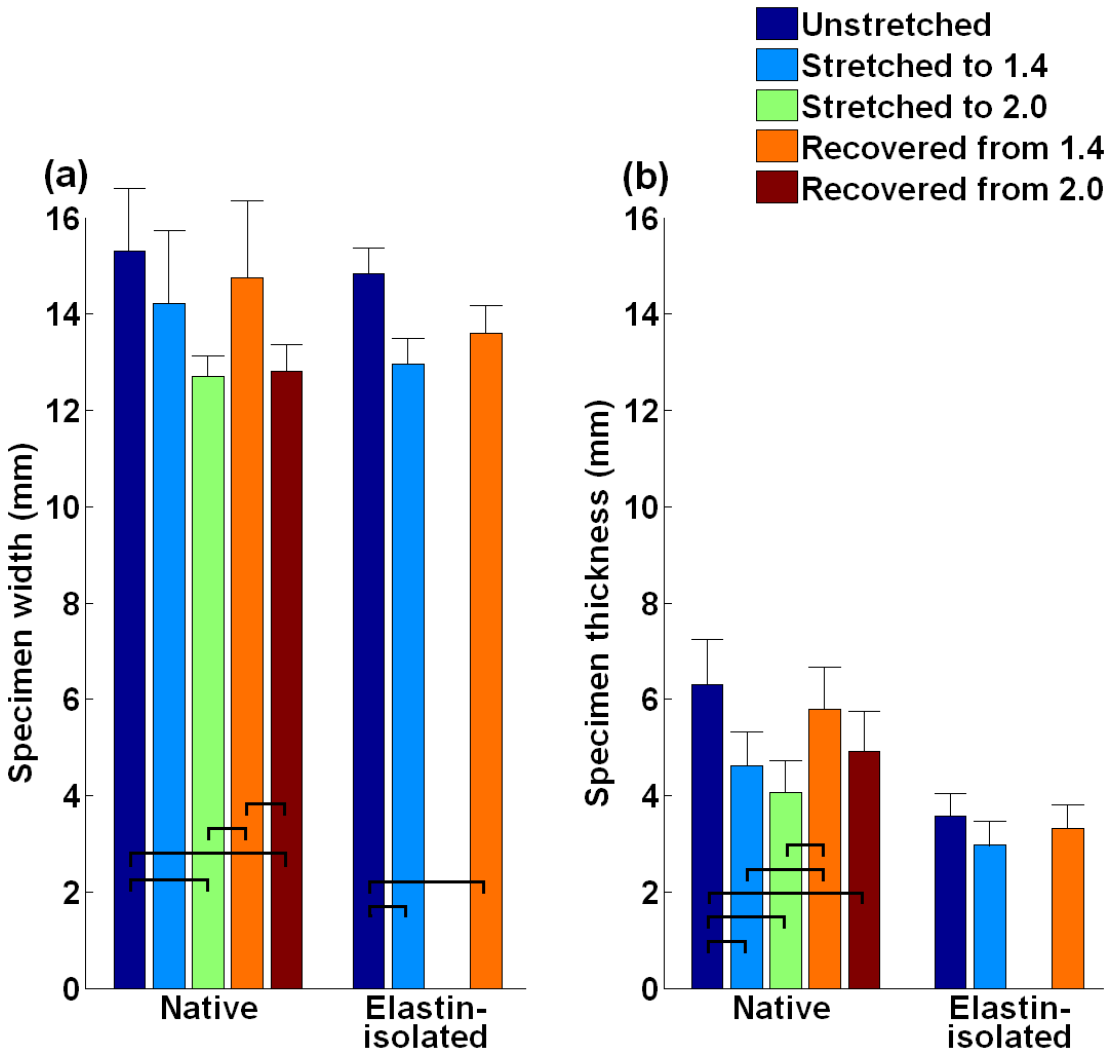

Figure 25- Change in (a)width, (b)thickness of native and elastin-isolated tissue specimens sorted for the loading state: (a)width, (b)thickness. Bars for data sets that are statistically different are connected with brackets.

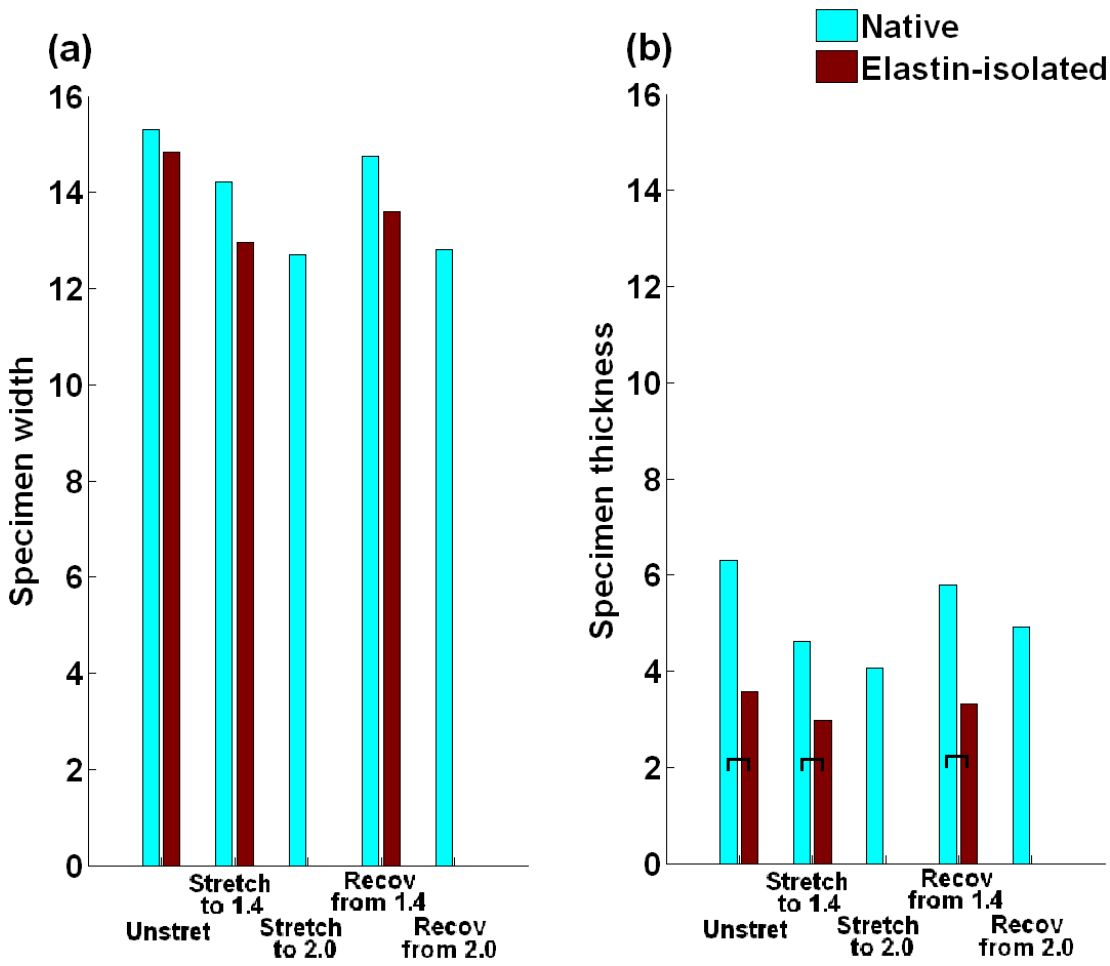

Figure 26- Change in (a)width, (b)thickness of specimens under different loading states sorted for naive and elastin-isolated tissues. Bars for data sets that are statistically different are connected with brackets.

One interesting observation is the inward bending of the specimens when released for deformation recovery, Fig. 27, likely due to higher recovery of deformation toward the inner layers of wall thickness, which have larger elastin density, when compared to outer layers.

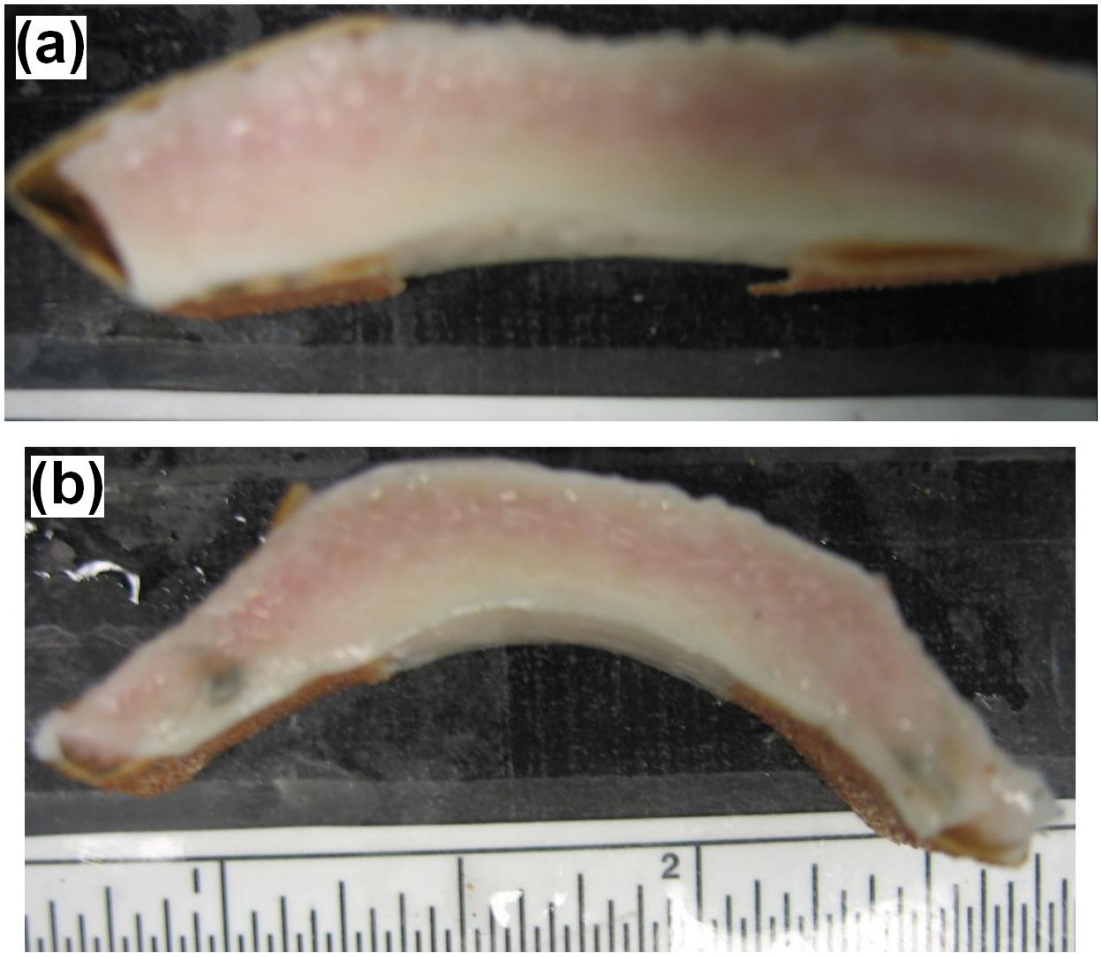

Figure 27- Side images of a tissue specimen (a) before loading, (b)after deformation recovery. Inward bending of the specimens after deformation recovery is likely due to the higher deformation recovery toward the inner layer caused by higher elastin density.

III.3.2. Macro-Scale Deformation Master Plots

Table 4 shows the width and thickness measurements on both native and elastin-isolated tissues at extension and recovery, normalized to measurements on the unstretched specimens. Data are also represented in the master plot of Fig. 28.

Table 4- Relative change in width and thickness of tissue specimens during loading and unloading normalized for measurements on unstretched specimens.

		Stretched $\lambda = 1.4$	Stretched $\lambda = 2.0$	Recovered $\lambda = 1.4$	Recovered $\lambda = 2.0$
Native	**Width**	0.91	0.85	0.95	0.86
	Thickness	0.72	0.66	0.90	0.80
Elastin-	**Width**	0.87	--	0.92	--
Isolated	**Thickness**	0.83	--	0.93	--

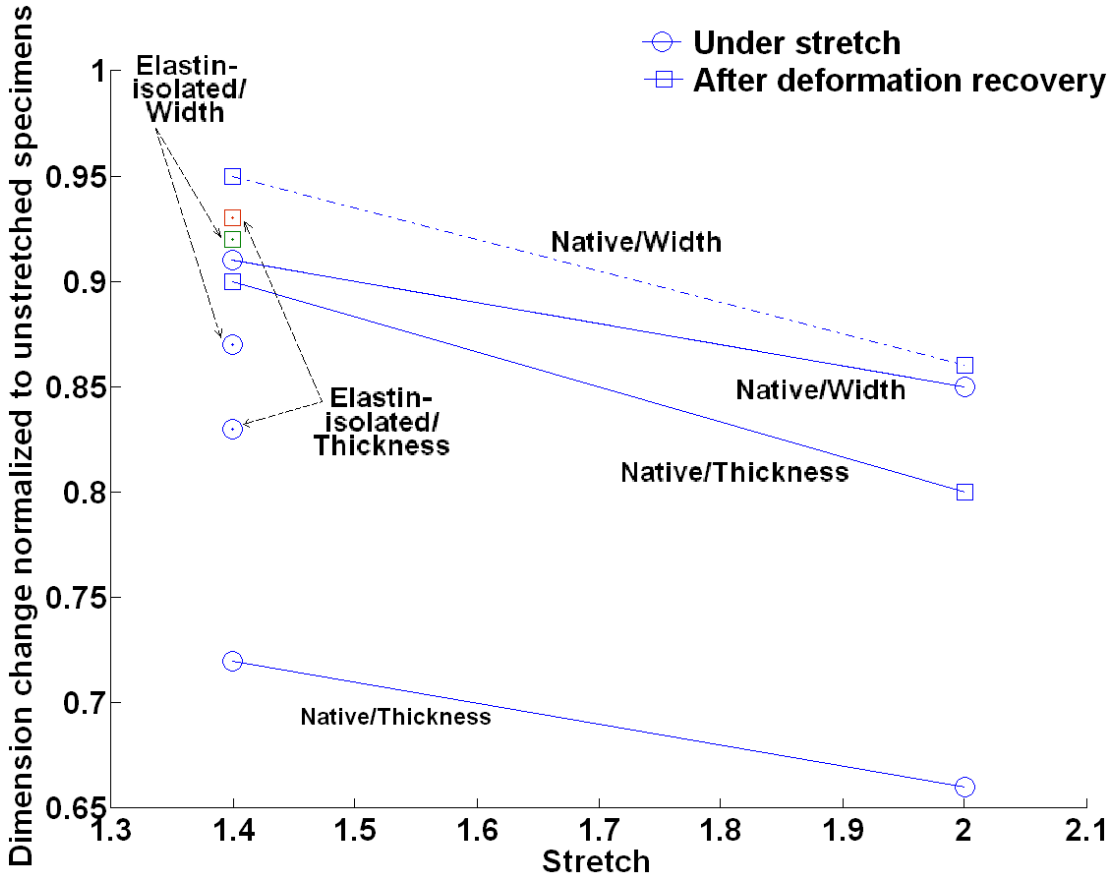

Figure 28- Master plot of relative change in width and thickness of tissue specimens during loading and unloading normalized to measurements on unstretched specimens.

III.3.3. Histological Observations at Different Sectioning Planes

One initial question to be answered before further histological examinations to be conducted is: What is the best plane for sectioning the tissue specimens to best capture the microstructural conformations? To answer this question, let's recall the polar coordinate system assumed on the aorta which transformed into the rectangular specimen as shown in Fig. 29. It should be noted however that the specimens extracted from the tissue do not usually stay in rectangular shape but bend around the z axis, Fig. 30, which is due to the fact that the specimens tend to recover the ring shape they used to posses originally before they cut from the aorta. Pilot histological examinations were initially performed on a few specimens sectioned in all three different planes, Fig. 31. Looking at images from different sectioning planes, it was observed that the r—θ plane gave the most accurate representation of the fibrillar structure in the tissue (see discussion section for more detailed description). The rest of the histological observations are therefore decided to be made in the r—θ plane.

Another interesting observation here was the change in the orientation of the fibrillar structure across the wall layer. Figure 32 shows histology images of specimens under no stretch, under stretch and after deformation recovery, sectioned in both the r—θ and r—z planes. It is observed that the dominant orientation of the fibrillar network toward the very inner layer (intima) is along the z direction and by moving toward the media layer it abruptly changes to be along the θ direction. This observation is particularly evident when simultaneously comparing histology at two different planes, Fig. 32.

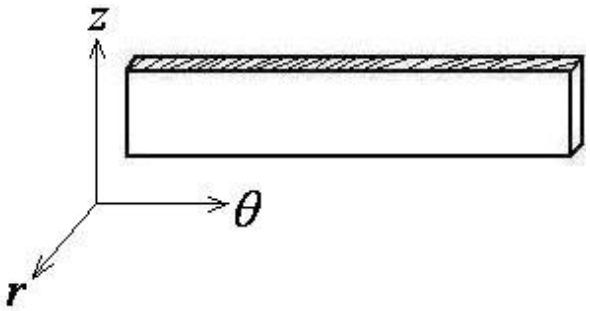

Figure 29- Polar coordinate system oriented on the circumferential rectangular specimen.

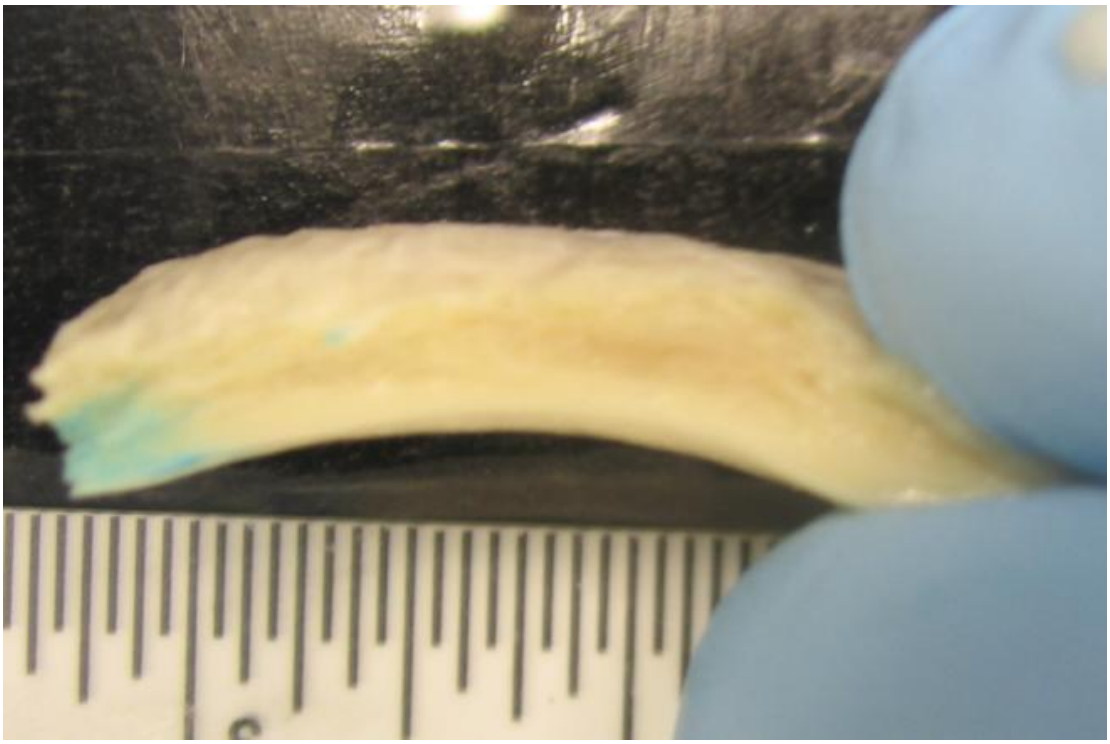

Figure 30- r—θ view of an unstretched specimen which shows the bending around the z axis. The specimens bend because they tend to go back to the ring shape they originally possessed before being cut from the aorta.

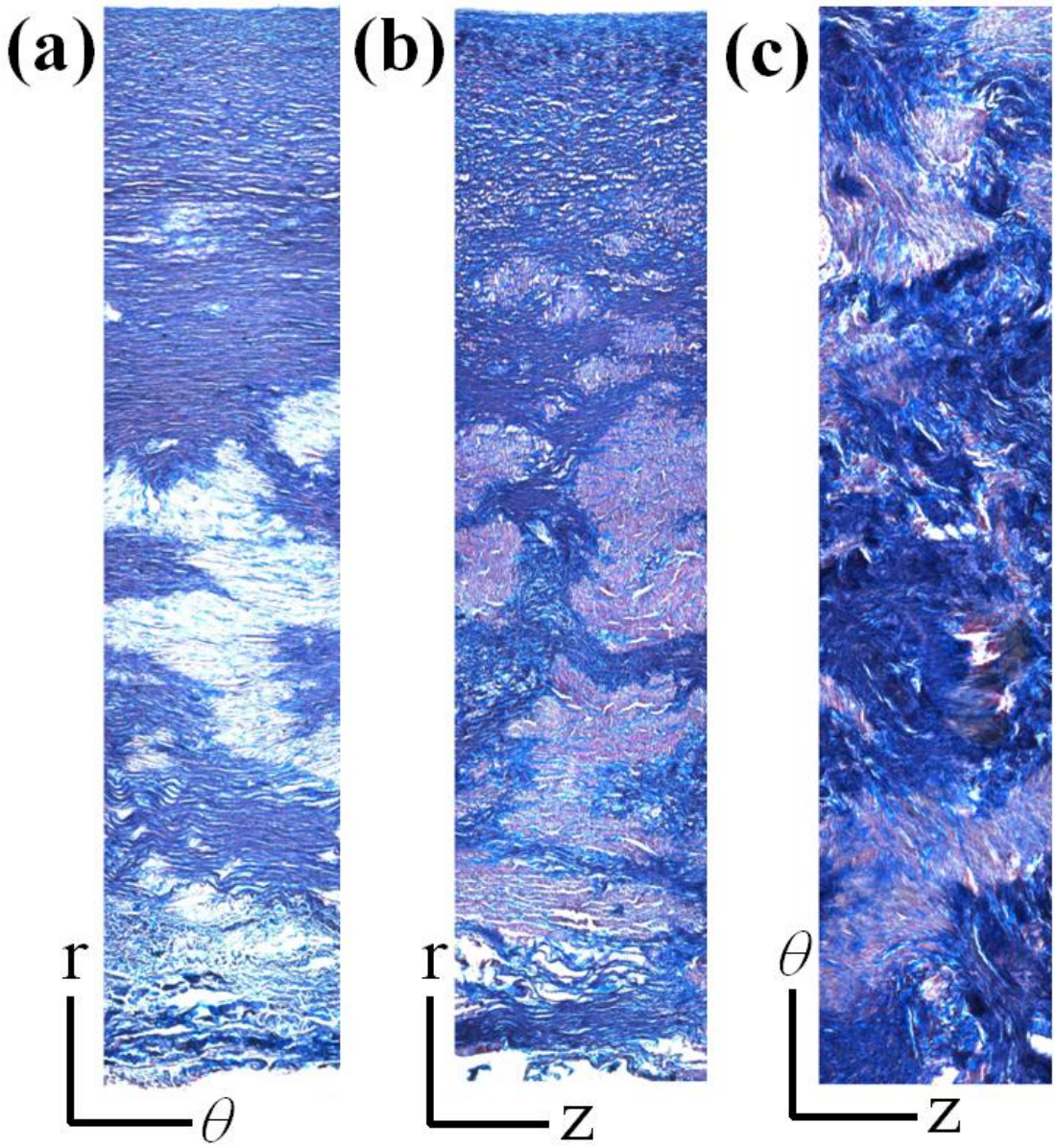

Figure 31- Panoramic views of histology images along three different sectioning planes. The r—θ plane is found to be the best plane to represent the fibrillar conformations in the media layer.

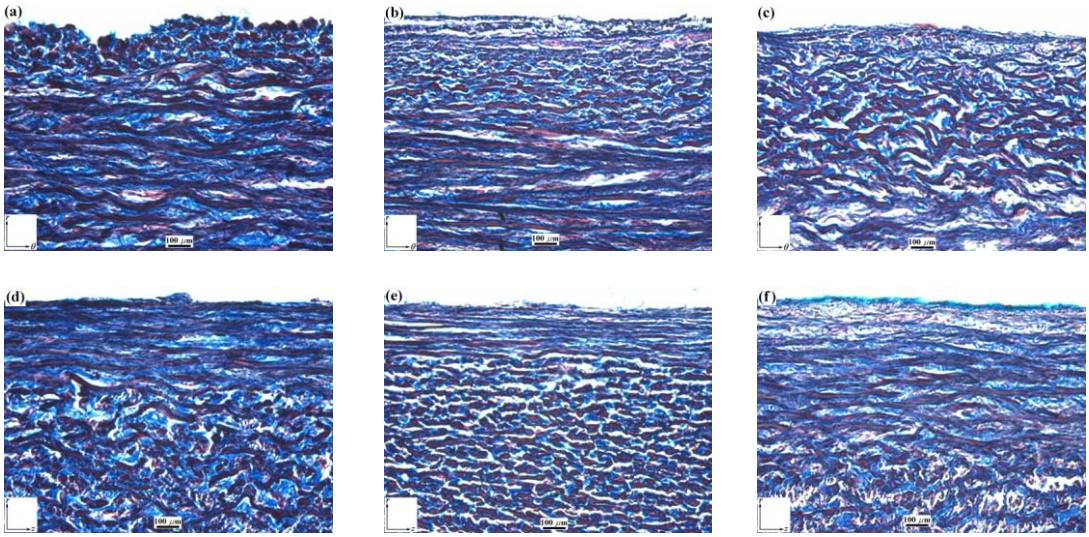

Figure 32- Histology images of aortic tissue (a) r—θ section of unstretched specimen, (b) r—θ section of specimen under stretch, (c) r—θ section of specimen after deformation recovery, (d) r—z section of unstretched specimen, (e) r—z section of specimen under stretch, (f) r—z section of specimen after deformation recovery.

III.3.4. Histological Observations on Microstructural Deformations

Particular consideration was paid to the change in microstructural configurations during tissue deformation by looking at histology images from unstretched specimens, specimens under stretch and specimens after deformation recovery. Given the expected difference between inner layers and outer layers of the wall thickness due to the higher density of elastin toward the inner layers, histological images are considered separately for each region. Figures 33 and 34 show the histology sections from respectively inner and outer regions of specimen from native tissue. In each figure, (a) shows the microstructure of the unstretched specimen, (b) shows the microstructure of the specimen stretched to 1.4, (c) shows the microstructure of the specimen after recovery from 1.4 stretch, (d) shows the microstructure of the

specimen stretched to 2.0 and (e) shows the microstructure of the specimen after recovery from 2.0 stretch.

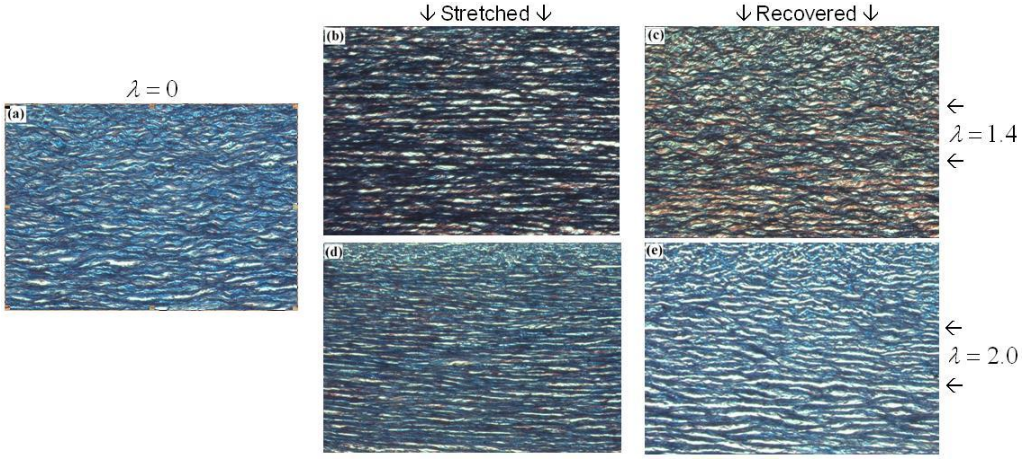

Figure 33- Histology of specimens from wall "inner" thickness of "native" tissue. (a) unloaded; (b) under 1.4 stretch; (c) under 2.0 stretch; (d) after recovery from 1.4 stretch; (e) after recovery from 2.0 stretch.

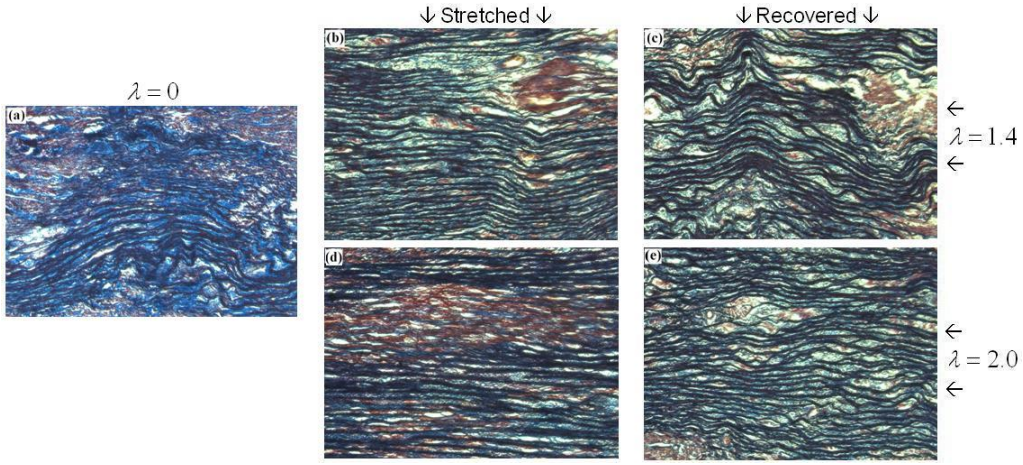

Figure 34- Histology of specimens from wall "outer" thickness of "native" tissue. (a) unloaded; (b) under 1.4 stretch; (c) under 2.0 stretch; (d) after recovery from 1.4 stretch; (e) after recovery from 2.0 stretch.

The specimens from elastin-isolated tissue were only examined under low stretch because loosing the collagen drastically decreases their strength and they were not able to tolerate higher stretch. Figures 35 and 36 show the histology sections from respectively inner and outer regions of specimen from elastin-isolated tissue. In each figure, (a) shows the microstructure of the unstretched specimen, (b) shows the microstructure of the specimen stretched to 1.4 and (c) shows the microstructure of the specimen after recovery from 1.4 stretch.

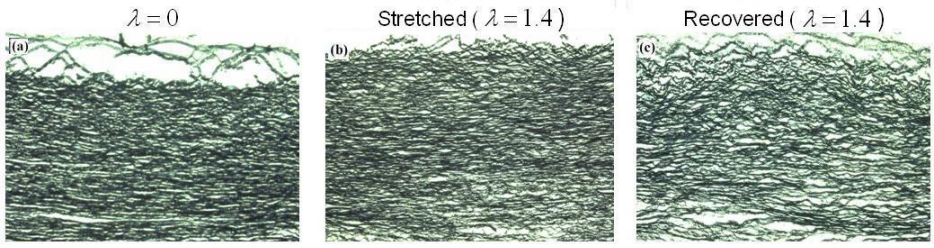

Figure 35- Histology of specimens from wall "inner" thickness of "elastin-isolated" tissue. (a) unloaded; (b) under 1.4 stretch; (c) under 2.0 stretch; (d) after recovery from 1.4 stretch; (e) after recovery from 2.0 stretch.

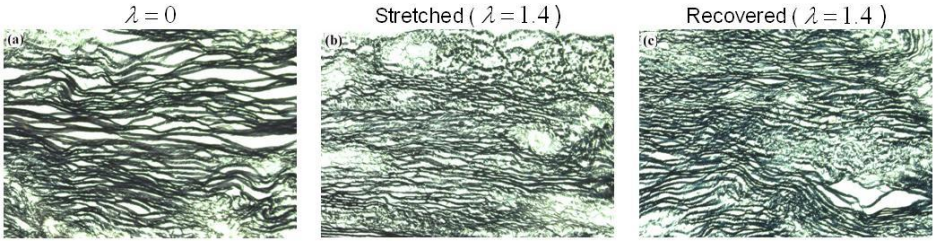

Figure 36- Histology of specimens from wall "inner" thickness of "elastin-isolated" tissue. (a) unloaded; (b) under 1.4 stretch; (c) under 2.0 stretch; (d) after recovery from 1.4 stretch; (e) after recovery from 2.0 stretch.

III.3.5. Frequency-Domain Characterization

The Fourier transformation was applied to histology images in order to extract a numerical measure of the fibrillar directionality. The method was applied to images from native and elastin-isolated specimens tested unstretched, under stretch and after recovery. The average measurements on the diameter aspect ratio made on the Fourier images are shown in Table 5. Larger values of aspect ratio indicate higher fibrillar directionality along the circumferential orientation. Figure 37 shows the bar graph of the data along with the standard deviation for each group, sorted in terms of the loading state. The same data are shown in Fig. 38 which are sorted in terms of tissue type/layer. Bars for data sets that are statistically different are connected with brackets.

Table 5- Average measurements of aspect ratio of the diameters along the main axes in 2-dimendional fast Fourier transform of the histology images obtained from different tissue specimens. Higher values of aspect ratio indicate more directionality levels of the fibrillar network in the circumferential direction (horizontal).

		Unstretched	**Stretched** $\lambda = 1.4$	**Stretched** $\lambda = 2.0$	**Recovered** $\lambda = 1.4$	**Recovered** $\lambda = 2.0$
Native	**Inner**	4.41	7.27	9.33	6.01	6.70
	Outer	2.70	5.61	8.56	4.46	5.63
Elastin-	**Inner**	6.51	7.24	--	6.71	--
Isolated	**Outer**	5.70	5.99	--	5.98	--

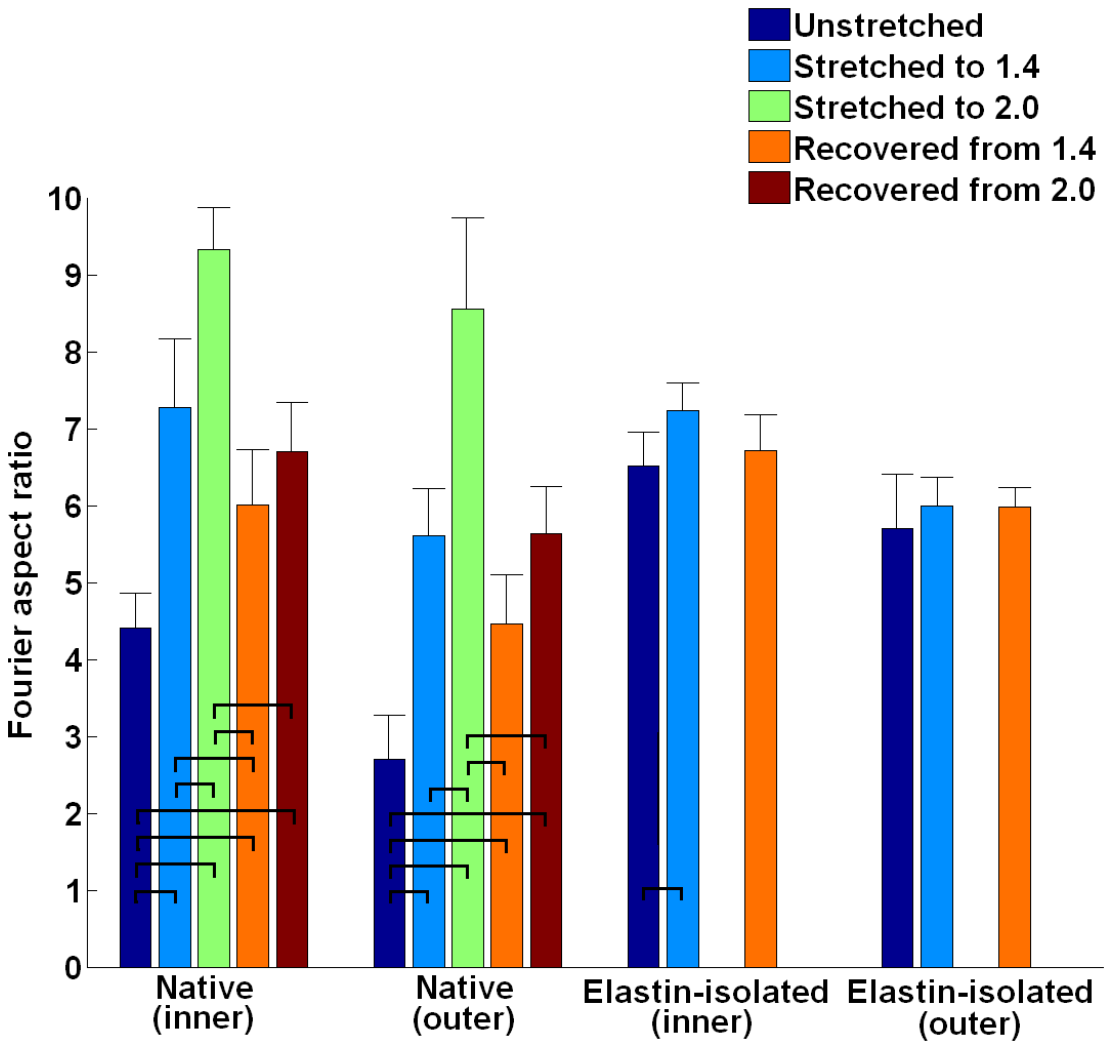

Figure 37- Aspect ratio of the main diameters on Fourier transform images from native and elastin-isolated tissue specimens sorted according to loading state. Bars for data sets that are statistically different are connected with brackets. Higher values of aspect ratio indicate more directionality levels of the fibrillar network in the circumferential direction (horizontal).

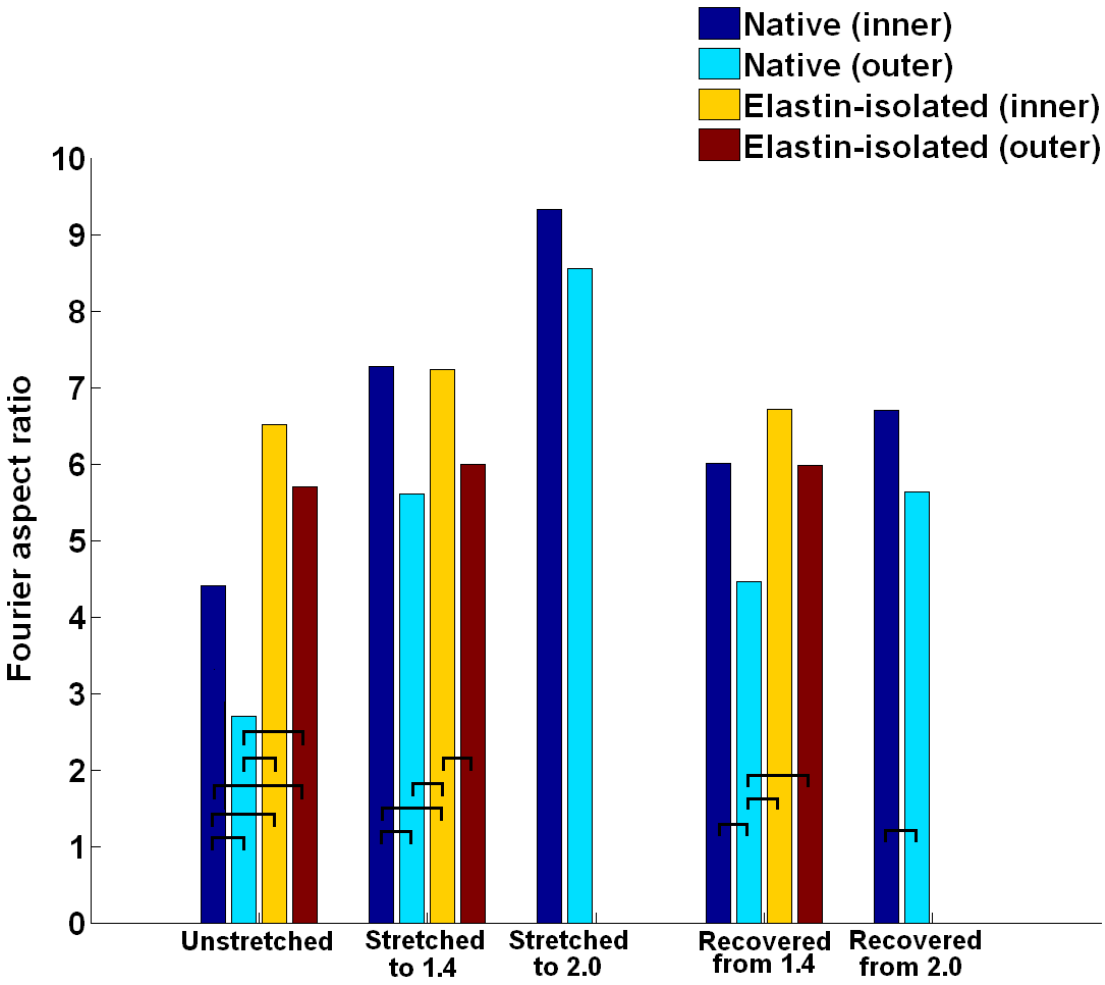

Figure 38- Aspect ratio of the main diameters on Fourier transform images from specimens under different loading states sorted for native and elastin-isolated tissues. Bars for data sets that are statistically different are connected with brackets. Higher values of aspect ratio indicate more directionality levels of the fibrillar network in the circumferential direction (horizontal).

III.3.6. Spatial-Domain Characterization

Figures 39 and 40 illustrate histology sections from 1/3 inner and outer wall thickness regions, obtained from unstretched specimens from native and elastin-isolated tissues, respectively, along with the histogram of fibrillar orientation calculated through Hough transformation of histology images. Similar results are shown in Figs. 41 through 46 for native and elastin-isolated tissue specimens under stretch and after deformation recovery.

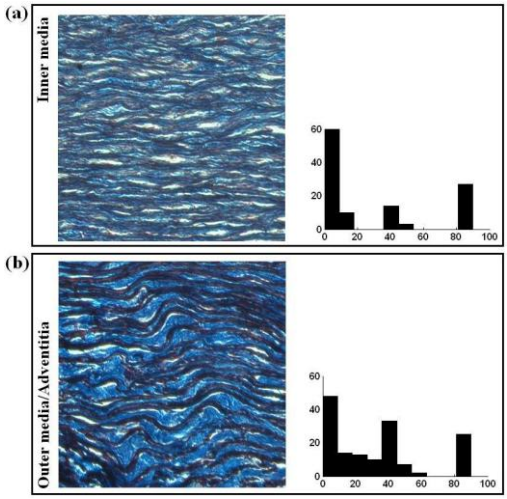

Figure 39- Histology sections of ‘native’ aortic tissue obtained from ‘unstretched’ samples, along with histogram of the fibrillar orientation angles: (a) inner wall, (b) outer wall.

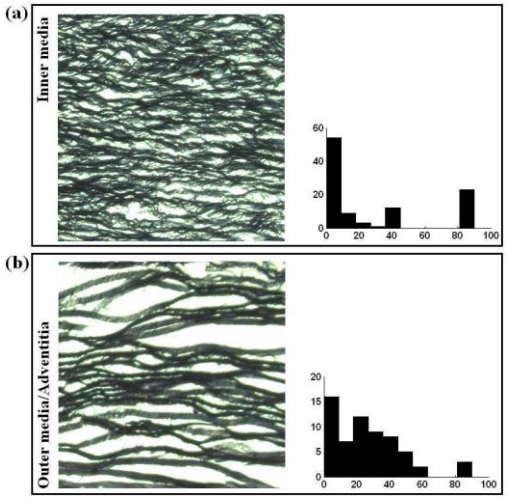

Figure 40- Histology sections of ‘elastin-isolated’ aortic tissue from ‘unstretched’ samples, along with histogram of the fibrillar orientation angles: (a) inner wall, (b) outer wall.

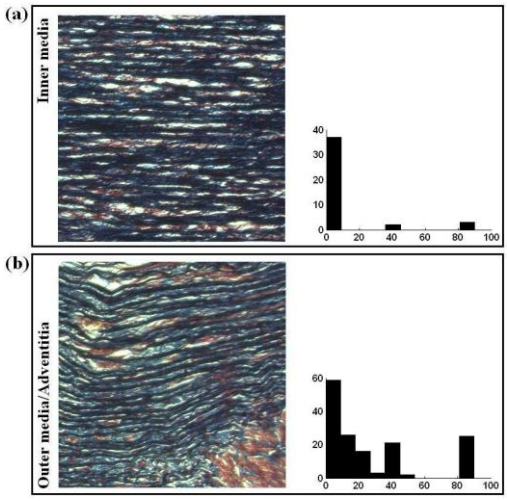

Figure 41- Histology sections of ‘native’ aortic tissue obtained from samples ‘stretched to $\lambda = 1.4$’, along with histogram of the fibrillar orientation angles: (a) inner wall, (b) outer wall.

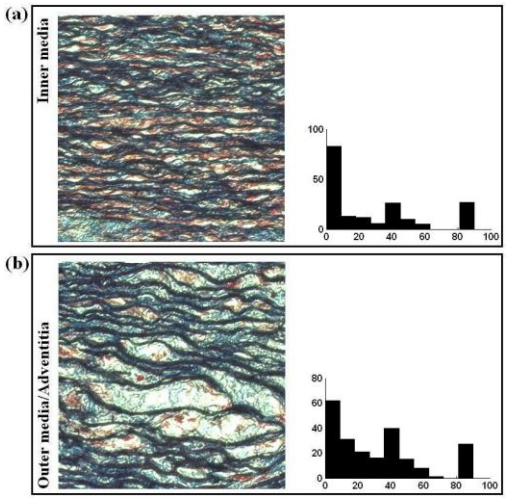

Figure 42- Histology sections of ‘native’ aortic tissue obtained from samples ‘recovered from $\lambda = 1.4$’, along with histogram of the fibrillar orientation angles: (a) inner wall, (b) outer wall.

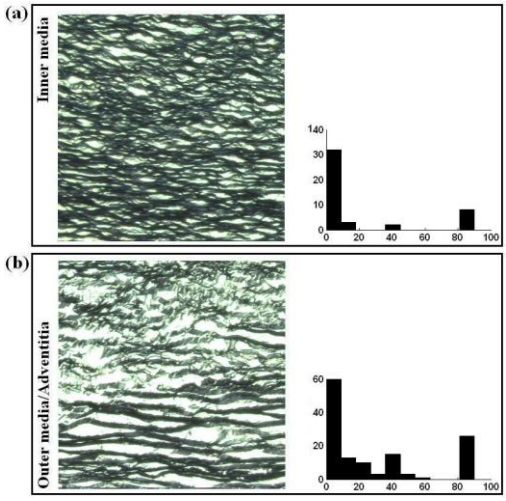

Figure 43- Histology sections of 'elastin-isolated' aortic tissue from samples 'stretched to $\lambda = 1.4$', along with histology of the fibrillar orientation angles: (a) inner wall, (b) outer wall.

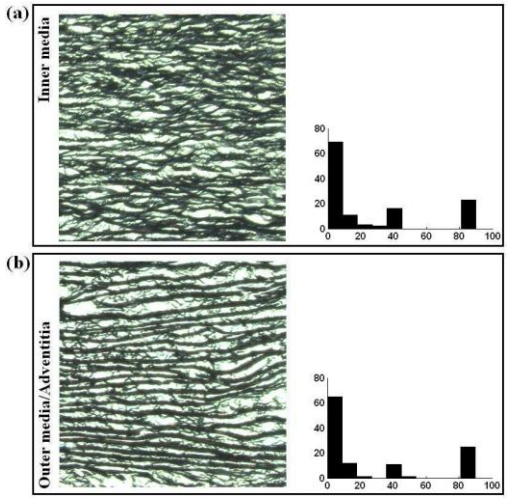

Figure 44- Histology sections of 'elastin-isolated' aortic tissue from samples 'recovered from $\lambda = 1.4$', along with histology of the fibrillar orientation angles: (a) inner wall, (b) outer wall.

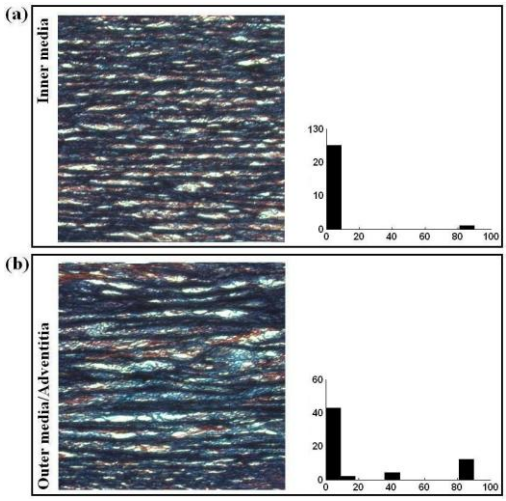

Figure 45- Histology sections of 'native' aortic tissue obtained from samples 'stretched to $\lambda = 2.0$', along with histology of the fibrillar orientation angles: (a) inner wall, (b) outer wall.

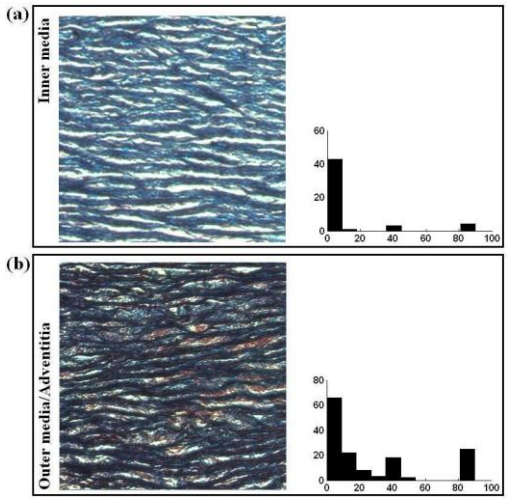

Figure 46- Histology sections of 'native' aortic tissue obtained from samples 'recovered from $\lambda = 2.0$', along with histology of the fibrillar orientation angles: (a) inner wall, (b) outer wall.

For better comparison of tissue microstructure in different cases, the angle distribution in each histogram is averaged to obtain a single value. The average of the averaged-angle measurements are shown in the Table 6 for different types of specimens. Figure 47 shows the bar graph of the data along with the standard deviation for each group, sorted in terms of the loading state. Same data are shown in Fig 48 which are sorted in terms of tissue type/layer. Bars for data sets that are statistically different are connected with brackets.

Table 6- Average of fibrillar orientation angles for different tissue samples. Angles were detected using Hough transformation of the histology images. Angles were measured with respect to the horizontal axis; the closer to 0 the angle is, the higher level of directionality the microstructure shows.

		Unstretched	**Stretched** $\lambda = 1.4$	**Stretched** $\lambda = 2.0$	**Recovered** $\lambda = 1.4$	**Recovered** $\lambda = 2.0$
Native	**Inner**	30.75°	9.55°	3.71°	28.71°	11.90°
	Outer	33.16°	27.77°	22.43°	31.57°	26.89°
Elastin-Isolated	**Inner**	28.99°	19.61°	--	26.20°	--
	Outer	26.77°	22.02°	--	23.35°	--

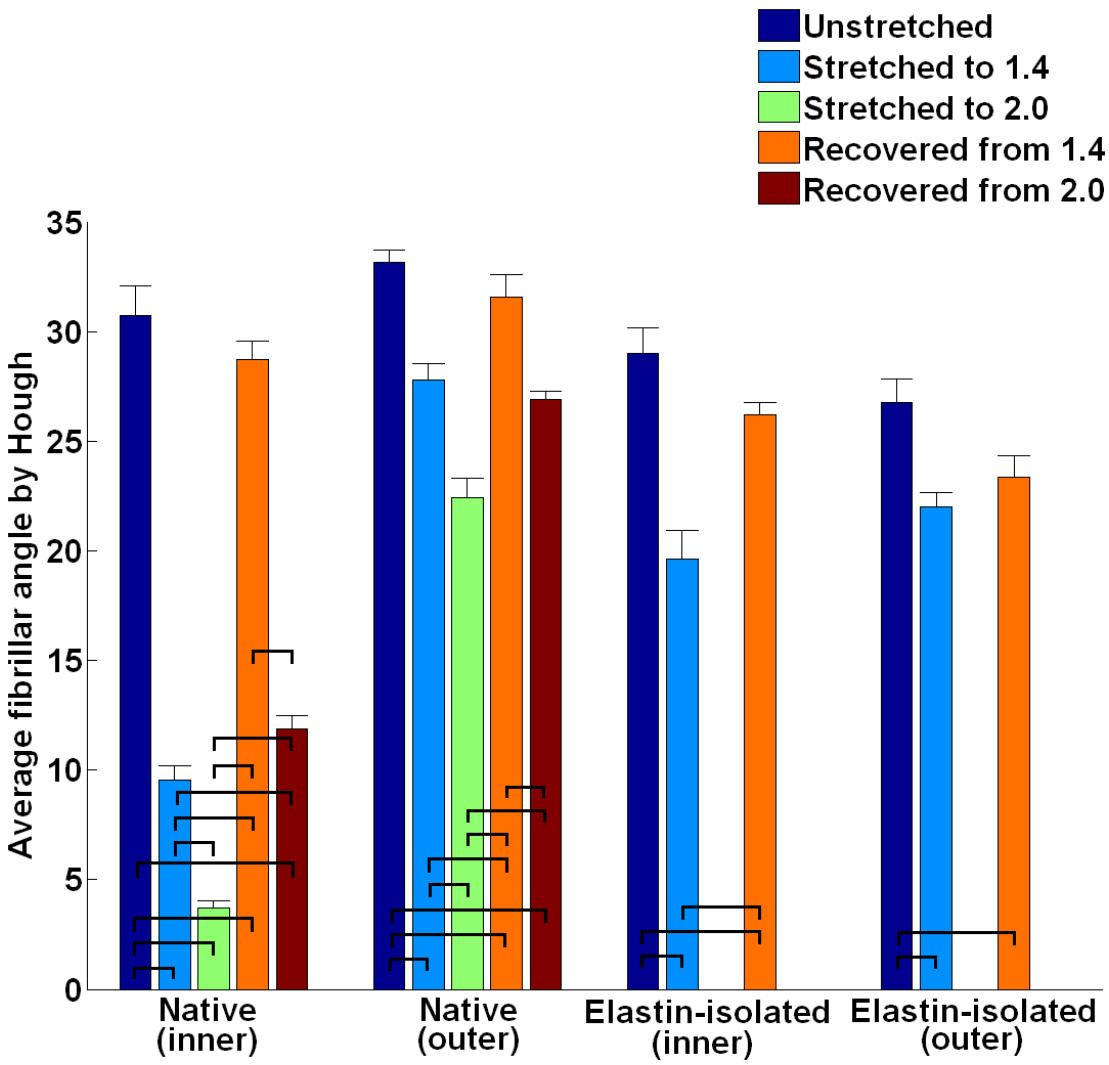

Figure 47- Average of fibrillar orientation angles -measured w.r.t. horizontal axis and using Hough method- from native and elastin-isolated tissue specimens sorted according to loading state. Bars for data sets that are statistically different are connected with brackets.

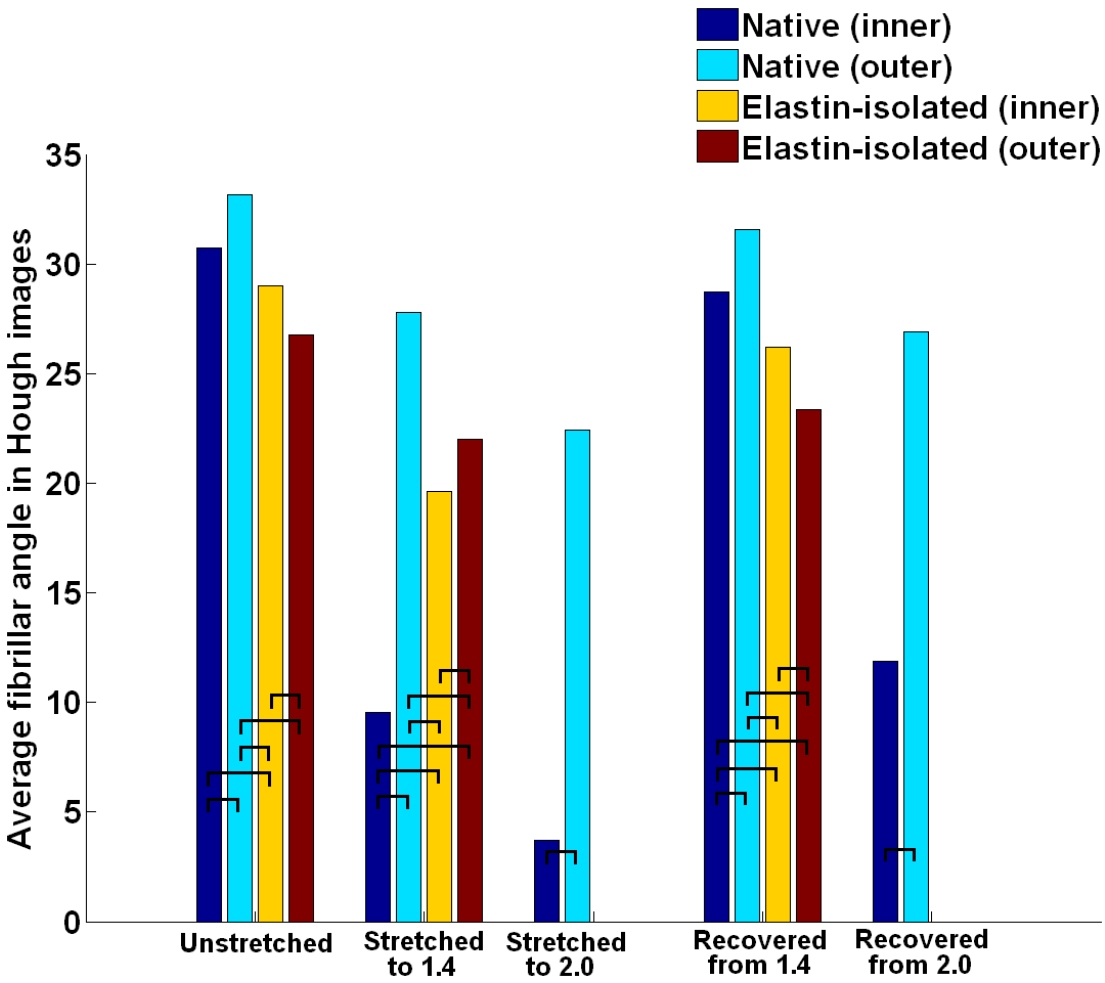

Figure 48- Average of fibrillar orientation angles -measured w.r.t. horizontal axis and using Hough method- from specimens under different loading states sorted according to native and elastin-isolated tissues. Bars for data sets that are statistically different are connected with brackets.

III.3.7. Microstructural Deformation Master Plots

In order to better compare the change in microstructural configurations between different tissue types and under different loading conditions, the measurements from tissue specimens under stretch and after deformation recovery are assessed relative to measurements on unstretched specimens. Tables 7 and 8 illustrate the relative data

based on the Fourier and Hough analyses, respectively. The Fourier data are normalized by dividing the aspect ratio of the specimens at each of the loading states by the aspect ratio of the unstretched specimens. The Hough data are normalized by subtracting the fibrillar angles of the unstretched specimens from the fibrillar angles of the specimens under stretch and after deformation recovery. The results are shown in so-called master plots for easy visualization under different conditions, Figs. 49 and 50 for Fourier and Hough data, respectively.

Table 7- Relative measurements of aspect ratio of the diameters along the main axes in 2-dimendional fast Fourier transform of the histology images obtained from different tissue specimens under stretch and after deformation recovery. Values are normalized with respect to measurements on unstretched specimens.

		Stretched $\lambda = 1.4$	Stretched $\lambda = 2.0$	Recovered $\lambda = 1.4$	Recovered $\lambda = 2.0$
Native	**Inner**	1.65	2.12	1.36	1.52
	Outer	2.08	3.17	1.65	2.09
Elastin-	**Inner**	1.11	--	1.03	--
Isolated	**Outer**	1.05	--	1.05	--

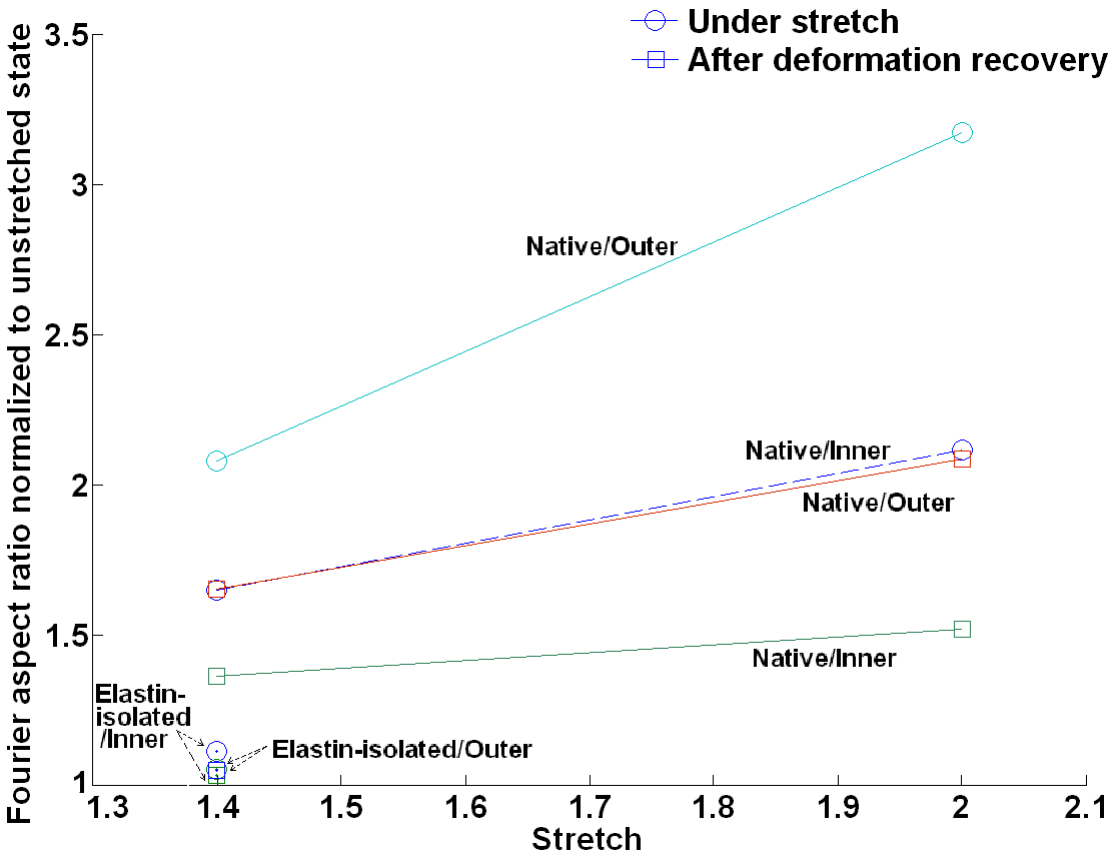

Figure 49- Master plot for the relative measurements of Fourier aspect ratio obtained from different tissue specimens under stretch and after deformation recovery. Values are normalized with respect to measurements on unstretched specimens.

Table 8- Relative fibrillar orientation angles of different tissue specimens obtained by Hough transformation. Values are subtracted from the measurements on unstretched specimens.

		Stretched $\lambda = 1.4$	Stretched $\lambda = 2.0$	Recovered $\lambda = 1.4$	Recovered $\lambda = 2.0$
Native	**Inner**	21.20°	27.04°	2.04°	18.85°
	Outer	5.39°	10.73°	1.59°	6.27°
Elastin-Isolated	**Inner**	9.38°	--	2.79°	--
	Outer	4.75°	--	3.42°	--

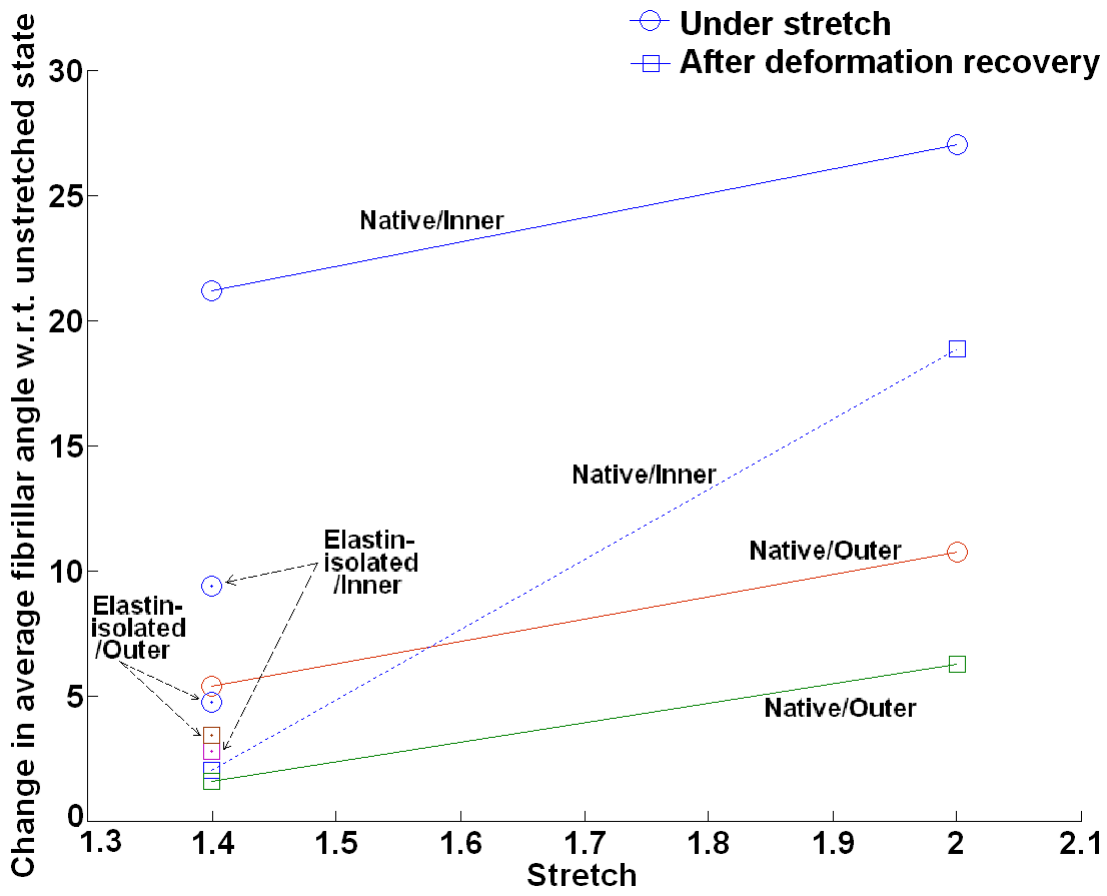

Figure 50- Master plots for the relative fibrillar orientation angles of different tissue specimens obtained by Hough transformation. Values are subtracted from the measurements on unstretched specimens.

III.4. Discussion

The main goal of this chapter was to investigate the microstructural changes in the tissue when it undergoes deformation. The tissue-scale and histological alterations were measured on the circumferential specimens from the native and elastin-isolated tissue specimens. In studying the tissue microstructural configurations, it should be noted that the potential effects from residual stress in the tissue are not considered. It is known that when unloaded, the aorta maintains the residual stress inside the wall thickness and it is released when the aorta is cut axially. In the protocol adapted here to prepare the circumferential specimens, the residual stress inside the ring piece is relieved when the ring is cut axially, and that causes the cut ring to open up into an arch. The argument here is that the microstructural conformations in the tissue might change first during the release of residual stress. Therefore, what we consider as an unstretched specimen might not really represent the microstructure of unstretched aortic tissue, but that of a residual stress-free tissue. Having in mind the distinction between stress-free and load-free aorta caused by the residual stress, the analysis in this chapter is valid for the stress-free aorta, and the stretched and deformation recovered states are evaluated relative to the unstretched state.

Based on the macro-scale examinations, the rather intuitive observation was that the circumferential specimens shrink along both thickness and width when they undergo stretch. It is found that there is a higher inverse correlation between the elongation of circumferential specimens and the shrinkage along the thickness than along the width, Table 4. After deformation recovery, the specimens show levels of permanent deformation in both thickness and width as neither recovers the initial

values for the unstretched specimen, Table 4. Particularly, the thickness shows higher permanent deformation than the width does, which can be attributed to the fact that the fibrillar network is oriented off angle from the circumferential direction and so the deformation of the fibers has a component in the width direction. Whereas in the thickness direction, the shrinkage effects are more from squeezing out of extracellular water during the stretching of the specimen. Comparing the native and extraccelular matrix specimens, Table 4 indicates that the elastin-isolated specimens show higher shrinkage in width and thickness as well as higher recovery, which can be due to higher relative contribution of elastic properties.

In the microstructural domain, first a remark should be made about the loading and unloading protocols adapted here to test the histology of specimens. Although it is sought to chemically fix the microstructure of the tissue specimens at different states during stretch and after deformation recovery, there would still be stress relaxation taking place inside the fixative agent. This is because the fixative agent takes few hours to fully take effect and meanwhile the specimens continue to stress-relax. As a result, what is captured here as the histology of tissue specimens under specific stretch or after deformation recovery might not be accurately quantified. However, given that the major part of our analysis is on a comparative basis between different loading states, the current protocol provides measures to describe the deformation mechanisms. The test protocols can be improved by developing better fixative agents so as to obtain a more efficient and quick method to fix the tissue microstructure and minimize the post-fixation relaxation.

The first step of our approach to study the microstructural changes was to find the best plane for sectioning the tissue specimens. Given the almost circumferential orientation of fibrillar network around the aorta, the r—z plane is intuitively not a proper sectioning plane since it is technically crossing the fibers and not lying along them. This is observed in Fig. 31(b) where the elastin network in the media layer appears as a set of elongated dots, supposedly the cross sections of the fibers. Now between the z—θ and r—θ planes which should supposedly describe the fibrillar network, Figs. 31(a) and 31(c) show that the r—θ plane is a better representative. One main reason that prevents the fibrillar structure from being shown in the z—θ section is that the circumferential specimens always tend to bend back into an arch segment, Fig. 30. Therefore, as much as it is tried to keep them straight during tissue fixation and paraffin embedding so as to obtain straight sections within the z—θ plane, the outcome nonetheless are sections partly within and partly crossing the z—θ plane. This is confirmed by Fig. 31(c) which shows network of detached bundles.

As discussed, the r—θ sections best represent the fibrillar structure in the media layer, but at the same time, the r—θ sections show cross-sectional microstructure in the intima layer, Fig. 32(a). Looking at the similar r—z sections, the pattern is almost reversed as they show cross-sectioning in the media which transits into fibrillar orientation toward the intima, Fig. 32(d). Observations in both planes suggest that the dominant orientation of the fibers is changing from circumferential within the media layer into axial in the intima layer. The dominant circumferential orientation of the fibrillar network in the aortic wall media has long been known and attributed to strengthening the tissue in the circumferential orientation where the

maximum stress is experienced due to blood pressure-induced dilation of the aorta. However, longitudinal orientation of the fibrillar structure in the intimal layer has hardly been noticed before. To the best of the author's knowledge, it is the first time that such revealing histology images are obtained to highlight the change in orientation of the fibrillar network when moving from the media to the intima layer. Similar to a physiologically-sound rationale for maximizing the strength of the aortic tissue at the wall media layer when circumferential stress is the largest wall stress, the longitudinal orientation of the fibrillar network in the intima regions can be attributed to increasing tissue strength against maximum stress from shear force caused by blood flow. The histology results further show how the microstructure changes when tissue-scale deformations take place, Figs. 32(a) through 32(f). Given that it is extremely thin and that it does not have any measurable effects in the biomechanics of the tissue in the circumferential direction, the endothelial layer is not considered in microstructural studying. The r—θ histology of the released specimen, Fig. 32(a), shows a relatively organized set of crimping elastin fibrils, and they turn into a more oriented elastin network with drastically less crimping when the specimen is extended, Fig. 32(b). For the specimens recovered from extension, Fig. 32(c), the microstructure takes a highly disorganized pattern with an increasing degree of crimping, higher than that in the initial released specimen. However, although it is already figured out that the histological quantification should rely on r—θ histology sections, observations in r—z sections still provide some qualitative understanding of microstructural deformations. For instance, the specimen in extension shows a uniform pattern of small cross sections, Fig. 32(e), compared to larger clots of

(inclined) cross sections in released samples, Fig. 18(d), which indicates that fibrils get thinner under stretch.

In examining the microstructural changes in the tissue, given that the density of elastin is much higher toward the inner media compared to the outer media/adventitia, histological examinations were separately conducted on 1/3 inner wall thickness and 1/3 outer wall thickness. The observations on inner media are expected to be more representative of elastin biomechanics.

The histological examinations of the tissue specimens under no stretch, stretches of 1.4 and 2.0 and after deformation recovery from stretches 1.4 and 2.0 shed light on morphological mechanisms of deformation at the microstructural scale. The networks in the wall inner layer show straighter fibrillar structure under stretch, which partly returns to the crimping structure after deformation recovery, Fig. 33. The fibrillar network in the wall outer layer shows a more undulated network, Fig. 34, which is hypothetically due to the sparser extracellular matrix, which allows free configuration of the network. Similar patterns are seen for elastin-isolated tissue, Figs. 35 and 36, with higher levels of crimping in the elastin network, which again could be due to the sparser extracellular matrix after digesting the non-elastin components.

Two image-based methods were used to quantify the histological observations, the Fourier method in frequency domain and the Hough method in spatial domain. Technically, the two methods complement and verify each other. Except in very few cases, the findings from both Fourier and Hough methods were

consistent in quantifying the level of microstructural directionality during tissue stretch and recovery, Tables 7 and 8.

The Fourier method indicates that for the inner part of the native tissue, the microstructure gets straightened by 65% and 112% when loaded up to 1.4 and 2.0 stretch, respectively, 29% and 60% of which is restored after deformation recovery, respectively, Table 7. Similarly for the outer region of the native tissue, while the microstructure is less organized, Table 5, but on comparative basis, the fibers get more straightened when loaded to 1.4 and 2.0 stretch, 108% and 217% respectively, 43% and 108% of which are restored after deformation recovery, respectively. The lower deformation recovery in the outer regions is likely due to the lower density of elastin (the most elastic component of the tissue) within the outer regions. Furthermore, it is seen that higher permanent deformation (lower deformation recovery) is seen at a stretch of 2.0 which could be caused by damages of elastin network which makes the network lose integrity and does not recover the deformation. The occurrence of this phenomenon is more plausible given the very low ultimate stretch of elastin of about 1.1. Looking at the Fourier measurement for the elastin-isolated tissue, Table 7, one notices that the inner part of the elastin-isolated tissue is straightened by 11% when stretched to 1.4, 8% of which is restored after deformation recovery. This is presumably due to fact that the elastin-isolated tissue is drastically weaker and stretching the specimen to 1.4 stretch can apply very high loads on the elastin network causing more damage and fracture to the network. Looking at the outer region, the directionality increases by only 5% almost none of

which is restored after deformation recovery. The observation is similar for the lower stretch, but a higher damage level is expected at stretch 2.0.

Similar qualitative results are obtained based on the Hough method, although they are slightly different in quantitative measures. Comparing the histology of unstretched native and elastin-isolated tissue samples -Figs 39 and 40, respectively- it is found that elastin-isolated tissues, on average, show less directionality in the microstructural networks. The reason could be the larger number of degrees of freedom for elastin networks in moving and reconfiguring within the vacant extracellular matrix after the rest of the components are digested out of the matrix of the treated tissues. Studying the microstructural alterations in native samples under increasing stretch is possible with the aid of Figs. 39(a), 41(a) and 45(a). The figures show that both in the inner and the outer media, stretching the tissue sample has a direct effect on the microstructure by straightening the fibers. Table 6 shows that the average angles of the fibrillar elastin in the inner media for unstretched, 1.4 stretched and 2.0 stretched samples are 30.75°, 9.55° and 3.71°, respectively. A similar pattern is seen for the elastin fibrillar orientation in the outer media, part (b) of the same figures. Considering the effects of sample stretching on the microstructural alterations in the elastin-isolated tissue, Figs. 39 and 43, it is observed that the elastin network tends to orient along the direction of applied stretch. However, due to fragile nature of elastin-isolated tissue specimens (primarily due to inexistence of collagen fibrils), we were unable to observe the tissue microstructure when stretched to 2.0 as the specimen's microstructure was already damaged. Less intuitive observations can be made on the microstructure of recovered tissue specimens after being released from

stretch. Figs. 42 and 44 show the microstructure of native and elastin-isolated tissue specimens, respectively, recovered from 1.4 stretch; where Fig. 45 illustrates that of a native tissue recovered from 2.0 stretch. For specimens recovered from 1.4 stretch, it is found that a large portion of the microstructural deformation is recovered, but yet the microstructure does not fully recover to the initial conformation in the unstretched tissue specimen. This observation suggests that while the aortic tissue biomechanics is primarily (visco)elastic, it nonetheless possesses a certain level of plasticity. Furthermore, when recovered from 2.0 stretch, an even lower level of microstructural restoration occurs; perhaps due to microstructure damage and dislocation. Table 8 summarizes the change in microstructure angular orientation under stretch and deformation recovery. For the inner part of the native tissue, there is a 21.20° and 27.04° change in angle for stretch at 1.4 and 2.0, respectively, of which 90.37% and 30.29% is restored after deformation recovery, which shows much higher deformation recovery for lower tissue stretch. For the outer region, a 5.39° and 10.73° change is observed in the microstructure angle when subjected to 1.4 and 2.0 stretch respectively, of which 70.50% and 41.57% is restored after deformation recovery, respectively. The elastin-isolated tissue shows a 9.38° and 4.75° change in microstructure angle under 1.4 stretch, of which 70.26% and 28.00% is restored after deformation recovery, respectively.

There are a few sources of inaccuracy in the quantitative results obtained from the histology images. Firstly, the histology images used for the analysis were prepared such that the horizontal axis on the image coincides with the circumferential direction of the tissue. However, image setting was performed manually and could be

prone to subjective errors. Given the sensitivity of the Fourier and Hough techniques with respect to image orientation, the interpretations of the quantification results could be slightly off depending on the accuracy of the initial image alignment. Secondly, although the primary fibrillar structure in the histology images belongs to elastin, the existence of other components in the images impedes the exact identification of the elastin fibrillar network. Therefore, the results might be contaminated with data detected on non-elastin regions of the image. In particular, some of the unexpected observations in the Hough results —such as a high density of fibrillar angle at 90° for stretched samples— could be due to detection of localized line edges on random particles and sub-microstructure in the images which should not technically be counted as fibrillar orientation of the elastin network. This issue can be addressed by developing homegrown computer codes, instead of using commercial ones, to specifically detect items of interest and reject others as noise. Thirdly, in order for the methods to yield sensible interpretations on the microstructural configurations, each selected image window should contain uniform and similar patterns of microstructural conformations; otherwise, the heterogeneity in the microstructural features will be lost through an averaged single outcome. Therefore, selecting a proper window size for image analysis purposes and a careful utilization of the techniques are crucial for obtaining meaningful and accurate readings. We believe that some of the discrepancies in interpreting the results obtained through the Fourier and Hough methods, comparing Tables 7 and 8, are due to adverse effects of the locality of the methods.

A quantification of the Fourier results can also suffer from subjectivity. As outlined in the methodology section above, we identify the high-intensity region in the Fourier images and use ImageJ to measure the length of the main axes; whereby the entire procedure is subject to human inaccuracy. An item of future work could be enhancing the current computer code to automatically extract quantified features from Fourier transformation images.

IV. VISCOELASTIC MECHANICAL TESTING

Elucidating how the biomechanics is affected by hydration in soft biological tissues is critical for understanding the potential effects of diseases where the tissue extracellular matrix (ECM) is altered. The ability to control the ECM water content is necessary for studying hydration-dependent tissue mechanics and for minimizing confounding effects caused by differences in tissue water content among specimens. In this section, we describe an approach to adjust and maintain the water content using a two-stage hydration technique, in order to overcome unique challenges faced in the mechanical testing of biological tissues. As in the rest of this study, bovine aortic tissue was used to illustrate the approach. A liquid phase approach using polyethylene glycol (PEG) solutions allowed for efficient initial adjustment of tissue hydration. This was followed by a vapor phase approach using a humidity chamber for maintaining a stable water content for 45 minutes. Incubation in PEG solution brought the bovine aortic tissue samples to equilibrium water content in approximately 6 hours, much more efficiently than using a humidity chamber alone. Characteristic relationships between tissue water content and PEG concentration as well as relative humidity were obtained. It was found that PEG concentrations ranging from 0-40% had an inverse relationship with tissue water content ranging from 80-380%, which corresponded to relative humidities between 53-99%.

IV.1. Background

Quantifying hydration effects is an important, but sometimes overlooked, aspect of studying mechanical properties and material behavior in synthetic and biological materials [Koplik 1985; Rubio 1989; Cieplak 1990; He 1992; Dougherty 1998; Bru 2006]. Various theoretical and experimental methods have been utilized to characterize the material-water interaction and swelling properties of different materials. Simulation tools have been applied to some applications of studying hydration behavior in biological tissues. Molecular dynamics simulations have been used to predict the hydration of a tissue's protein constituents and verify experimental results [Mogilner 2002; Scharnagl 2005; Ravikumar 2008; Orecchini 2009].

The ability of existing theoretical methods to describe solid-fluid interaction [Koplik 1985; Kardar 1986; Kessler 1991] diminishes when the complexity of a material's structure increases. The majority of biological soft tissues possess structural networks with variable pore size and crosslinking, and are composed of different extracellular matrix (ECM) protein constituents [Humphrey 2002]. Soft tissue properties rely largely on how these structural constituents interact with each other and with the interstitial fluid. Mechanical behaviors of soft biological tissues have been universally linked to ECM hydration both in vivo and in vitro [Grigera 1979; Setton 1994; Buckwalter 1995; Adams 1996; Kerin 1998; Lillie 1998; Talman 2001; Taylor 2004; Guo 2007; Gainaru 2009]. For instance, the viscoelastic behavior of aortic tissue during normal operation of the cardiovascular system is highly dependent on proper hydration of vascular elastin [Gosline 1979; Silver 1989; Guo 2007]. Ramifications of improper tissue hydration include the disruption of tissue

homeostasis and can be a root cause of various diseases, and present a concern for biologists, clinicians, and bioengineers who work on therapeutic measures or synthetic substitutes [Maroudas 1985; Wexler 1985; Han 2001; Rochette 2005; Harley 2007]. Dehydration of elastin causes a transition in material behavior from ductile to brittle in synthetic polymers [Kausch 1976; Hertzberg 1980] and it is found that only 10% loss of water, for example, causes significant stiffening of elastin [Taylor 2004]. Blockage of fluid motion by binding of elastin to cholesterol esters or by alteration in glycosaminoglycans, both of which may occur during atherosclerosis, causes stiffening of arterial tissue [Lillie 1990; Lovekamp 2006]. Loss of water also reduces elastin's fatigue resistance to cyclic loading, particularly at high frequency caused by post-stenotic resonance [Rodbard 1967; Trillo 1975]. It has been further shown that alterations in tissue hydration produce comparable changes in elastin's viscoelastic behavior as does an alteration in temperature [Lillie 1990].

Reported experimental soft tissue mechanics studies are generally concerned about maintaining hydration to avoid drying out samples, but typically employ methods that either do not allow control over specific hydration levels or induce suprahydration. For cartilage tissues, samples are often fully submersed in saline solutions to study swelling and mechanical behavior under external loading [Grodzinsky 1981; Lehner 1989; Kerin 1998; Torzilli 1999]. To maintain corneal samples fully hydrated for studying biomechanical contributions of the epithelium, tissues have been incubated in Optisol, a corneal preservation medium used for transplantation purposes [Elsheikh 2008]. Taylor et al. examined avian keratinous tissue samples submerged in $22^{\circ}C$ deionized water in order to mimic a full hydration

environment [Taylor 2004]. Samples from lumbar spine are sometimes hydrated by incubating them in a saline water bath for several hours before testing [Pflaster 1997; Costi 2002] or infusing saline solutions into spinal discs to enhance consistency in the measured mechanical behavior [Huber 2007]. Hydration of heart valve cusp tissue was shown to depend on the incubation solution including porcine blood, Hanks solution (physiologic saline), phosphate buffered saline and dextran solutions over the course of an hour [Talman 2001].

Considering that biological tissues exist in vivo under conditions that are less than fully swelled, a procedure to maintain steady tissue hydration during in vitro mechanical testing would be useful for studying more physiologically-relevant behaviors. Likewise, experimental determination of the role of hydration-dependent changes in tissue mechanics requires the capability to adjust a tissue over a range of partial hydration levels. Both published reports [Ferrans 1978; Hopwood 1985] and our own experiences indicate that different laboratory procedures can have a marked influence in tissue hydration. Thus, in order for valid comparisons to be made across different in vitro tests, standardized tissue preparation and sample hydration levels need to be implemented. Intrafibrillar water is believed to be primarily involved with stiffening of protein molecules [Lillie 1990; Lillie 1996], while interfibrillar water is thought to play a greater role in solid-fluid interactions. Water content is typically used as a quantitative measure of intrafibrillar and interfibrillar water to represent total tissue hydration [Wasano 1983; Lillie 1996].

Given the potential for biomaterials to degrade, together with often lengthy procedures in experimental set-up, controlling the water content of a sample becomes

a time-sensitive process. Efficient and reproducible methods are needed to ensure integrity of the sample and the test. Several studies have reported methods whose goals were to generate specific hydration levels in tissue samples, primarily by relying on generating osmotic pressure. Sequential incubation of vocal fold tissue sample in Krebs-Ringer isotonic solution, dehydrating in sucrose hypertonic solution and rehydrating in distilled water hypotonic solution, was performed to induce certain hydration in tissue samples [Chan 2002]. Talman et al. monitored the change in hydration of heart valve cusp tissue when incubated in different concentrations of dextran solutions over up to 1000 minutes [Talman 2001]. Using various concentrations of NaCl solution has also been shown to be effective in adjusting hydration of cartilage and aortic tissues [Grodzinsky 1981; Narmoneva 1999; Flahiff 2004; Guo 2007]. Basser et al. used polyethylene glycol (PEG) solution to study cartilage biomechanics under various hydration levels [Basser 1998]. PEG solution has also been used to control the hydration of the pectin network using the osmotic pressure produced across the molecular network media [MacDougall 2001; Zsivanovits 2004]. Others further elaborated on formulating the osmotic pressure balance between PEG and tissue constituents [Maroudas 1973; Basser 1998]. One limitation is that these procedures require immersion in solution, which may not be ideally suited for certain testing procedures.

In this study, we describe a liquid-vapor method (LVM) that sequentially uses a liquid phase method (LPM) and vapor phase method (VPM) to adjust and maintain specific levels of tissue hydration in a practical, efficient, and reproducible manner. The approach is amenable to scale-up for processing multiple specimens, to being

incorporated into a mechanical testing set-up for measuring tissue sample mechanical properties, and to the use of optical techniques for characterizing deformations without distortions caused by surrounding fluid. Using this method, we report the relationships between water content and solute concentration as well as air relative humidity for specimens from bovine arterial tissue. These relationships can be used directly in other preparations using similar tissues, or modified for application to other materials.

IV.2. Materials and Methods

This section provides the main steps taken to conduct the experimentation and analysis relevant to investigating viscoelastic behavior of tissue specimens with a degraded matrix.

IV.2.1. Sample Preparation

Please refer to subsections III.2.1 through III.2.3 for a detailed description of procedures for preparing specimens from native, matrix-degraded and elastin-isolated tissues.

IV.2.2. Modulating Water Content

A sequential two stage approach was used to adjust and maintain the water content of vascular tissue specimens. The first stage utilizes solutions containing different concentrations of PEG for efficient adjustment of tissue hydration, bringing

the water content to a desired target level. The second stage consists of maintaining the water content of the tissue specimen constant using a humidified chamber. The following subsections describe each stage in detail.

IV.2.3. Liquid Phase Method

The LPM is based on the concept of osmotic pressure causing fluid flow across a porous barrier until equilibrium is reached [Lillie 1996]. This approach has been widely used to identify swelling pressure of intervertebral disc [Urban 1981; Urban 1988; Johnstone 1992] and cartilage tissues [Maroudas1981; Basser 1998], and to prevent swelling of explant cultures in vitro [Bayliss 1986]. Based on this principle, when a porous barrier is placed between the tissue and a solution of higher solute concentration, water travels out of the tissue across the media into the solution, Fig. 51(a). The amount of water leaving the tissue depends on the solute concentration.

For our study, tissue specimens were removed from PBS and placed inside a piece of dialysis tubing with molecular weight cutoff of 12kD (Sigma Aldrich, St. Louis, MO). The tubing was closed off at both ends with small clips and immersed in an excess volume of 20kD PEG solution (Fisher Scientific, Pittsburgh, PA), Fig. 51(a). As such, we monitored the time-dependent changes in mass of the specimens over the course of 30 hours to determine when the water content reached equilibrium.

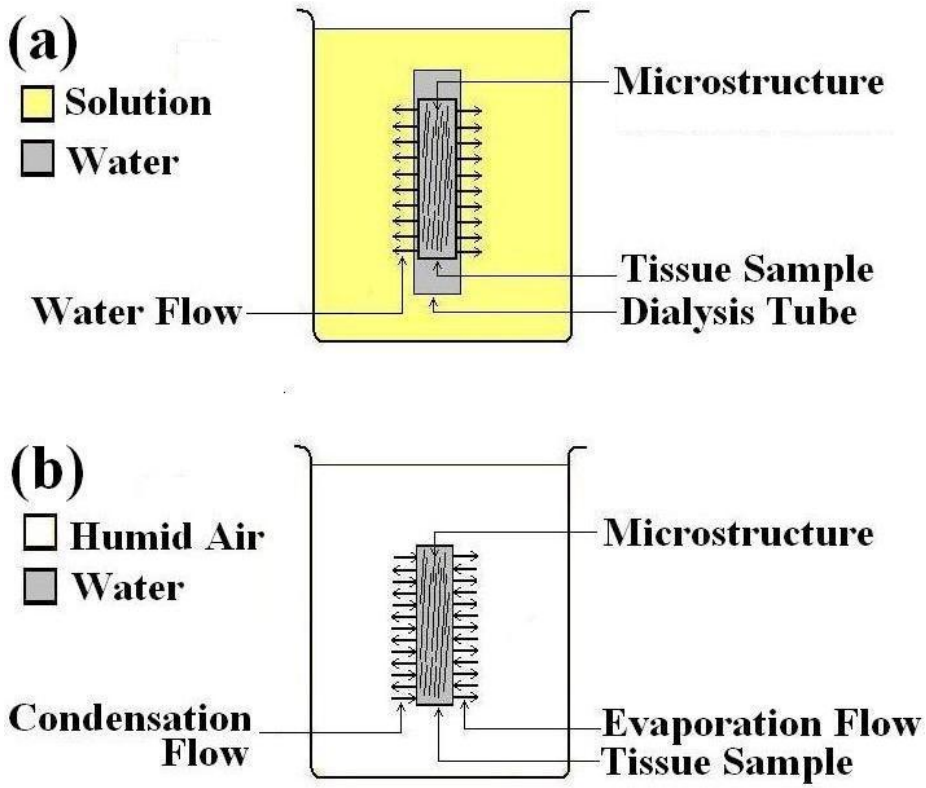

Figure 51— (a)Schematic illustration of LPM hydration set up. The tissue specimen is enclosed inside dialysis tubing and placed inside the PEG solution. Proper tubing pore size, smaller than the molecular size of the PEG solution, should be selected. (b)Schematic illustration of VPM method to hydrate tissue specimen. The specimen is placed inside the humidity chamber with a specific relative humidity percentage to maintain the sample water content.

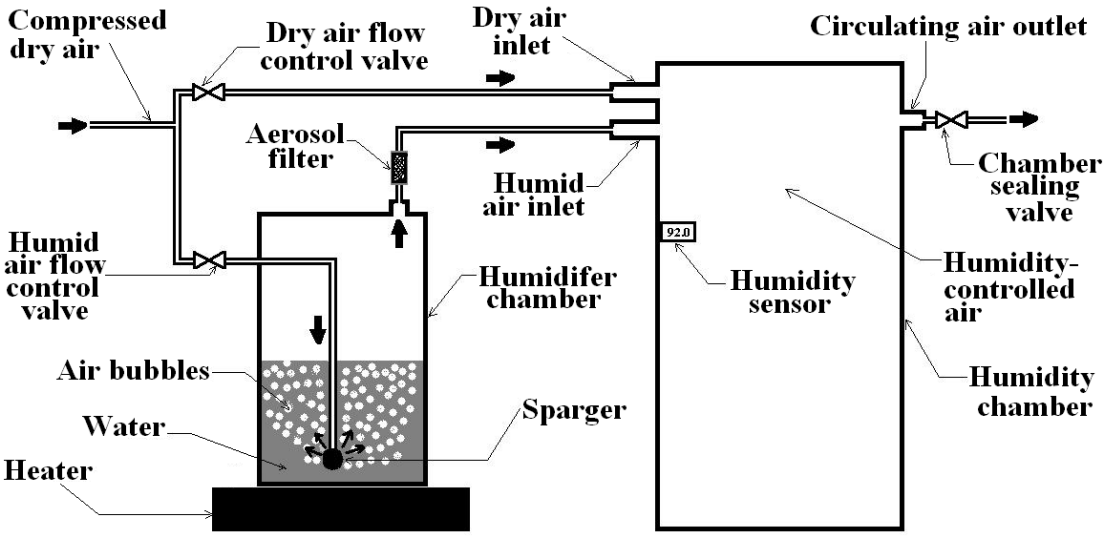

Figure 52— Humidity chamber with sparging mechanism used as the humidifier system. Circulating a flow of air through water causes the air to absorb humidity. By adjusting the humid and dry air flows into a chamber, the chamber humidity can be controlled.

IV.2.4. Vapor Phase Method

The VPM is based on moisture exchange between the tissue surface and a humidified atmosphere [Lillie 1996]. During this process, water evaporates into the surrounding air and water vapor condenses on the tissue surface, Fig. 51(b). The rates of vaporization and condensation are dependent on the relative humidity, the percent partial pressure of water vapor with respect to the saturation vapor pressure of water in the air. A higher percentage of ambient humidity causes greater condensation on the tissue surface, and the change in water content on the tissue surface causes redistribution of interstitial water within the sample. Thus, for a certain percentage of ambient humidity, the water exchange between tissue and surrounding air would

eventually reach equilibrium, where the tissue sample maintains certain water content.

Generating a humidified environment can be achieved using different methods [Lillie 1990; Lillie 1996]. A sparging system was deemed most appropriate for our application in which dry air was passed through water. The small air bubbles generated in the water cause air molecules to absorb humidity. Upon reaching the surface of the water, the humidified air [Lillie 1996] is passed through an aerosol filter at the sparger outlet to prevent water droplets from entering the humidity chamber, Fig. 52. In addition to the humid air inlet, the chamber was also equipped with a dry air inlet, flow of both of which can be adjusted using designated valves to allow greater control over the relative humidity inside the chamber, which was measured using a solid state humidity sensor *(Essick Air, Little Rock, AR)* with $\pm 0.5\%$ precision. Increasing the temperature of the water inside the sparger improved the water absorbability of the air and increased its humidity. To reach humidity percentages above 90%, we placed the sparging system over a heater and were able to achieve humidity values as high as 99%.

IV.2.5. LVM Sorption Relations

Incubation of tissues in hypertonic solutions and humidified air results in the absorption of water into the pores of the bulk tissue as well as adsorption of water molecules into extracellular matrix proteins through electrochemical forces. In order to utilize the two-step LVM effectively, the sorption behavior of the sample must first be described during each step. This allows us to associate a solute concentration with

a relative humidity for the LPM and VPM stages, respectively. Because computing volumes of the solid ECM requires assumptions and approximations, we chose to express sample hydration as gravimetric water content, $\%WC_g$, rather than volumetric water content. This involves direct measurements of mass:

$$\%WC_g = \frac{m_w}{m_d} \times 100 \tag{22}$$

where m_w and m_d are the mass of water in the sample and dehydrated mass of the sample, respectively. The total water mass, m_w, was computed by calculating the difference between sample's hydrated mass, m_h, and dried mass, m_d [Jeffrey 1995; Naka 2005], leading to:

$$\%WC_g = \frac{m_h - m_d}{m_d} \times 100 \tag{23}$$

The measured gravimetric water content, $\%WC_g$, was first used to quantify changes in tissue hydration using the LPM as a function of solute concentration, $\%SC$. Similarly, the hydration behavior in the VPM was characterized by relating $\%WC_g$ and chamber relative humidity $\%RH$. Taking the $\%WC_g$ as the common parameter, the corresponding $\%SC$ and $\%RH$ were related to each other.

IV.2.6. Entire Hydration Protocol

After sample preparation, the initial mass of hydrated specimens was measured. Tissue specimens were removed from PBS, with special care taken not to squeeze them. Excess water was then carefully wicked off of only the tissue surface, and samples were placed on a PB403-S laboratory balance with ± 0.5mg precision

(Mettler Toledo, Columbus, OH). Specimens were then placed inside individual pieces of dialysis tubing and both ends of the tubing were closed off using clips. Samples were then incubated in a PEG solution of known concentration (0, 5, 10, 20, or 40% w/v). Some specimens were incubated in PEG solutions and their mass periodically measured over the course of 30 hours to determine the time necessary to reach equilibrium. Upon determining a 6-hour equilibration period, subsequent specimens were incubated in PEG solutions overnight, and then used for VPM analyses. For these specimens, an iterative procedure was used to determine the appropriate chamber humidity to maintain a stable gravimetric water content for each concentration of PEG solution. Samples were removed from PEG solutions, weighed, and then left in the humidity chamber for 45 minutes at a known humidity level. Samples were then re-weighed to determine mass changes. Humidity adjustments were made and the iterative process continued until the observed changes in mass were within 10% of the fully swelled mass for four sequential specimens. Each sample was then oven-dried for 7 hours and weighed again to obtain the dry mass.

IV.2.7. Stress Relaxation Testing

The mechanical testing of the specimens was performed using the MTS® 858 Mini Bionix mechanical testing system, Fig. 53(a). Stress relaxation was conducted using the displacement-control mode by applying constant stretch and collecting the force data measured by the machine. Dividing the force by the initial area of the specimens, measured before loading the specimen, results in the stress.

Standard rectangular specimens were cut with an OML-customized cutting fixture, Fig. 11, in the circumferential direction. Superglue was used at the two ends of the specimen to attach both sides to the pieces of sandpaper in order to increase the friction. The sandpaper-reinforced parts of the specimen were then secured in the OML-customized fixture, Fig. 53(b).

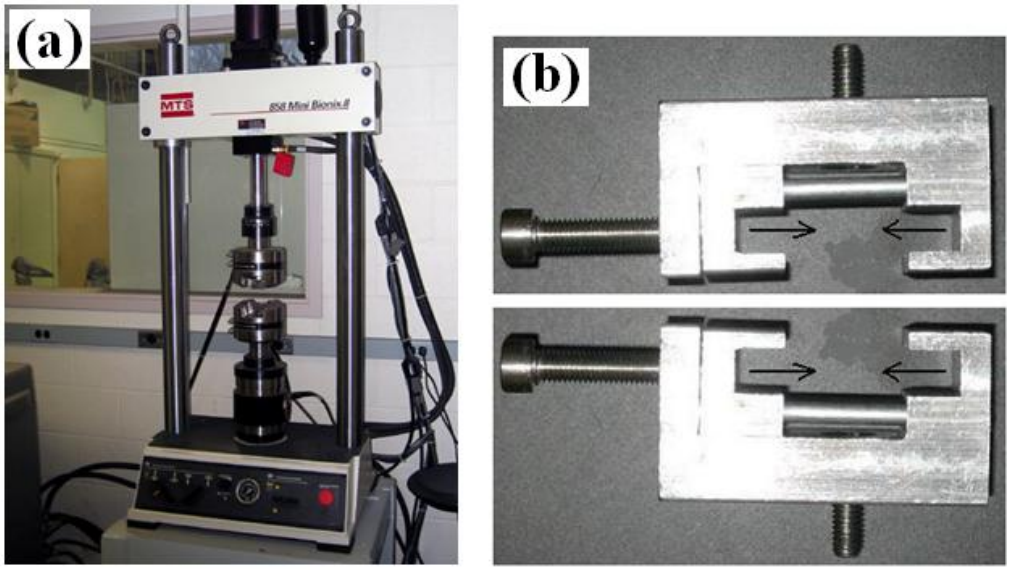

Figure 53- (a)MTS® 858 Mini Bionix mechanical testing system available in OML, (b) OML-customized fixtures to grip rectangular arterial specimens.

Given the necessity of maintaining tissue hydration during the test, the entire humidifying setup was incorporated around the MTS machine, Fig. 54. Figure 55 shows a close up image of the tissue specimen secured by the grips inside the humidity chamber.

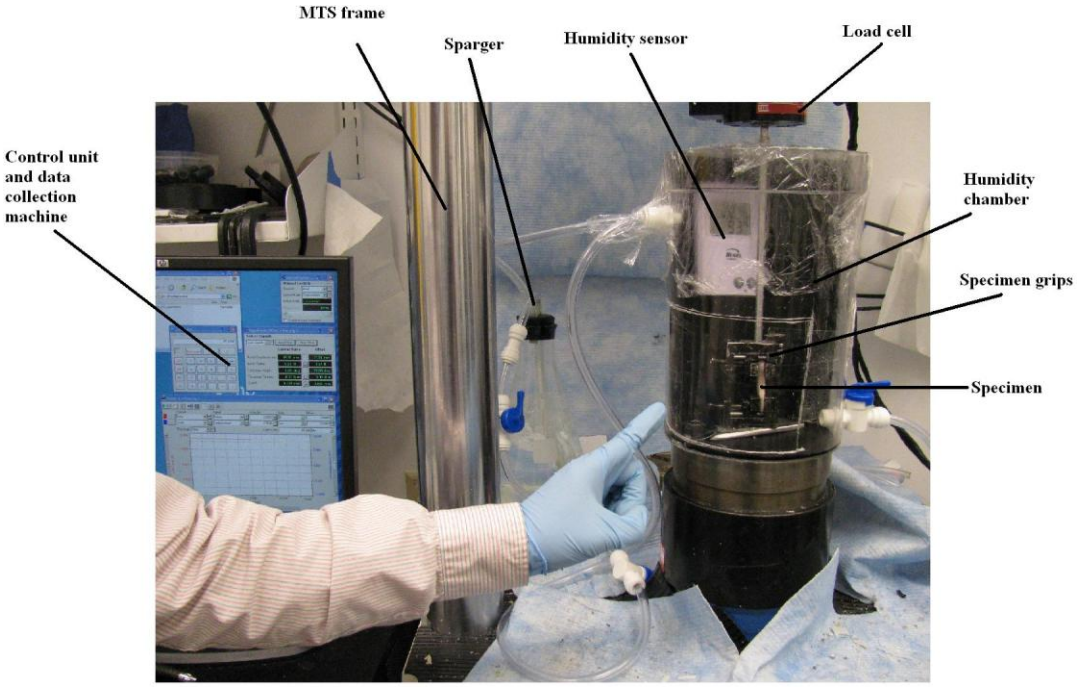

Figure 54- Entire experimental setup for conducting stress-relaxation test on aortic specimens under controlled relative humidity.

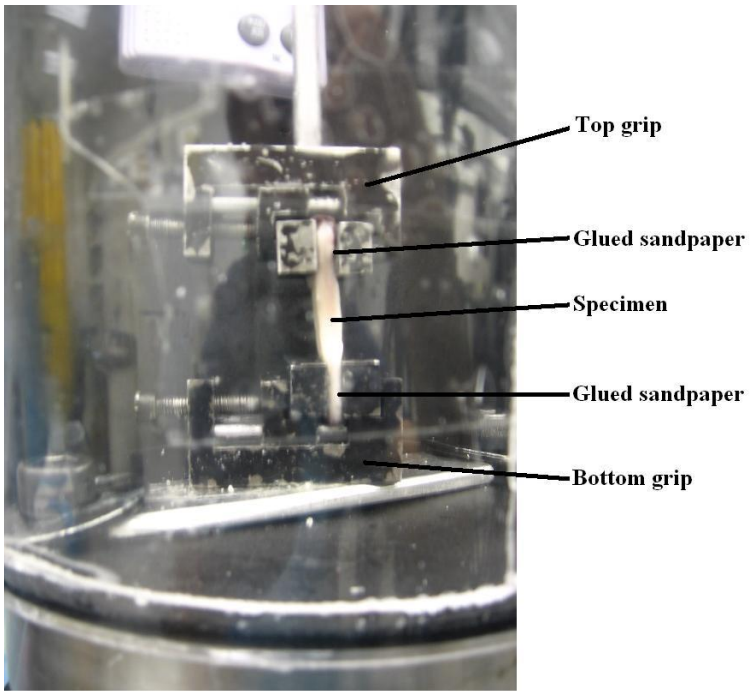

Figure 55- Close up of the specimen grips. Two ends of the specimen are glued to small pieces of sandpaper for increasing friction and secured between to parts of the top and bottom grips.

IV.3. Results

This section provides the experimental results relevant to hydration mechanisms and mechanical testing of the specimens.

IV.3.1. Time-dependent changes in water content

In order to characterize how quickly tissue hydration changes using the LPM and VPM, we measured time course changes in water content in 40% (w/v) PEG solution and 60% relative humidity, values selected based on pilot data. The data emphasize the superior efficiency by which hydration can be adjusted using the LPM. For LPM specimens, the equilibrium water content was reached in 6 hours after fully swelled specimens were introduced into the PEG solution, Fig. 56(a). For VPM specimens, however, the mass continued to change over 55 hours, at which point the experiments were terminated, Fig. 56(b).

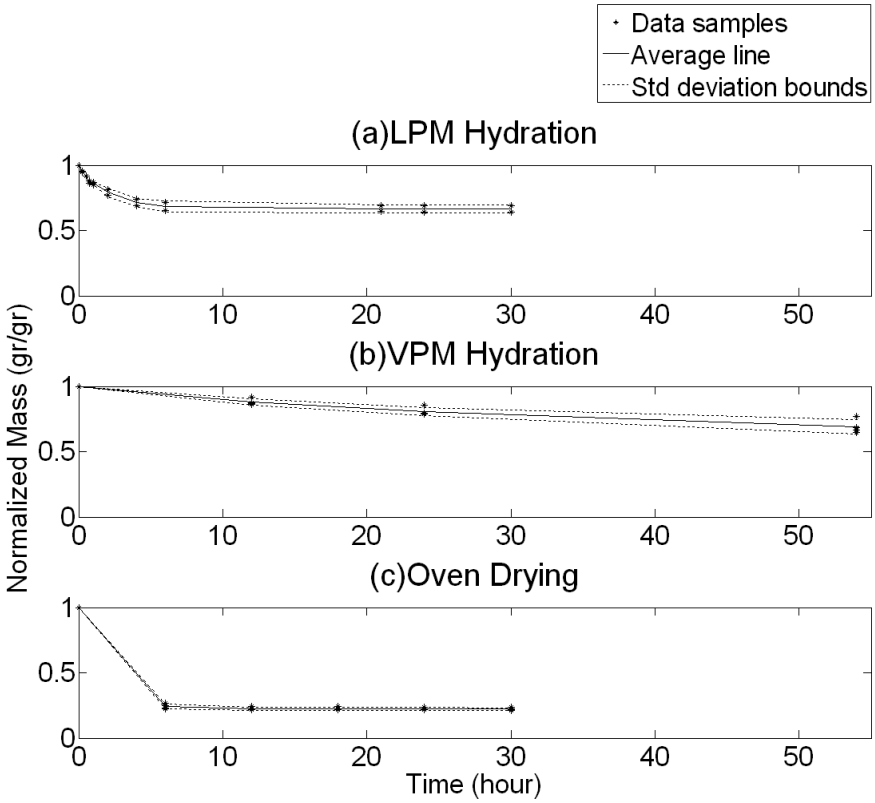

Figure 56— Rate of change of sample mass during (a)Liquid phase hydration method with 40% PEG solution, (b)Vapor phase hydration method with 60% chamber humidity, (c)Oven drying. Figures (a) and (c) show that LPM and drying equilibrium states were reached in approximately 6 and 7 hours, respectively. Figure (b) shows that no equilibrium was achieved for the VPM method even after 5 days.

IV.3.2. LVM Sorption Characteristics

As expected, higher solute concentrations resulted in lower levels of water content. Figure 57 illustrates the dual sorption characteristics for the entire LVM method obtained for native tissue. Figure 57(a) shows results from the LPM method, relating water content and solute concentration. Having determined the required solute

concentration from the LPM stage, Fig. 57(b) can then be used to specify the corresponding relative humidity in the VPM method. In order to approximate the solute concentration and relative humidity for any water content other than the exact examined values, the following sigmoid curves might be used to facilitate the interpolation procedure:

$$\%SC = -2 + \frac{44}{\left[1+\exp\left(\%WC_g - 80\right)\right]^{0.01}} \tag{12}$$

$$\%RH = 52 + \frac{47}{\left[1+\exp\left(\%SC - 8\right)\right]^{0.15}} \tag{13}$$

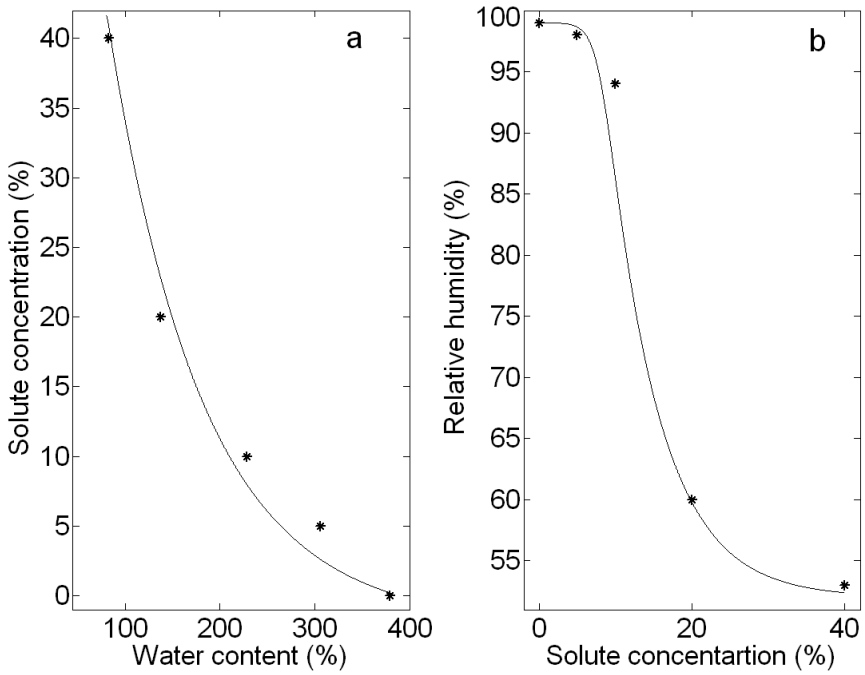

Figure 57— Sorption characteristics data for the entire LVM method along with interpolating curves determined for native tissue. (a)LPM stage: Water content-solute concentration data, (b)VPM stage: Solute concentration-relative humidity data.

Figure 57 shows the above relations within the working range of water content. The coefficients of determination (R^2) of 0.98 and 0.97, respectively for solute concentration and relative humidity, indicate an acceptable fit of the curves to the experimental data points. The water content of fully submersed samples was around 370% (Fig. 57 for 0% PEG). Thus, for a dehydrated sample to retain a water content of $\%WC = 200$, Eqs 12 and 13 indicate that it should be tested in a solution with a concentration of approximately $\%SC = 11.25$ and in an environment with a relative humidity of approximately $\%RH = 80.69$.

Similar sorption characteristic relations for matrix-degraded tissue were calculated and are shown in Fig. 58. The coefficients of determination for solute concentration and relative humidity data fitting are 0.93 and 0.99, respectively.

$$\%SC = -68 + \frac{120}{\left[1+\exp\left(\%WC_g\right)\right]^{0.002}} \tag{24}$$

$$\%RH = 39 + \frac{60}{\left[1+\exp\left(\%SC - 7\right)\right]^{0.024}} \tag{25}$$

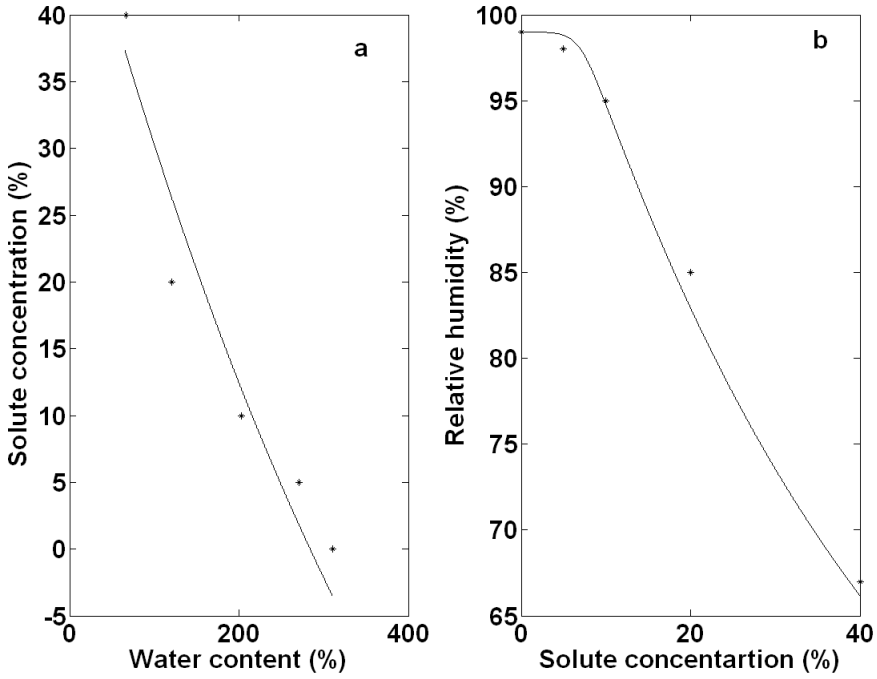

Figure 58— Sorption characteristics data for the entire LVM method along with interpolating curves determined for matrix-degraded tissue. (a)LPM stage: Water content-solute concentration data, (b)VPM stage: Solute concentration-relative humidity data.

Finally, for elastin-isolated tissue, sorption characteristic relations were calculated using Eqs. 16 and 17, and are shown in Fig. 59. The coefficients of determination for solute concentration and relative humidity data fitting are 0.89 and 0.98, respectively.

$$\%SC = -15 + \frac{120}{\left[1+\exp\left(\%WC_g + 180\right)\right]^{0.004}} \tag{26}$$

$$\%RH = 47 + \frac{52}{\left[1+\exp\left(\%SC - 5\right)\right]^{0.022}} \tag{27}$$

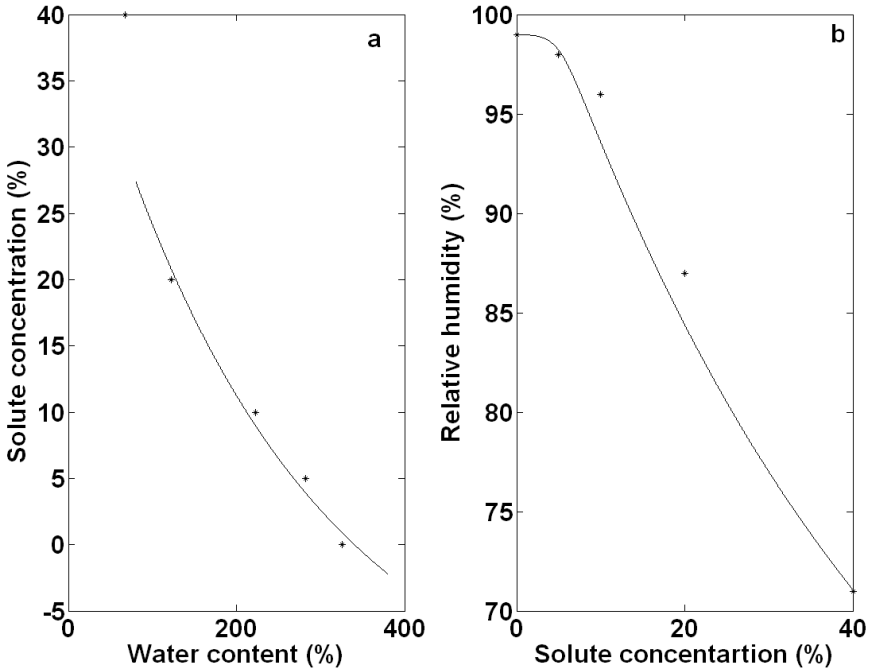

Figure 59— Sorption characteristics data for the entire LVM method along with interpolating curves determined for elastin-isolated tissue. (a)LPM stage: Water content-solute concentration data, (b)VPM stage: Solute concentration-relative humidity data.

IV.3.3. Effect of Stretch on Stress-Relaxation

The stress relaxation behavior for native aortic tissue is shown in Fig. 60 for two different stretch levels of 1.4 and 2.0.

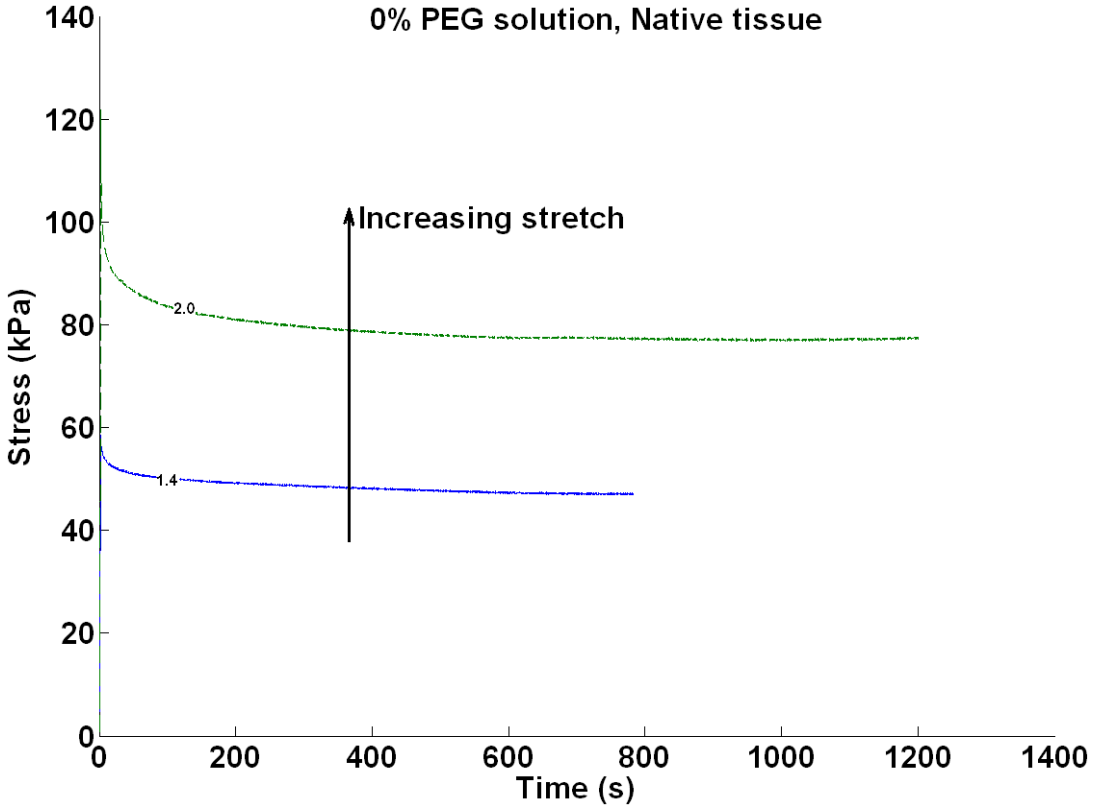

Figure 60— Stress-relaxation behavior of aortic tissue under two stretch levels of 1.4 and 2.0. All specimens were from native aortic tissue and fully hydrated in 0% PEG solution.

To better perceive the relaxation trend of the tissue, Fig. 61 shows the same behavior normalized to the initial and final values of stress.

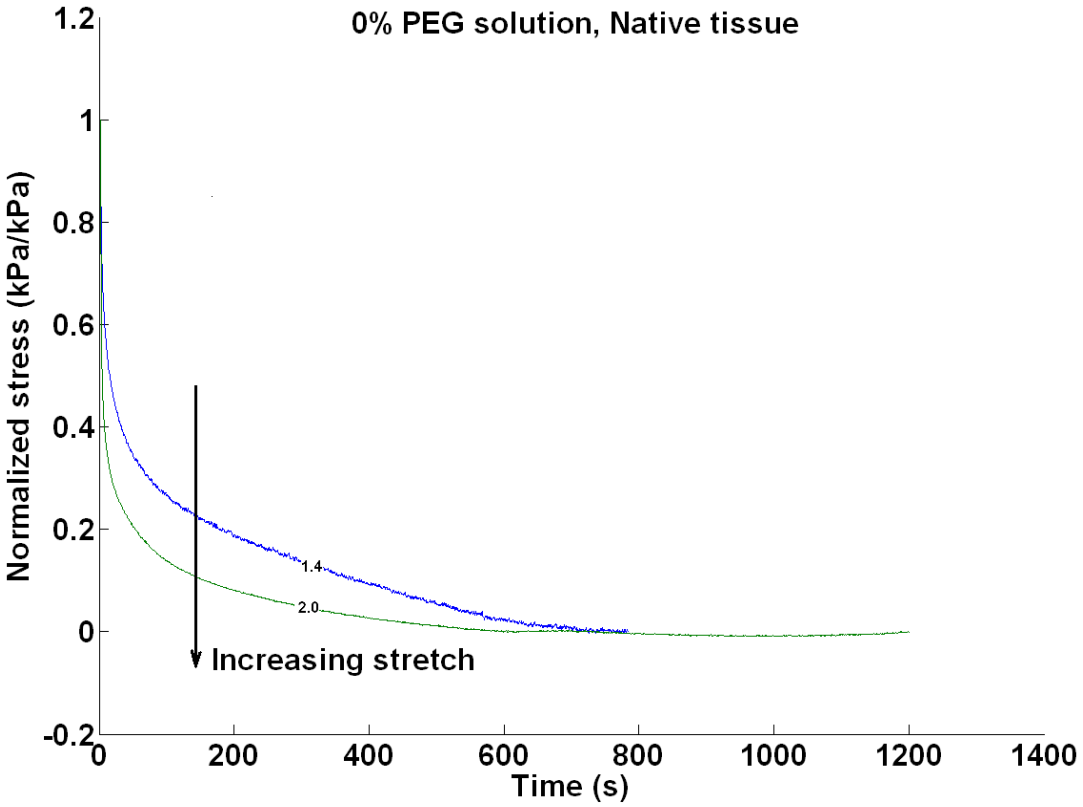

Figure 61— Stress-relaxation behavior of aortic tissue under two stretch levels of 1.4 and 2.0. All specimens were from native aortic tissue and fully hydrated in 0% PEG solution. Relaxation data are normalized for initial and final stress values.

IV.3.4. Effects of Matrix Alteration on Stress-Relaxation

To understand the effects of alteration in the tissue extracellular matrix, stress relaxation of native, matrix-degraded and elastin-isolated tissue samples are obtained under comparable test conditions (fully hydrated and tested under 1.4 stretch), Fig. 62.

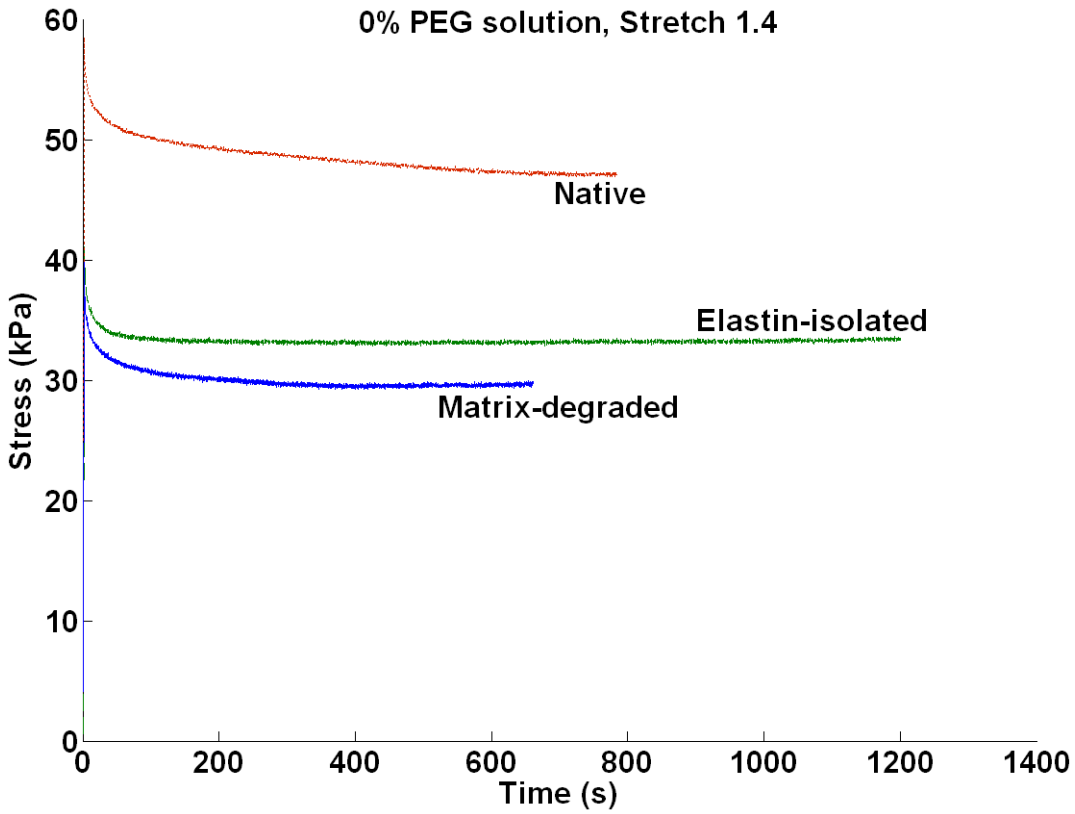

Figure 62— Stress-relaxation behavior of native, matrix-degraded and elastin-isolated specimens. All specimens were fully hydrated in 0% PEG solution and were tested under 1.4 stretch.

Figure 63 shows the same relaxation behaviors normalized by initial and final stress values.

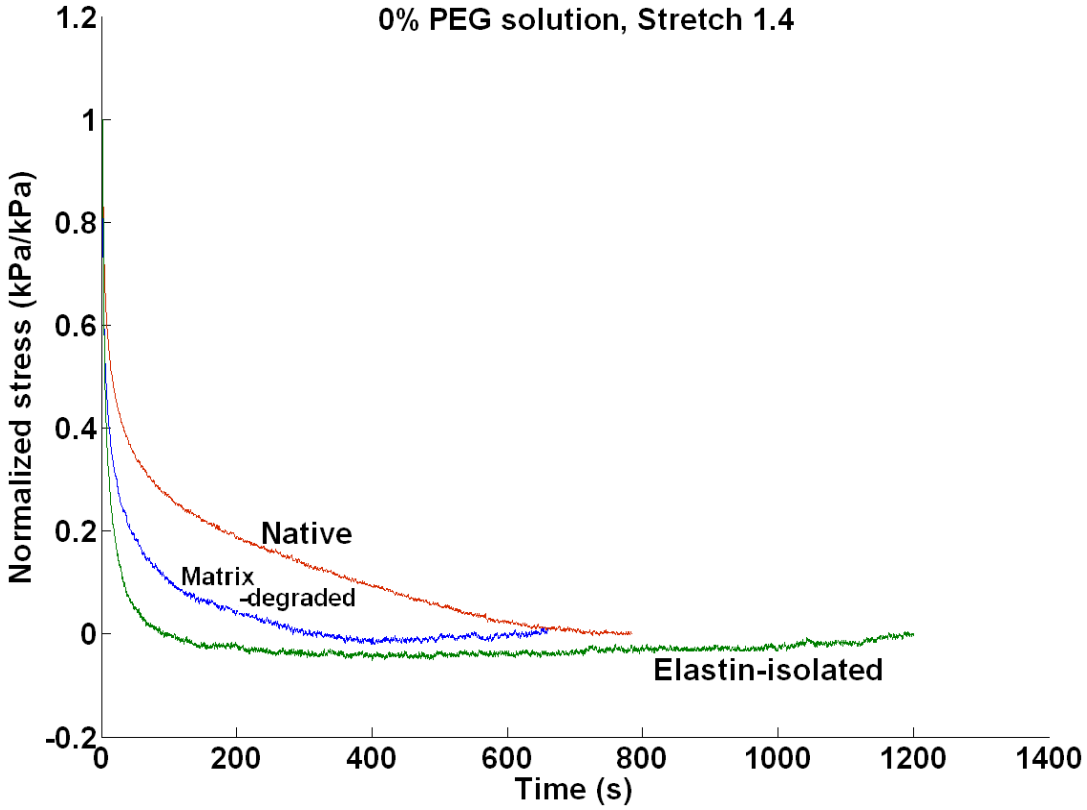

Figure 63— Stress-relaxation behavior of native, matrix-degraded and elastin-isolated specimens. All specimens were fully hydrated in 0% PEG solution and were tested under 1.4 stretch. Relaxation data are normalized for initial and final stress values.

IV.3.5. Effects of Hydration on Stress-Relaxation

The effects of hydration on the tissue are investigated by testing the stress-relaxation of specimens from native tissue under three different decreasing hydration levels with 378.97, 137.57 and 82.43 water contents, Fig. 64. The water contents are induced using PEG solutions of 0%, 20% and 40% concentrations, respectively.

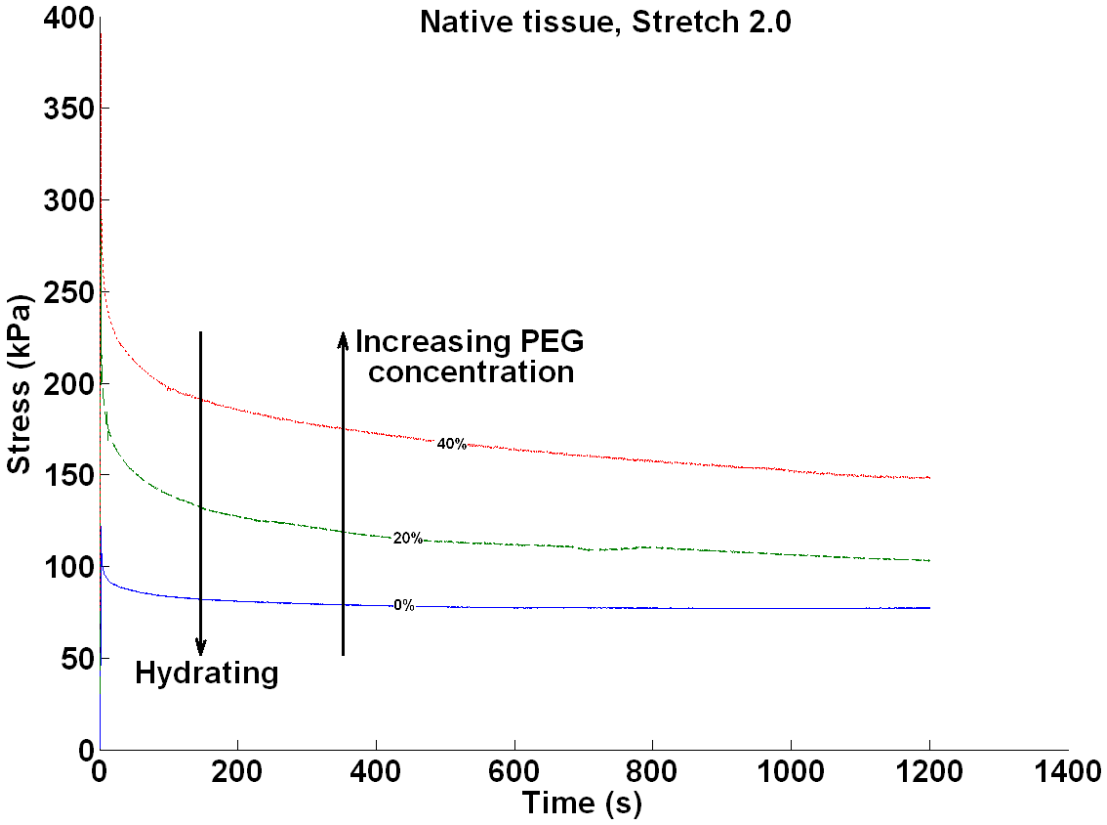

Figure 64— Stress-relaxation behavior of specimens from aortic tissue specimens hydrated under 0%, 20% and 40% PEG solution, respectively. All specimens were extracted from native tissue and were tested under 2.0 stretch.

For better comparison of relaxation trends between different hydration levels, Fig. 65 illustrates same data normalized by initial and final values of stress.

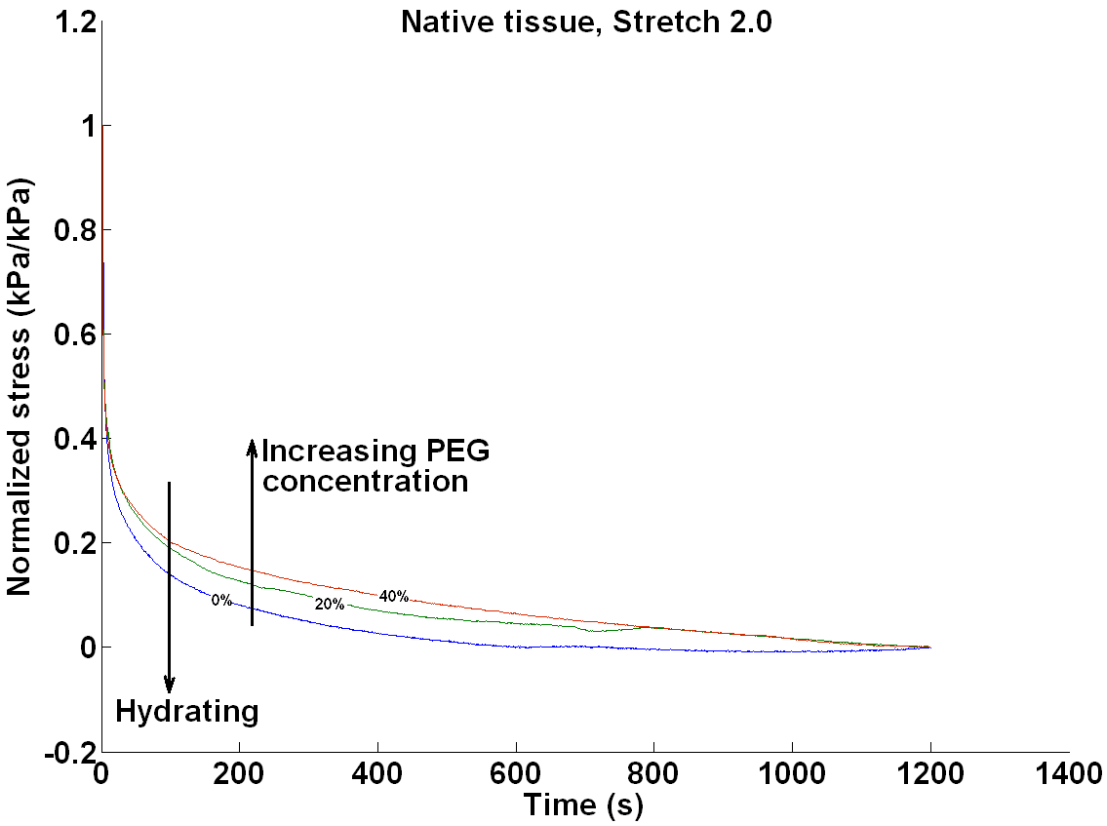

Figure 65— Stress-relaxation behavior of specimens from aortic tissue hydrated under 0%, 20% and 40% PEG solution, respectively. All specimens were extracted from native tissue and were tested under 2.0 stretch. Relaxation data are normalized for initial and final stress values.

IV.3.6. Stress Relaxation Master Plots

In order to provide a general reference for looking up relaxation data for all different test conditions, a master plot of the actual relaxation behavior is given in Fig. 66.

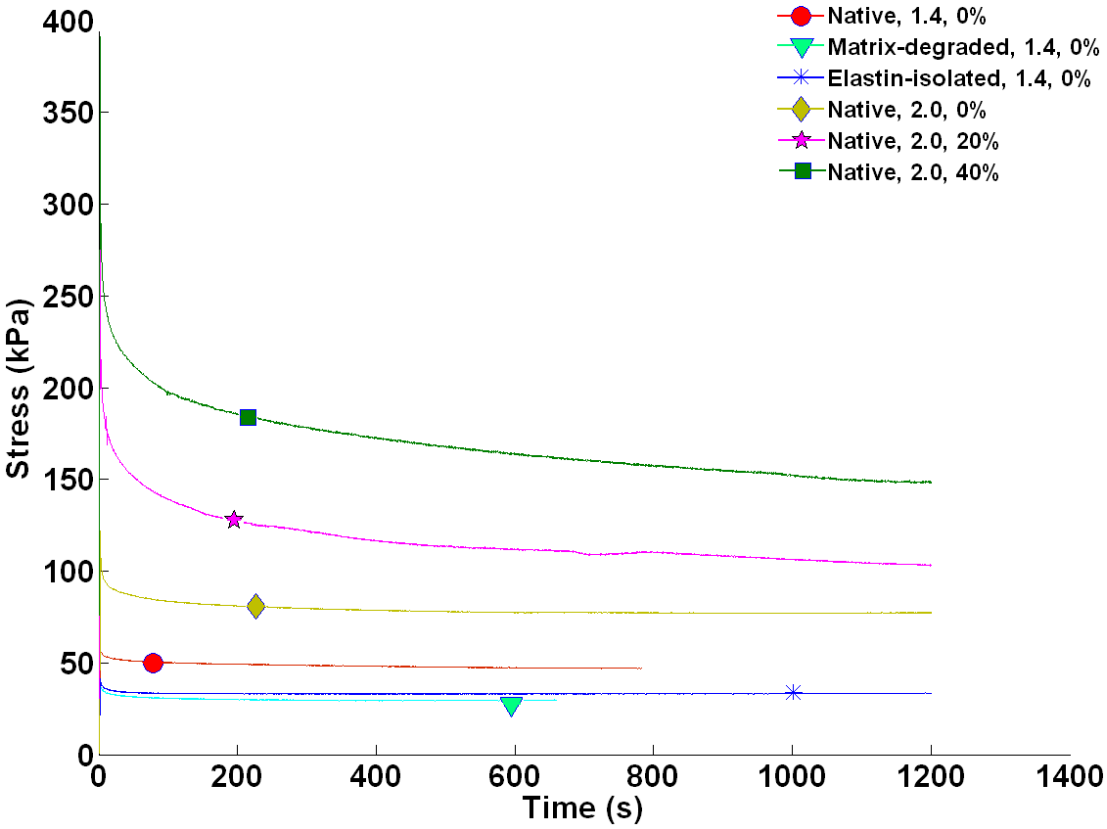

Figure 66— Stress-relaxation master plot for aortic specimens under different conditions of tissue type, stretch level, and PEG concentration.

In order to compare the relaxation features for all different test conditions, the previous master plot is normalized to initial and final stress values and the data is shown in the normalized master plot of Fig. 67.

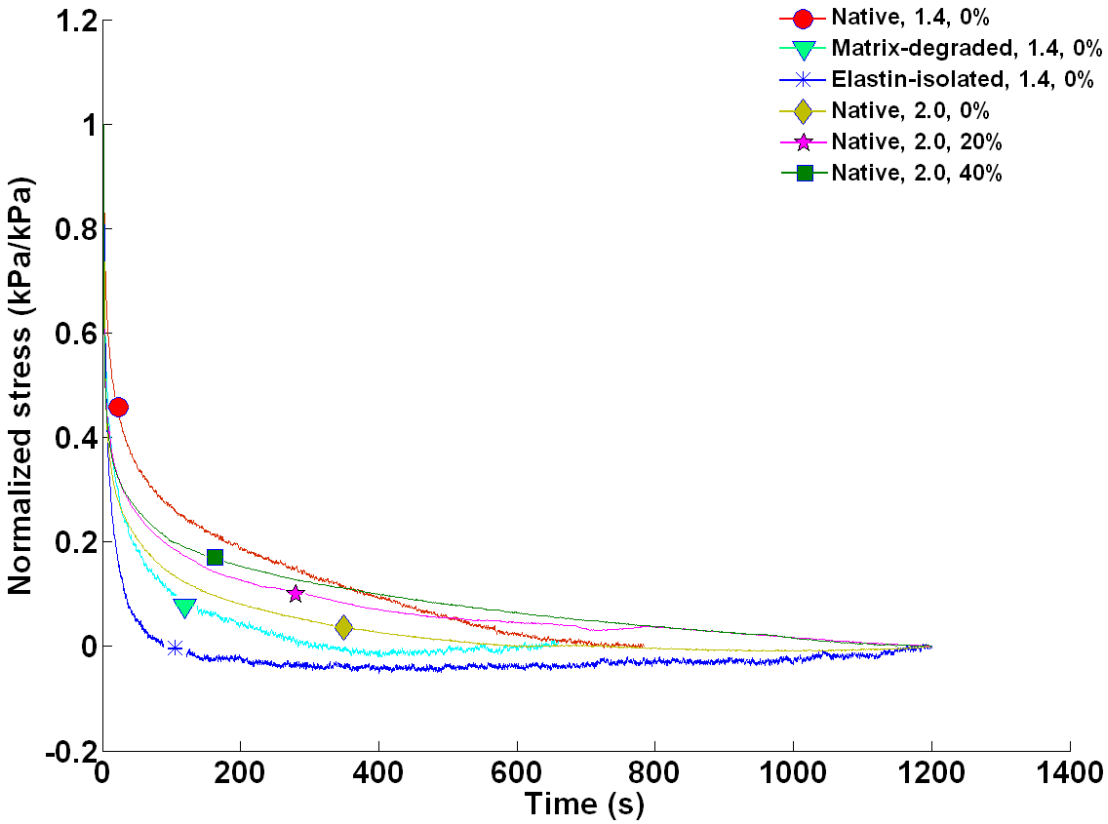

Figure 67— Stress-relaxation master plot for aortic specimens under different conditions of tissue type, stretch level, and PEG concentration. Relaxation data are normalized for initial and final stress values.

As a quantitative measure of comparing the transient behavior for relaxation behavior under different test conditions, it is assumed that the decay trends obtained

here follow exponential behavior, which is an accurate-enough assumption given the close match of the trends to exponential decay. Having assumed exponential decays, a decay constant, λ_s, and a settling time, t_s, are defined and measured. On each stress relaxation curve, the λ_s is defined as the time where the response reaches 63% of its decay, in this case 0.37, and the t_s is defined as the time where the response reaches 95% of its final decay, in this case 0.05, Fig. 68.

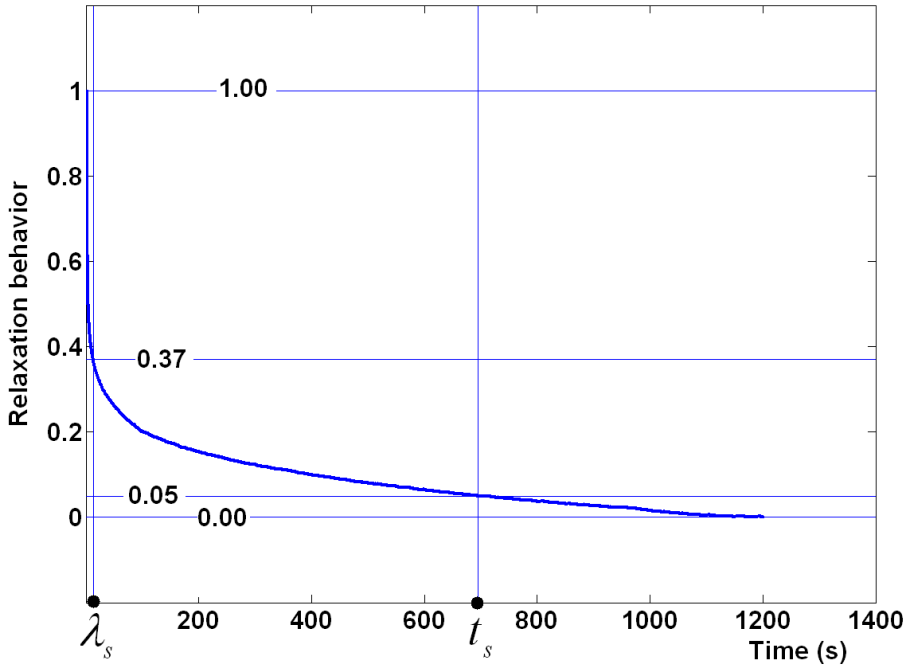

Figure 68— Illustration of decay constant, λ_s, and settling time, t_s, on a stress relaxation curve.

Table 9 lists the λ_s and t_s constant for the stress relaxation curves of all different test conditions.

Table 9- Decay constant and settling time for stress relaxation behavior of aortic specimens in all different test conditions.

Tissue type, stretch, %PEG	λ_s (s)	t_s (s)
Native, 1.4, 0%	40	520
Matrix-degraded, 1.4, 0%	14	180
Elastin-isolated, 1.4, 0%	8.5	50
Native, 2.0, 0%	10	300
Native, 2.0, 20%	14	550
Native, 2.0, 40%	12.8	695

IV.3.7. Stress Rate

The rate of change of stress is known as a good measure of viscosity in the material behavior. Given the decreasing stress during the stress-relaxation test, the negative rate of stress change is shown in Figs. 69 through 71 respectively sorted for effects of stretch, matrix type and PEG concentration.

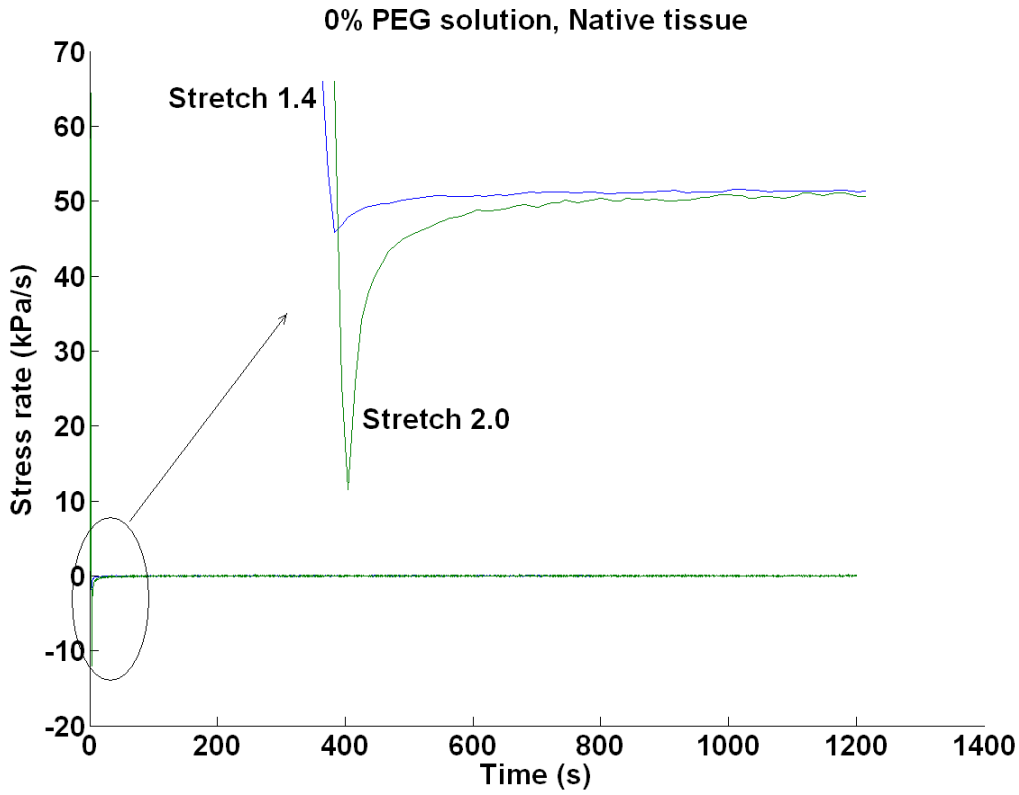

Figure 69— Rate of stress decrease during stress-relaxation behavior of native aortic tissue under two stretch levels of 1.4 and 2.0. It is observed that higher stretch causes a higher rate of change in stress.

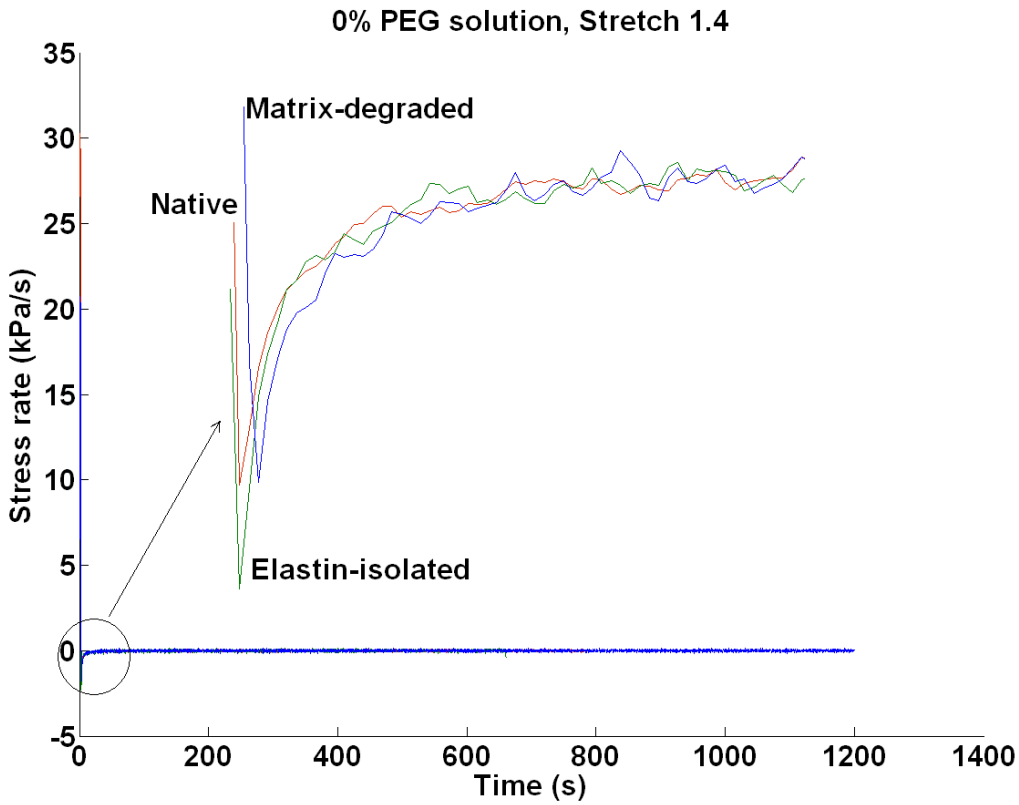

Figure 70— Rate of stress decrease during stress-relaxation of native, matrix-degraded and elastin-isolated tissue specimens under 1.4 stretch. A higher rate of change in stress is observed for elastin-isolated tissue compared to an almost equal rate of change for native and matrix-degraded tissues.

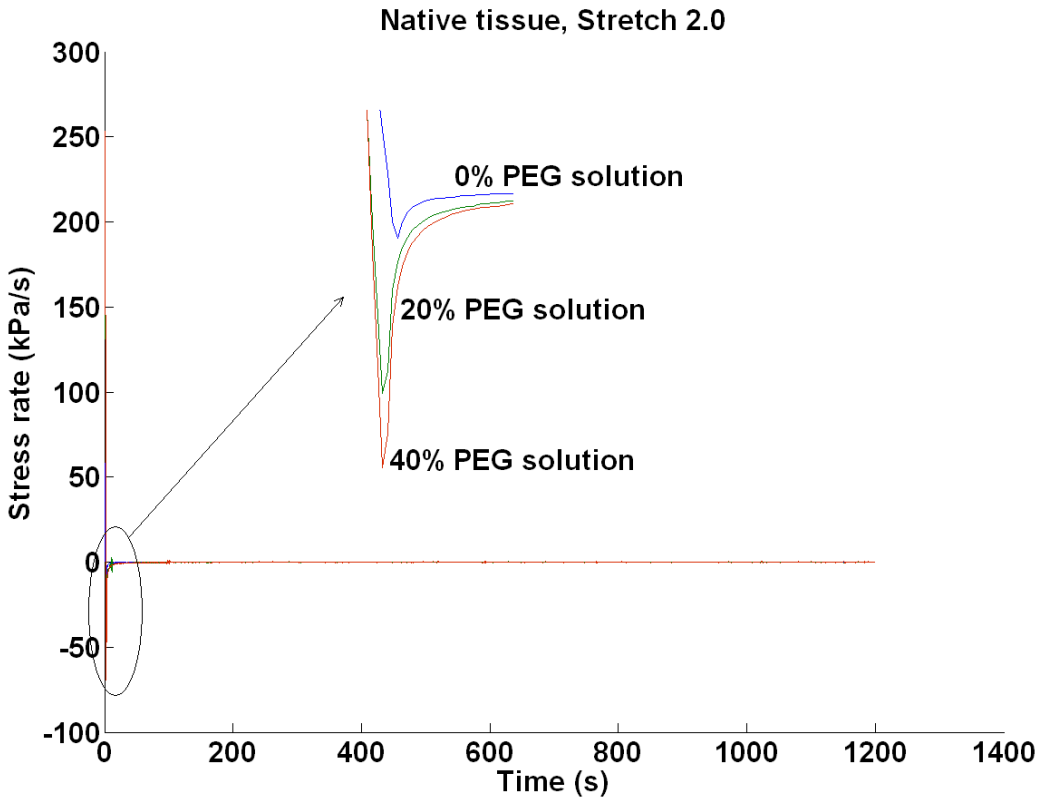

Figure 71— Rate of stress decrease during stress-relaxation behavior of specimens from native aortic tissue specimens hydrated under 0%, 20% and 40% PEG solution, respectively. It is observed that tissue dehydration causes higher rate of change.

IV.3.8. Comparison to Spring-Dashpot Models

Among the common component-based models of Maxwell, Kelvin-Voigt and standard-linear, the Kelvin-Voigt is inherently not suitable for modeling stress-relaxation but creep, since it gives a constant stress for a constant strain. The Maxwell and Kelving-Voigt models were also tested in this study and were found incapable of describing the observed behaviors. Both a manual systematic fitting procedure and the MATLAB® fitting toolbox were used and both models failed to provide a good fit for almost all curves.

Going a step further, putting two Maxwell models in parallel was found capable of modeling the observed stress-relaxation behaviors. The arrangement of springs and dashpots are shown in Fig. 72. For this arrangement, the time behavior of stress, $\sigma(t)$, during stress-relaxation test under constant strain ε_0 can be calculated based on the following formula:

$$\sigma(t) = \varepsilon_0 k_1 \, \mathrm{e}^{-k_1 t / c_1} + \varepsilon_0 k_2 \, \mathrm{e}^{-k_2 t / c_2} \tag{28}$$

where k_1 and k_2 are spring constants, and c_1 and c_2 are dashpot constants.

The Matlab® curve fitting tool was used to extract the four parameters of the parallel Maxwell model for all of the stress-relaxation behaviors, which are listed in Table 10. The table also lists the root mean squared errors (RMSE) for each of the fits which indicate that this model can reasonably describe the behaviors.

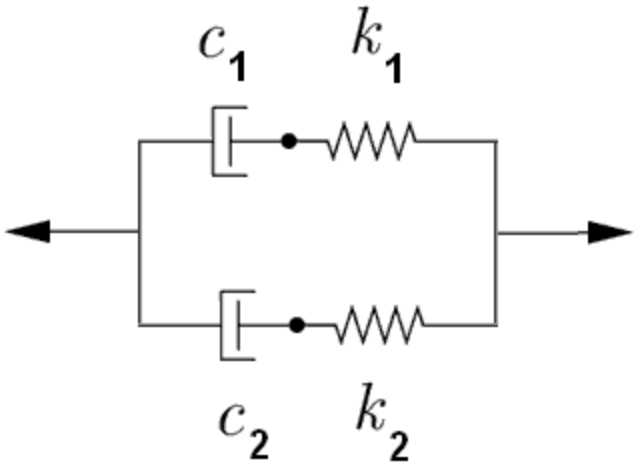

Figure 72— Arrangement of two Maxwell models in parallel. The parameters k and c represent spring and dashpot constants.

Table 10- Spring and dashpot coefficients of the parallel Maxwell model shown in Figure 53 for describing the stress-relaxation behavior of different tissue specimens.

Test condition	$k_1(KN/m)$	$c_1(MNs/m)$	$k_2(KN/m)$	$c_2(MNs/m)$	**RMSE**
Native, 1.4, 0%	12.75	0.43	125.00	1860.10	0.09
Matrix-degraded, 1.4, 0%	13.10	0.44	75.45	1524.20	0.06
Elastin-isolated, 1.4, 0%	13.13	0.26	23.93	310.00	0.04
Native, 2.0, 0%	15.58	1.56	79.45	2600.00	0.63
Native, 2.0, 20%	62.20	2.83	125.50	836.67	1.05
Native, 2.0, 40%	69.32	3.46	189.50	789.58	0.97

Figures 73 through 75 show the variation of the spring and dashpot constants respectively with stretch, matrix type and PEG concentration.

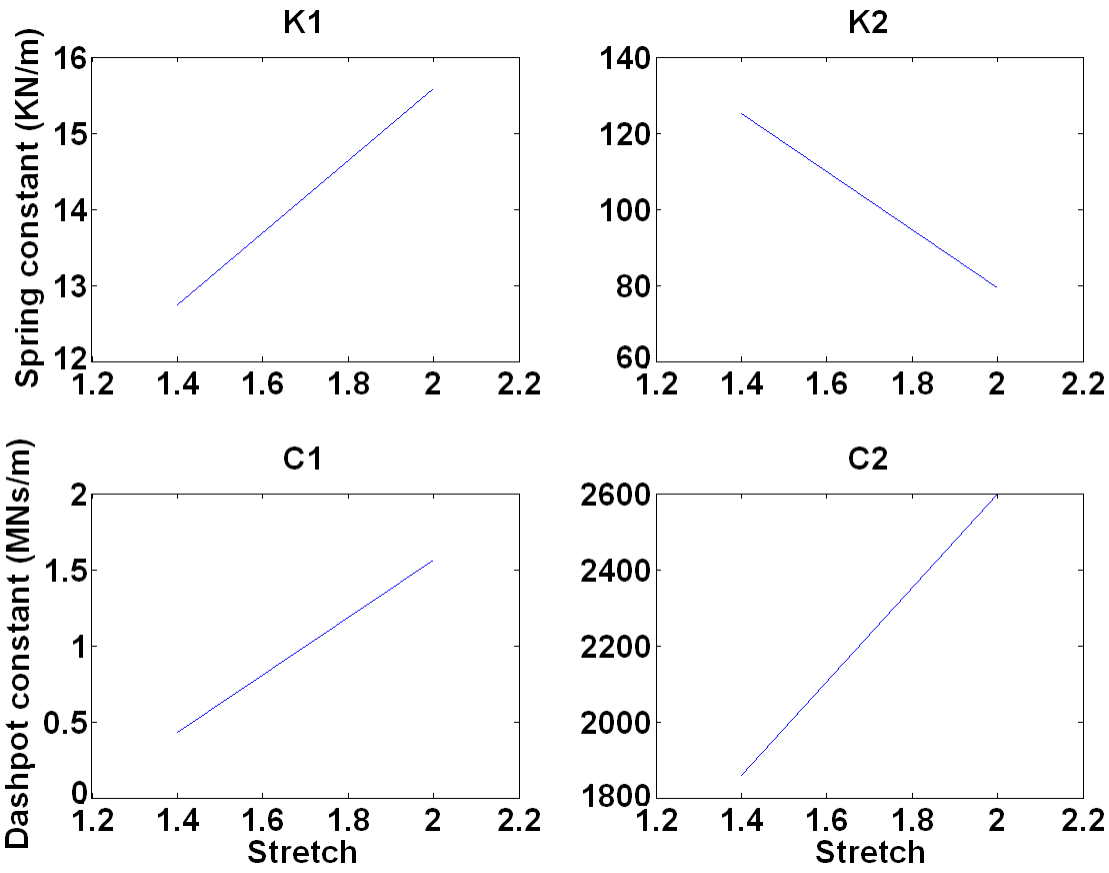

Figure 73— Relation between the tissue stretch and the spring and dashpot constants of the parallel Maxwell model for the native tissue.

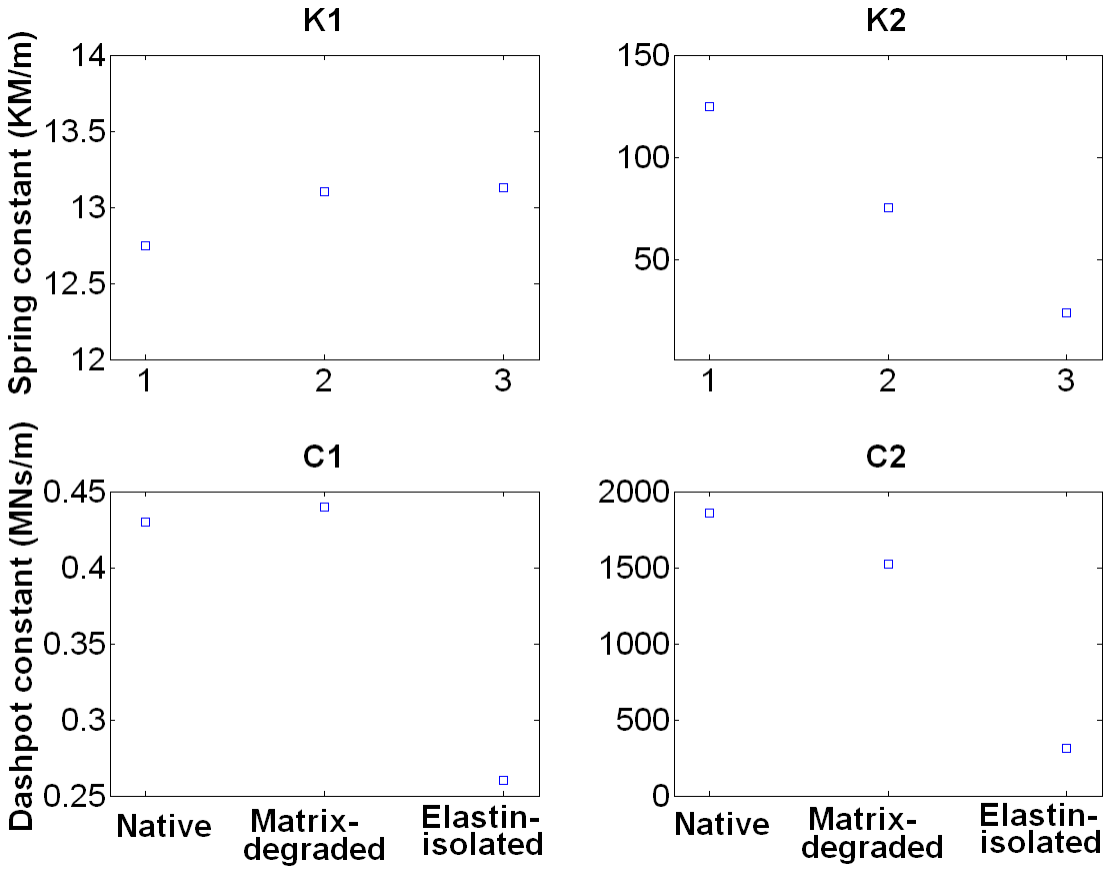

Figure 74— Change in spring and dashpot constants of the parallel Maxwell model for tissues with different matrix composition.

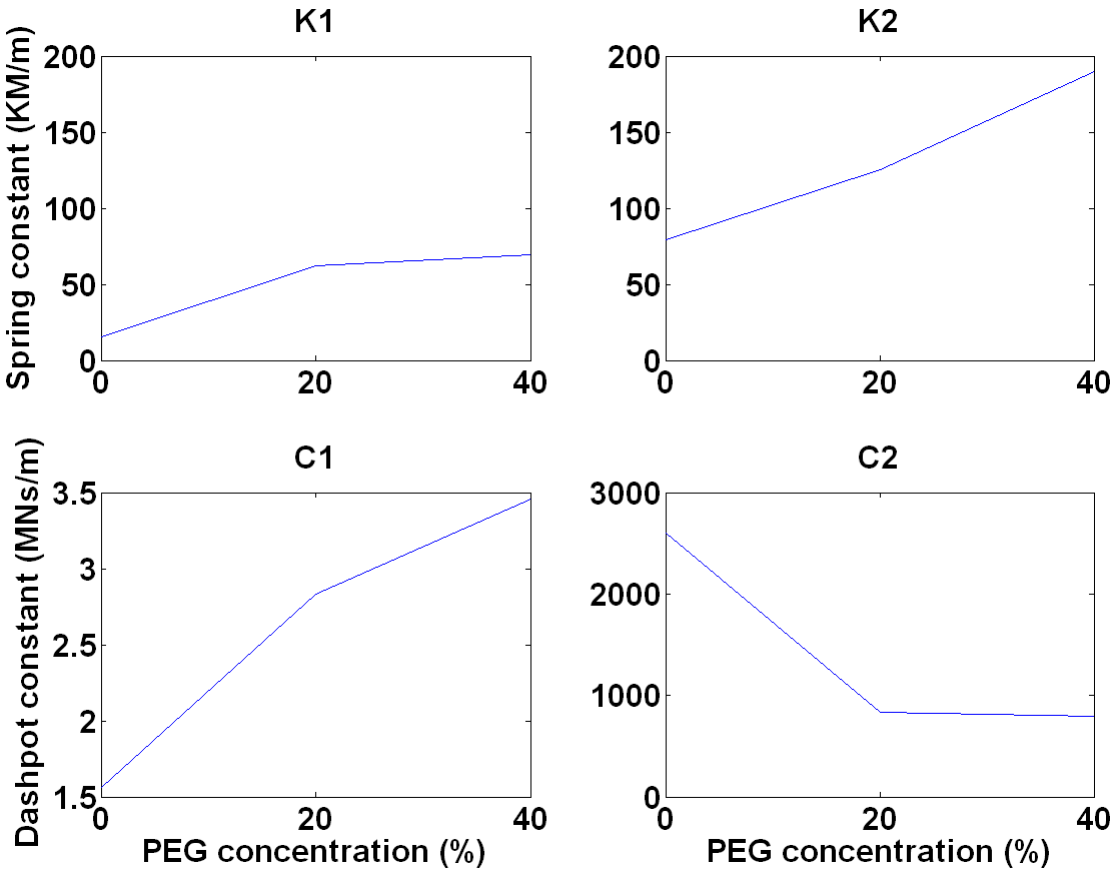

Figure 75— Relation between the PEG concentration and the spring and dashpot constants of the parallel Maxwell model for native tissue. PEG concentration is inversely related to tissue hydration level.

IV.4. Discussion

The initial efforts in this chapter concern the use of a combined solution- and humidity-based approach for modulating tissue hydration, one that is amenable to mechanical testing procedures. The approach takes advantage of the merits of the LPM and the VPM, and overcomes their individual limitations. Advantages of the LPM include the relative ease with which it can be implemented, since tissues can be

immersed directly in a bath containing the appropriate PEG concentration, and the relative speed to achieve equilibrium in sample water content. Different incubation times have been reported for samples hydrated using the LPM. For example, 45 minutes for pig aorta [Lillie 1996], 1-2 hours for animal lumbar spine [Bayliss 1986], 1 day for pectin networks [Zsivanovits 2004], 2 days for human lumbar spine [Urban 1988] and human articular cartilage [Basser 1998] have been used. While equilibrium times may vary depending on tissue, in many cases the time course changes may not have been characterized. Thus, incubation times may have been overestimated to ensure equilibrium or simply assumed. Our own observations indicate that, for bovine aorta samples of our chosen size, an equilibrium time of 6 hours was appropriate, Fig. 56(a). Our time course results also show that much of the change in water content takes place within first hour —a consistent observation with other reports [Pflaster 1997; Urban 1981; Rand 1989]. Yet, the LPM presents a number of challenges for mechanical testing of tissues. Placing tissues in a solution of fixed PEG concentration necessarily imposes a boundary condition that will induce osmotic pressures under tissue deformation. In addition, the use of a bathing solution may introduce artifacts or inaccuracies when tracking surface markers or textures for strain measurements. This could be particularly problematic during dynamic loading regimes that may induce significant fluid movement.

With the VPM, the advantages and challenges are essentially reversed. The primary advantage of the humidified environment is that it does not impose any additional forces that may influence tissue mechanics and is amenable to optical techniques for strain measurement. However, as we confirmed, this approach requires

excessively long incubation times. For biological tissues, such durations may be unacceptable considering the potential for degradative processes and contamination to confound mechanical measures. It has been reported that porcine aortic samples placed in a humidified environment required approximately 14 days to reach equilibrium water content [Lillie 1990; Lillie 1996]. To gauge how gravimetric water content changes in bovine aortic tissues using the VPM as the exclusive method, we found that sample hydration does not reach equilibrium even after 55 hours at 60% relative humidity, Fig. 55(b). There would arguably be a strong potential for matrix degradation by this point.

Based on these factors, the shorter equilibrium times found using the LPM are highly appealing for testing tissues in vitro, yet the incorporation of the VPM to maintain water content during actual testing procedures is also critical. The necessity of having some form of humidified environment for samples outside the PEG solution was supported by our measurements on samples placed in room air after performing the LVM. Tissues removed from PEG concentrations of 0% and 10% after LVM equilibrium lost 21% and 14% of their hydrated mass, respectively, after just 30 minutes in open laboratory conditions (35% RH and $25^{\circ}C$).

In conducting the VPM, we decided to use the sparging system primarily for two reasons. The first is that this system allows rapid change of the chamber humidity when needed. Using the humid/dry air inlet valves, the chamber humidity can be adjusted on the order of 5 %/min (though changes are slower when the humidity exceeds 90%). This is a critical feature when using the chamber as part of the mechanical testing set up, because the chamber might need to be opened and closed

during the experiment and the target humidity inside the chamber needs to be quickly restored every time an interruption occurs. The second advantage is that the sparging system provides a transparent humid environment inside the chamber that does not introduce artifacts into the optical measurements. This is critical for accurate measurements of tissue deformation. Other methods using a humidity chamber have been proposed but have some limitations. For instance, tissues can be suspended in a chamber containing a salt solution. Varying the salt concentration allows precise control over humidity but sample equilibration reportedly takes about 14 uninterrupted days [Lillie 1990]. Additionally, samples need to be hydrated one at a time, unlike with our method which can be used to hydrate batches of samples. This imposes additional time constraints when dozens of samples need to be tested from each fresh tissue harvest. Another method is simply blowing a stream of water vapor on the tissue specimens, but this would impair sample visualization and optical measurements, as well as introduce mechanical disturbances.

Although combining the LPM and the VPM techniques offers important advantages, some limitations were introduced and some existing limitations of the LPM and the VPM could not be overcome. One new limitation in this technique is the increased handling of specimens required during preparation. With our current equipment, tissues cannot be both equilibrated and tested in a single apparatus, but must be transferred from one to the other. The exposure to ambient air and manual manipulation of the specimen may temporarily perturb tissue hydration. A second limitation is the increase in groundwork needed to establish complementary osmotic pressure/humidity relationships with tissue hydration. While this effectively doubles

the workload to establish a foundation for a specific tissue type, it can be argued that the time saved and accuracy gained over using either the LPM or the VPM alone justifies this additional effort.

Among the inherent limitations of modulating tissue hydration in vitro, one potentially important consideration is the water distribution within the tissue. How water is re-distributed in the tissue ECM and fibrillar network during the LPM and VPM are not known, but it is likely that time-dependent changes in water distribution occur throughout the tissue when traveling from the surface to the central regions of the sample. It is also likely that fluid transport occurs anisotropically in many tissues, including bovine aorta. Depending on the efficiency of fluid movement in the radial thickness, the length and width of the tissue specimen may or may not be important. Water distribution mechanisms could be partially responsible for long equilibrium durations using the VPM. If this is the case, local inhomogeneities in water distribution could affect mechanical property measurements, even though the bulk sample is controlled for water content. Therefore, using the VPM it may not be precise to say that the hydration state of the sample does not change, but because the time window of our application of the VPM (a fraction of an hour) is much shorter than the duration for hydration equilibrium in the VPM (on the order of tens of hours), changes are likely to be small and/or limited to the surface. The larger standard deviation of the VPM normalized water content measurements compared to those obtained with the LPM —0.052 versus 0.021— shows greater uncertainty with the VPM, an observation that has also been reported by Rand *et al* [Naka 2005].

A final inherent limitation of artificially controlling water content is the specificity to the type and size of tissue specimens. Outcomes of this study establish a platform for studying the role of hydration on tissue biomechanics. However, extending the LVM from bovine aorta tissue samples reported here for implementation with other biological or synthetic materials requires similar evaluation of the sorption characteristics for the material of interest. Furthermore, sorption characteristics for a particular material may vary with geometry. The relative magnitude of water distribution inhomogeneities and a sample's surface/volume ratio may differentially impact these characteristics and necessitate development of separate sorption curves. Although such investigations directly reveal the behavior of tissues in vitro, the implications on tissue biomechanics can potentially be interpreted in a more physiologically relevant context. Several methods have been reported for estimating in vivo tissue hydration noninvasively, including MRI [Han 2001; Wexler 1985], energy-disperse X-ray diffraction [Caracciolo 2005] and Tetrahertz spectroscopy [Png 2008]. Such methods can be used to quantify changes in tissue hydration during physiologic and pathophysiologic conditions in vivo, and their biomechanical and mechanobiologic impact assessed.

Differences in tissue properties during degrading the extracellular matrix are first evident in the different sorption characteristic curves, Figs. 57 through 59. This indicates that the mechanisms through which the tissue hydration changes depend on the composition of the extracellular matrix. One factor which can be responsible for such alterations in tissue hydration can be effective porosity which changes during tissue treatment procedures. Knowing that tissue hydration is an important factor in

controlling mechanical behavior, changes in tissue hydration features for different native, matrix-degraded and elastin-isolated tissues can be used to predict changes in tissue biomechanics as well.

Based on the results obtained from examining the mechanical behavior of tissue specimens, deeper insights into morphological and phenomenal changes in the tissue can be achieved. It is seen that increasing the stretch in the native tissue makes the tissue stiffer, Fig. 60, but faster relaxation is obtained based on either stress relaxation or rate of change of stress, Figs. 61 and 69, respectively. Quantitatively, compared to 1.4 stretch, 2.0 stretching of the specimens results in 25.00% lower decay constant and 57.69% lower settling time, Table 9. The reason for such increase in viscosity under increasing stretch could be the fact that stretching the tissue can cause the water content to be squeezed out from within the tissue interfibrillar spaces. Assuming the overall mechanical behavior of the tissue as a matrix-water composite, dehydrating the tissue decreases the role of (incompressible and non-viscoelastic) water in tissue biomechanics and lets the tissue microstructure play a more dominant role in the overall tissue biomechanics revealed through stress-relaxation testing. However, such trend is limited to certain stretch level beyond which it is expected that the tissue microstructure starts to damage and collapse and so the stress-relaxation would contain discrete sudden jumps.

Looking at the effects of alteration in the tissue matrix on the stress-relaxation behavior, Figure 62 shows that treating the elastin-isolated and matrix-degraded tissues results in structures that are weaker than the native tissue (lower initial stresses for same stretch). Weakening of the matrix-degraded and elastin-isolated tissues is

due to denaturing the collagen which is responsible for a large part of the tissue integrity and strength. Evaluating the relaxation trends in different tissue types, Fig. 63, it is observed that native, matrix-degraded and elastin-isolated tissues respectively show faster relaxation trends; 35% and 21.25% decrease in decay constants for matrix-degraded and elastin-isolated tissues, respectively, as well as 34.62% and 9.62% decrease in settling time, respectively, Table 9. It can be argued that the difference in mechanical behavior of native, matrix-degraded and elastin-isolated tissues mainly reflects the contributions of biomechanics of each of the individual constituents versus the contributions from the interactions between them primarily through the extracellular matrix. Especially because the stress-relaxation tests are performed in stretch 1.4, expectedly low enough for collagen to engage, the difference in relaxation behaviors mainly reflects that of the elastin and matrix interaction. In the matrix-degraded tissue, elimination of collagen as the main load-tolerating component makes the role of elastin and water more dominant and since the tissue can recover the deformation faster, so does the change in stress. By further removal of the disintegrated collagen network, the elastin network in the elastin-isolated tissue can reconfigure more freely and play an even more highlighted role in the tissue biomechanics. In addition, treating the tissue and altering the extracellular matrix changes the entire water-matrix composition in the tissue which on the other hand means changes in the amount of water available to the elastin.

Studying the direct effects of hydration on the mechanical behavior of native tissue, Figure 64 shows that dehydrating the tissue makes the tissue stiffer (larger initial stress for same constant stretch). By normalizing the stress relaxation

behaviors, Figure 65 shows that dehydration causes slower stress-relaxation; 140% and 128% increase in decay constant and 183.33% and 231.66% increase in settling time, respectively when the tissue is dehydrated in 20% PEG and 40% PEG solutions compared to fully hydrated tissue in 0% PEG solution, Table 9. It has already been postulated that elastin protein shows rubbery-like behavior when sufficient hydrating water is available and its behavior shifts to crystallized-like behavior when not enough hydrating water is available [Lillie 1996]. The viscoelastic mechanical behaviors obtained here are good verifying observations, which show that hydrating the tissue increases its viscosity. The main reason for this phenomenon is that, given the hydrophilic nature of elastin molecules, for them to bond with each other and to relocate within the protein structure, they first should bond to water molecules [Lillie 1996]. However, it is seen that the relation between the change in PEG concentration and the change in viscosity is not linear, meaning that the amount of drop in viscosity by comparing dehydrated tissue in 20% PEG to that of fully hydrated tissue in 0% PEG is not the same as that obtained by comparing dehydrated tissue in 40% PEG to dehydrated tissue in 20% PEG, Fig 65. One reason for this loose correlation could be the distinction between intrafibrillar versus interfibrillar water. It has been already found that what practically regulates the viscoelastic behavior of elastin is that part of water which hydrates the elastin molecules, called intrafibrillar water, and not the water that fills the vacancies in the extracellular matrix, called interfibrillar water [Lillie 1996]. Since in the current study, what is being measured is the amount of tissue water content, which is the summation of intrafibrillar and interfibrillar water,

unless one can find methods to measure them separately, it is not possible to derive a correlation between tissue viscosity measurements and intrafibrillar water.

Finally, it was attempted to describe the experimental mechanical behaviors with traditional spring-dashpot models. As it is discussed earlier, the common Maxwell and Linear solid models were found incapable of describing the stress relaxation behaviors. However, a model composed of two parallel Maxwell model - Fig. 72- was found able to describe different stress relaxation behaviors with reasonably acceptable accuracy, see RMSE numbers in Table 10. Looking at the values for spring and dashpot constants in the model, Table 10, it is being argued here that each of the springs and dashpots in the model can be associated with relevant microstructural components in the tissue. Given the higher spring and dashpot constants for the branch number 2, the lower branch can be associated with collagen and the upper branch, branch number 1, can be associated with the contributions from elastin and the anchoring effects from the extracellular matrix. However, it is being strongly emphasized that modeling the tissue with such spring-dashpot systems is only meant to describe the data in a mathematical manner but does not carry much physiological significance. After all, the parallel Maxwell model with the collagen/elastin/extracellular assumption can only make sense given how little is known about the actual extracellular matrix morphology and composition. The collagen and elastin are anchored to the extracellular matrix through GAGs and form the entire integrated tissue. So the model does capture the parallel attachment of collagen and elastin. As it is seen in the Table 10, denaturing the collagen from the native tissue decreases the K_2 and digesting out the collagen further does so which

both indicates that collagen is loosing its stiffness. Similar observations are made for the viscosity measures of elastin, C_2, which shows diminishing effects from collagen throughout the tissue treatment. However, the elastin contributions, represented by K_1 and C_1, remain almost constant during the tissue treatment. It is also seen that by dehydrating the tissue (increasing the PEG concentration), the spring constants increase, which means the tissue is getting stiffer. At the same time, the collagen's viscosity, C_2, decreases by dehydration but elastin's, C_1, increases. It is very difficult to connect such conclusions with the experimental observations made on the tissue mechanical behavior, because the mechanical behaviors represent the properties of the entire tissue and not the individual microstructural components of elastin and collagen.

V. SUMMARY AND FUTURE RESEARCH

This research was of benefit to the field of vascular tissue biomechanics by addressing some of the important existing problems in the field. Elucidating how cardiovascular biomechanics is regulated during health and disease is critical for developing diagnostic and therapeutic methods. There has been a general trend in recent years to develop models, which can describe the tissue behavior in a multiscale manner, meaning that morphological phenomena in the tissue can be captured at different length scales, from organ down to tissue, cell and molecule, and they can be put together in one single model to accurately describe the tissue biomechanics [Weinberg *in press*]. As of now, multiscale modeling of biological systems is in its infancy stages due to multiple reasons. Due to challenges in developing modeling techniques, there is a lack of meaningful and coherent data from an identical biological system under similar conditions gathered at multiple length scales. Having said this, the current study is a major step in reaching out to multiscale modeling of cardiovascular tissue. The study provides tissue-scale and microstructural level deformation measurements from the aorta under different deformation protocols, which can partly be used as a platform for setting up a multiscale deformation model. To the best of the author's knowledge, this is among very few studies that provide such sort of deformation measurements on the cardiovascular tissue.

The study also quantified microstructural deformation in the tissue, which has not been reported before. The Fourier and Hough transformations were used on histology images of tissue under different deformation states to quantify the microstructural conformations. It is being argued here that each method brings

separate insight to the microstructural deformation characterization. The Fourier method gives an average measure of relative directionality in the tissue microstructure, stating how different the directionality of the tissue is in each of the horizontal and vertical directions. So if positioned properly and accurately in the horizontal circumferential direction, the Fourier aspect ratio can be looked at as a good and efficient representative measure of directionality in the tissue microstructurte. On the other hand, the Hough method measures the average angular orientations in the tissue microstructure and again, if positioned properly and accurately in the horizontal circumferential direction, Hough measurements can quantify the average angular orientation of the microstructure. One difference between the Fourier and Hough methods is that Fourier measurements show a more overall evaluation of the tissue microstructure whereas in the Hough method, every single line measurement is being counted and so more local effects are taken into account. Even at its infancy stages of development, the Hough technique can serve the purpose rather effectively. The techniques establish a platform for further continuation of the methodology into developing more advanced devices for monitoring microstructural alterations, with potential implications in diagnosis of tissue abnormalities in pathological conditions.

Going back to tissue-scale examinations, stress-relaxation behaviors of the tissues were also studied under different conditions. Within the scope of this study, it is difficult to either draw conclusions on the microstructural mechanisms behind the tissue-scale mechanical behaviors or to interpret such behaviors in terms of morphological phenomena taking place during the tissue loading and deformation.

However, hypothetical discussions to describe such phenomena and the correlation between them were made, some of which require further study to probe the hypotheses. The responses were approximated by traditional spring-dashpot models and the results were interpreted in regards to the microstructural composition assumed in the model. As interesting as it sounds, using a spring-dashpot model is more significant from the mathematical point of view but not so much from the physiological point of view. Indeed, determining the model parameters for the experimental data is only a mathematical fit but there is no concrete evidence that each of the components necessarily represents physiological collagen or elastin. However, such models can be used to interpret some of the findings and set the guidelines for enhancing test protocols and enriching the models.

One of the aspects that can potentially improve the accuracy of the findings on microstructural alterations in the tissue is testing the aortic ring segments instead of rectangular circumferential specimens. In addition to all the similarities to internal pressure loadings in physiological conditions, the fundamental difference between testing the ring segments and circumferential specimens is the perseverance and relief of tissue residual stress, respectively. It is well known that the aorta in its unloaded form contains compressive residual stress which is verified by the opening of the aorta (or aortic ring segments) when cut axially. Although, the exact measures of residual stress in the tissue and the impact that it might cause on the microstructural conformations has not been quantified, the least expected is that there should be a difference between the histology of ring segments and circumferential specimens during loading and unloading. The main challenge in examining the ring segments

under loading and unloading is the lack of proper testing machines. One of the current lab projects under consideration is designing and testing a customized apparatus for loading the aortic ring segments, Fig. 76. The apparatus is designed to apply a given pressure inside the ring segment and to take multiple pictures from top and side views, which allows the measurement of stretch, width and thickness. The design of the apparatus and the procedures to test the ring segments and read the data are still under development.

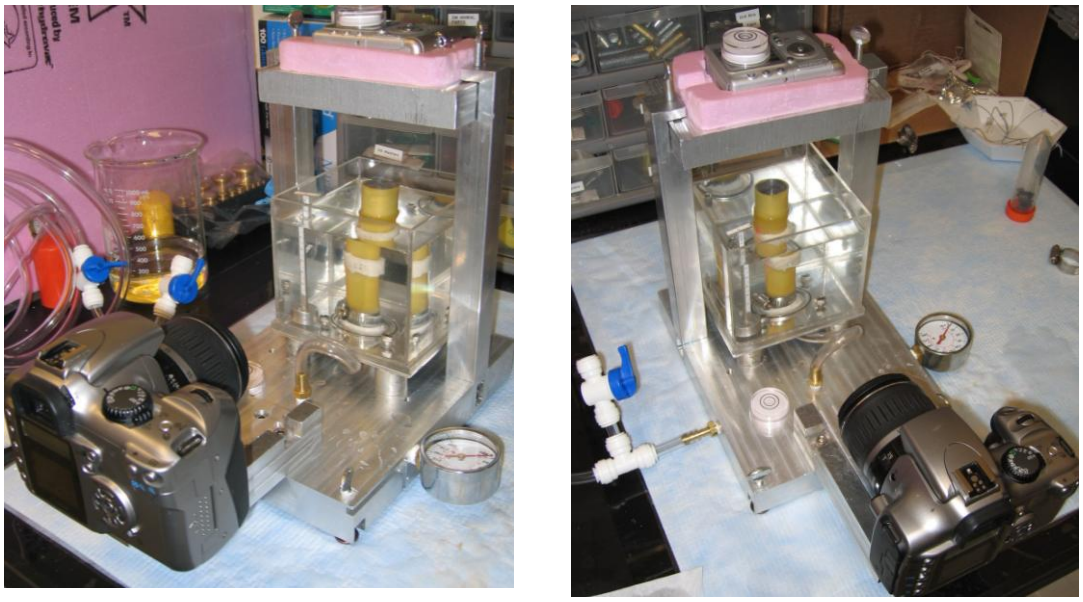

Figure 76- OML-customized equipment to inflate a rubber tube which is used for circumferential expansion of the arterial ring segment.

Another aspect that can be pursued is to examine the tissue macro- and microstructural changes under different loading protocols that can reveal other viscoelastic features. For instance, the mechanical behavior of the tissue under creep and cyclic loadings can be characterized. In particular, measuring phenomena such as

hysteresis and stiffening during cyclic loading in a wide range of frequencies can potentially be helpful in studying pathophysiological conditions such as poststenosis. Preliminary data on measuring the hysteresis loop in cyclic loading of native circumferential specimens under 1.4, 1.6 and 1.8 stretch are illustrated in Fig. 77, which suggests that definite trends exist.

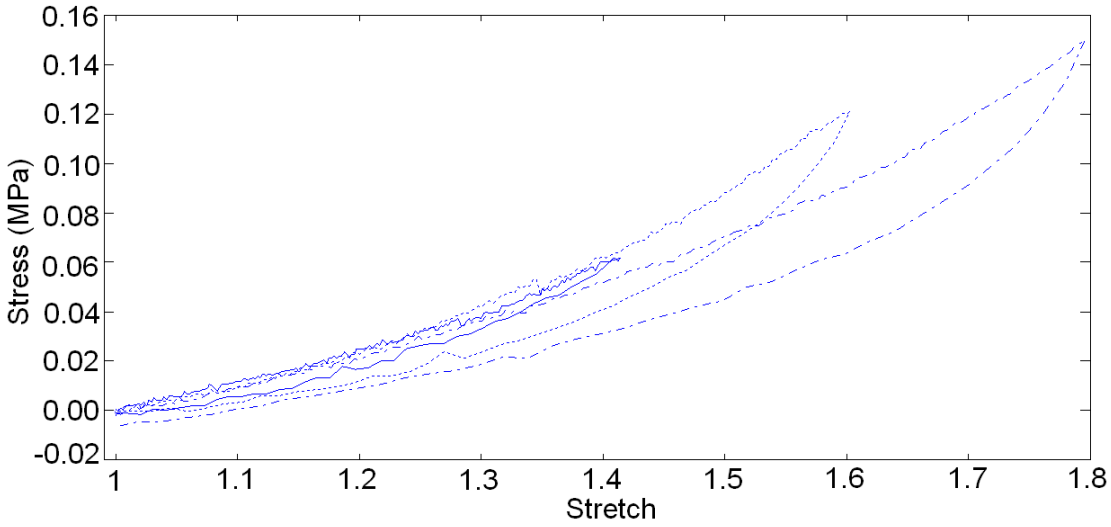

Figure 77- Hysteresis cycles during loading and unloading of native circumferential specimens under 1.4, 1.6 and 1.8 stretch.

In this study, the stress measurements on the test specimens were made at the tissue-scale dimensions. However, the tissue stress is not necessarily the same and even correlated to the stress in individual microstructural networks. Proper techniques, such as those similar to composite material characterization, can be used for arterial tissue to estimate the stress in individual microstructural components. In particular, estimating the stress in the elastin network, in the simpler case for elastin-isolated tissue, will enable a more accurate characterization of the elastin

biomechanics. Within the same path, examining the biomechanics of individual microstructural components of the extracellular matrix could be a significant step towards reaching the multiscale description of the entire tissue; however, this could be challenging and requires further development of probing techniques.

VI. APPENDICES

VI.1. Contributions

Following is a chronological list of journal articles and conferences proceedings/abstracts that have been contributed based on the outcomes of this dissertation.

VI.1.1. Experimental Measurement of Cardiovascular Tissue Viscoelastic Behavior under Controlled Tissue Hydration

Shahmirzadi D, Hsieh AH

Journal of Experimental Mechanics, to be submitted

Abstract not provided presently.

VI.1.2. Microstructural Deformations of Native and Elastin-Isolated Aortic Tissues under Loading

Shahmirzadi D, Hsieh AH

Invited paper to the Journal of Time-Dependent Materials, to be submitted

Abstract not provided presently.

VI.1.3. Quantification of Microstructural Alterations in Undeformed, Stretched and Recovered Specimens from Native and Elastin-Isolated Aortic Tissues

Shahmirzadi D, Bruck H, Hsieh HA

Journal of Vascular research, to be submitted shortly

(Abstract under review) Soft tissue biomechanics plays an important role in regulating tissue properties in health and disease. Understanding the mechanisms of biomechanical behavior in soft tissues is a crucial step in developing monitoring and therapeutic schemes or in synthesizing artificial replacements. Given the multiscale nature of tissue biomechanics, a full description can be obtained if the microstructural morphology is incorporated into the tissue deformation. Assessing alterations in microstructural morphology requires quantitative measurements which can be challenging given the complex, local and interactive conformations of tissue structural components embedded in the extracellular matrix. In this paper, we explore new image-based methods of quantification of tissue microstructure and examine the methods applied to aortic tissue under different deformation states. Though in their infancy stages of development, the methods yield reasonable results with acceptable interpretations. We believe that the outcome of this study paves the way for establishing enhanced methods of microstructural quantification with implications extendable to improving clinical diagnostic devices.

VI.1.4. In Vitro Mechanical Testing of Hydration-Controlled Arterial Tissue

Shahmirzadi D, Hsieh AH

Biomedical Engineering Society Annual Fall Scientific Meeting, October 6-9, 2010, Austin, TX, submitted

Elucidating how cardiovascular soft tissue biomechanics is affected by hydration is critical for understanding the potential effects of diseases where tissue extracellular matrix is altered. Ability to perform mechanical testing of cardiovascular tissue under hydration-controlled environment is a critical step to obtain a better understanding of hydration effects on tissue biomechanics in vitro. In this study, we conducted stress-relaxation testing on cardiovascular tissue specimens under different tissue hydration levels. We utilized a previously validated two-step protocol to modulate water content, first by incubating in solutions of varying osmolarity and then transferring the tissue into an MTS-mounted controlled humidity chamber to maintain water content throughout the tissue mechanical testing procedure. Circumferential tissue specimens were loaded in uniaxial tension to 100% strain, and the stress was measured over time. It was found that dehydrating the tissue makes it stiffer and causes higher drop of stress with higher rate of change during relaxation period. We argue that tissue dehydration undermines the effects from extracellular water on overall tissue biomechanics, and more closely reveals the relaxation of actual fibrillar structure, namely elastin-collagen network.

VI.1.5. Tissue- and Microstructural-level Deformation of Aortic Tissue under Viscoelastic/Viscoplastic Loading

Shahmirzadi D, Hsieh AH

Society of Experimental Mechanics Symposium on Time Dependent Constitutive Behavior and Failure/Fracture, June 7-9, 2010, Indianapolis, IN

Full description of soft tissue biomechanics requires multiscale characterization of phenomena spanning across organ to cellular scales. Proper tissue functioning in health and disease is regulated through physical interactions from one scale to another. Recent attempts in experimentation and modeling of tissue biomechanics aim to further understand either the phenomena at specific scale or the communication mechanisms between scales. In this study, we sought to determine how the microstructural organization of bovine aorta changes with fixed tissue deformation or after transient stretch and release. Circumferential aortic samples were subjected to small and large stretches, some kept stretched and some released to freely retract. Sample dimensions were measured before/after loading, then chemically-fixed and stained histologically to examine the microstructure. At tissue scale, it is found that sample's elongation is accompanied with width/thickness shrinkage in isochoric manner. Microstructural investigations reveal straightening of (undulated) fibrillar network when tissue stretches; with variations different at inner and outer layers of wall thickness. Once recovered, samples indicated larger permanent deformation toward outer layer, which possesses sparse elastic lamina. This study indicates a microstructural basis for observations of regional permanent

tissue stretch in artery tissues, and furnishes some early data for developing multiscale models of cardiovascular viscoelasticity/viscoplasticity.

VI.1.6. An Efficient Technique for Adjusting and Maintaining Specific Hydration Levels in Soft Biological Tissues In Vitro

Shahmirzadi D, Hsieh AH

Medical Engineering and Physics, in press

Elucidating how mechanics is affected by hydration in cardiovascular tissue is critical for understanding the potential effects of disease conditions. When studied in-vitro, hydration of tissue's extracellular matrix must be precisely controlled to provide repeatable test results. In this paper, we discuss a customized hydration technique developed to test viscoelastic mechanical properties of samples from different types of native and elastin-isolated aortic tissue. Autoclaving and NAOH treatment are routine procedures to isolate vascular elastin and study relevant mechanical properties. Tissue's extracellular matrix is altered throughout these procedures and our observations indicated that tissue's water content changes as a result. It is thus necessary to have the water content under control in order to provide comparable test conditions between different test samples. Time sensitivity of in-vitro examinations of biodegradable materials, together with constraints posed by experimental set up, makes the hydration problem challenging. Here, we utilized a biphasic hydration method composed of liquid phase dialysis tubing followed by vapor phase humidity chamber customized for testing viscoelastic mechanical properties of tissue samples under specific target humidity. The method is applied to samples from intact and

altered bovine tissues and characteristic sorption curves are developed. Numerical example is provided to better clarify the use of the technique. The proposed method is easily applicable to any other tissue types, provided that relevant sorption characteristic curves are developed.

VI.1.7. Controlling Vascular Tissue Hydration during In-Vitro Procedures

Shahmirzadi D, Hsieh AH

Biomedical Engineering Society Annual Fall Scientific Meeting, October 7-10, 2009, Pittsburgh, PA

Elucidating how mechanics is affected by hydration in cardiovascular tissue is critical for understanding the potential effects of disease conditions where tissue ECM is altered. For in vitro studies, extracellular matrix hydration must be precisely controlled during testing, particularly when different laboratory procedures are used to modulate tissue structure. For instance, sequential autoclaving and sodium hydroxide-treatment are procedures routinely used to isolate elastin network for studying elastin biomechanics. Understanding the change in tissue hydration allows us to achieve comparable test conditions between elastin-isolated and native samples; and eliminates confounding effects caused by differences in tissue hydration. In this study, we sought to quantify water content for native, autoclaved and autoclaved/NAOH-treated as well as another type of samples called cut/autoclaved/NAOH-treated samples which were prepared from autoclaved/NAOH-treated tissue, but the outer-half of the wall thickness was already cut out to obtain

more elastin-dense samples. We utilized a dialysis method to change tissue hydration in a controlled manner, and performed testing in a humidity chamber to maintain hydration constant. Compared to native samples, water content was found to be lower for both autoclaved and sodium hydroxide-treated samples. For different types of sample, the inverse relationships between PEG solute concentration and water content were also quantified. Characteristic sorption curves were obtained to describe water content in terms of both PEG concentration and humidity. Collectively, sorption characteristic curves for different sample types might be used to adjust sample water content in-vitro, which further enables characterizing the tissue biomechanics under controlled hydration.

VI.1.8. Microstructural Deformations of Arterial Tissue under Stress Relaxation and Deformation Recovery

Shahmirzadi D, Hsieh AH

Biomedical Engineering Society Annual Fall Scientific Meeting, October 7-10, 2009, Pittsburgh, PA

Elucidating how microstructural deformation is related to external loading is critical for understanding biomechanics of many cardiovascular disorders. In this study, we sought to examine the macro- and microstructural deformations of aortic tissue when circumferential tissue samples undergo stress relaxation at different levels of constant stretch. Macroscale deformations of the rectangular samples were characterized through photographs taken before and after stress-relaxation. At the end of each

experiment, samples were chemically fixed —while being kept stretched to minimize ongoing microstructural deformation during fixation—, processed for histological examinations and stained with a modified Verhoff's hematoxylin protocol. It was found that at the end of the relaxation period, width and thickness of the stretched samples decreased almost equally while the computed volume of the samples remained constant. For samples stretched at L=1.4, histology showed that the fibrous structure at the inner regions took an organized configuration with straighter lamellae along the load/stretch direction, whereas the outer regions showed undulated fibrillar structure. Higher stretching of the samples up to L=2 shifts the directed fibrillar structure toward the outer regions of the wall thickness, where the fibrillar microstructure at the inner regions became fractured into unorganized patterns. These observations reflect the transition of active load-carrying microstructural components from inner toward outer regions of wall thickness when external load/deformation increases.

VI.1.9. Characterizing Deformation-Induced Changes in Aortic Microstructure Using Image Processing Techniques

Shahmirzadi D, Hsieh AH

Society of Experimental Mechanics Fall Symposium and Workshop on Advanced Image-Based Measurement Methods, October 5-7, 2009, Columbia, SC

Elucidating how tissue deformations are transduced to the microstructural level is essential for understanding the role of mechanical stress on cellular function and

matrix damage in cardiovascular disease. Unlike at the tissue scale, where measurements of sample dimensions are sufficient to capture deformation, characterizing deformation at microstructural scale is a challenge. The primary obstacle in characterizing tissue fibrillar microstructure arises from the complex patterns of individual fibers with regional variations throughout the microstructure. In this study, we tested aortic tissue samples under different mechanical deformations, performed histological procedures to obtain microstructural images, and used image processing techniques to characterize fiber organization. Given the preferred direction of fibrillar structure around the aorta circumference, we aligned the main axis of the image along the circumferential direction and applied Hough and Fourier transformations to histology images in order to identify fibrillar directions, undulations and random distributions. Specifically, we were interested in distinguishing organized patterns of straightened fibrillar structure for loaded samples from disorganized patterns of undulated fibrillar structure for relaxed samples. Resulting Hough and Fourier images were averaged over entire samples in each of two categories which, collectively, enabled us to quantify microstructural changes during sample deformation.

VI.1.10. Quantifying Microscale Solid Area via Macroscale Measurements of Soft Tissues: Application to Elastin Fibers in Arterial Tissue

Shahmirzadi D, Hsieh AH

5th International Congress of Nano-Bio Clean Tech, October 27-30, 2008, San Francisco, CA

Characterization of micromechanical behavior of materials is a vital factor to engineering design of artificial materials or substitutes for biomaterials. A critical aspect for achieving this is accurate quantitation of stress and strain, a task that can be challenging when dealing with fiber-reinforced composites. Inherent is the ability to quantify solid cross-sectional area. Mechanics of most biological soft tissues is regulated by preferentially-oriented proteins networks embedded within amorphous ground matrix, compounded by hydration through interstitial fluid and interactions among different protein components. One approach to understanding these complex interactions is by initially characterizing the mechanics of individual structural components. In this study, a method is proposed to account for the area within arterial tissue that is occupied by elastin fibers, the primary component of the tissue that governs viscoelasticity. The method provides an adjustment factor, based on the elastin microstructure, to approximate the portion of the total (cross sectional) area of the tissue. This procedure provides a means to utilize routine macroscale measurement techniques to estimate microscale tissue features, which typically require destruction of the sample. The proposed method is a phenomenological one which reflects some of the structural alterations in the tissue during tissue hydration, which changes the effective area occupied by elastin fibers. Results were consistent with a few similar reports in the literature. The same fundamental approach can be adapted for other structural components and other tissues.

VI.1.11. Effects of Arterial Tissue Storage and Burst Failure on Residual Stress Relaxation

Shahmirzadi D, Hsieh AH, Haslach HW

Presented at the 34th Annual Northeast Bioengineering Conference, April 4-6, 2008, Providence, RI

This study examines how the relaxation of circumferential residual stress in the aortic tissue is altered with degradation of the tissue with in-vitro storage or circumferential expansion until failure. Results show that both treatments attenuate the effects of residual stress relaxation as assessed by the opening angle. Possible reasons for such alteration are discussed considering the mechanical and structural factors.

VI.2. Computer Codes

The majority of computations required in this research were performed in the MATLAB® environment *(The MathWorks Inc, Natick, MA)*. MATLAB® built-in codes were used whenever available, and customized programs were written whenever built-in codes were unavailable. The following section provides the main written computer codes.

VI.2.1. Hough and Fourier Transformation

```
clc

Fourier1=[
4.41    7.27    9.33    6.01    6.70;
2.70    5.61    8.56    4.46    5.63;
6.51    7.24    0.00    6.71    0.00;
5.70    5.99    0.00    5.98    0.00];
figure; bar(Fourier1)
xlabel('Native(inner)    Native(outer)    Elastin-isolated(inner)
Elastin-isolated(outer)')
ylabel('Aspect ratio in Fourier images')
figure; bar(Fourier1')
xlabel('Unstretched   Stretched to 1.4   Stretched to 2.0
Recovered from 1.4   Recovered from 2.0')
ylabel('Aspect ratio in Fourier images')

Hough1=[
30.75  9.55    3.71   28.71   11.90 ;
33.16  27.77  22.43   31.57   26.89;
28.99  19.61   0.00   26.20   0.00;
26.77  22.02   0.00   23.35   0.00];
figure; bar(Hough1)
xlabel('Native(inner)    Native(outer)    Elastin-isolated(inner)
Elastin-isolated(outer)')
ylabel('Average fibrillar angle in Hough images')
figure; bar(Hough1')
xlabel('Unstretched   Stretched to 1.4   Stretched to 2.0
Recovered from 1.4   Recovered from 2.0')
ylabel('Average fibrillar angle in Hough images')

figure; hold;
Fourier1_relative=[];
for i=1:4
    Fourier1_relative(i,:)=Fourier1(i,:)/Fourier1(i,1);
```

```
end
Fourier1_relative
plot([1.4,2.0],[Fourier1_relative(1,2),Fourier1_relative(1,3)],'O-')
plot([1.4,2.0],[Fourier1_relative(2,2),Fourier1_relative(2,3)],'O-')
plot([1.4],[Fourier1_relative(3,2)],'O-')
plot([1.4],[Fourier1_relative(4,2)],'O-')

plot([1.4,2.0],[Fourier1_relative(1,4),Fourier1_relative(1,5)],'s-')
plot([1.4,2.0],[Fourier1_relative(2,4),Fourier1_relative(2,5)],'s-')
plot([1.4],[Fourier1_relative(3,4)],'s-')
plot([1.4],[Fourier1_relative(4,4)],'s-')

figure; hold;
Hough1_relative=[];
for i=1:4
    Hough1_relative(i,:)=-Hough1(i,:)+Hough1(i,1);
end
Hough1_relative
plot([1.4,2.0],[Hough1_relative(1,2),Hough1_relative(1,3)],'O-')
plot([1.4,2.0],[Hough1_relative(2,2),Hough1_relative(2,3)],'O-')
plot([1.4],[Hough1_relative(3,2)],'O-')
plot([1.4],[Hough1_relative(4,2)],'O-')

plot([1.4,2.0],[Hough1_relative(1,4),Hough1_relative(1,5)],'s-')
plot([1.4,2.0],[Hough1_relative(2,4),Hough1_relative(2,5)],'s-')
plot([1.4],[Hough1_relative(3,4)],'s-')
plot([1.4],[Hough1_relative(4,4)],'s-')
```

VI.2.2. Sorption Characteristic Curve Fitting

```
clear
clc

% %---> Native tissue
% WC=[378.97 306.35 228.79 137.57 82.43];
% SC=[0 5 10 20 40];
% RH=[99 98 94 60 53];
%---> Matrix-fragmented tissue
% WC=[310.57 271.03 202.77 120.99 66.86];
% SC=[0 5 10 20 40];
% RH=[99 98 95 85 67];
% %---> Elastin-isolated Tissue
WC=[325.77 281.90 222.25 122.76 67.55];
SC=[0 5 10 20 40];
RH=[99 98 96 87 71];

%---------- WC-SC Interpolation
subplot(1,2,1)
hold off
x=WC;y=SC; plot(x,y,'*K'); hold
```

```
% %----> Native tissue
% X=[380:-0.01:80]; Y=-2+44*(1+exp(+X-80)).^-0.01;
% RSE1=(sum((y-(-2+44*(1+exp(+x-80)).^-0.01)).^2))^.5
% R2_1=1-[(sum((y-(-2+44*(1+exp(+x-80)).^-0.01)).^2))/(sum((y-
mean(y)).^2))]
%----> Matrix-fragmented tissue
% X=[310:-0.01:65]; Y=-68+120*(1+exp(+X-0)).^-0.002;
% RSE1=(sum((y-(-2+44*(1+exp(+x-80)).^-0.01)).^2))^.5
% R2_1=1-[(sum((y-(-68+120*(1+exp(+x-0)).^-0.002)).^2))/(sum((y-
mean(y)).^2))]
% %----> Elastin-isolated tissue
X=[380:-0.01:80]; Y=-15+120*(1+exp(+X+180)).^-0.0040;
RSE1=(sum((y-(-2+44*(1+exp(+x-80)).^-0.01)).^2))^.5
R2_1=1-[(sum((y-(-15+120*(1+exp(+x+180)).^-0.0040)).^2))/(sum((y-
mean(y)).^2))]
plot(X,Y,'K');xlabel('Water content (%)');ylabel('Solute
concentration (%)'); title('a. Curve fitting on WC-SC data')

%---------- SC-RH Interpolation
subplot(1,2,2)
hold off
x=SC;y=RH; plot(x,y,'*K'); hold
% %----> Native tissue
% X=[0:0.01:40]; Y=52+47*(1+exp(X-8)).^-0.15;
% RSE2=(sum((y-(52+47*(1+exp(x-8)).^-0.15)).^2))^.5
% R2_2=1-[(sum((y-(52+47*(1+exp(x-8)).^-0.15)).^2))/(sum((y-
mean(y)).^2))]
%----> Matrix-fragmented tissue
% X=[0:0.01:40]; Y=39+60*(1+exp(X-7)).^-0.024;
% RSE2=(sum((y-(52+47*(1+exp(x-8)).^-0.15)).^2))^.5
% R2_2=1-[(sum((y-(39+60*(1+exp(x-7)).^-0.024)).^2))/(sum((y-
mean(y)).^2))]
% %----> Elastin-isolated tissue
X=[0:0.01:40]; Y=47+52*(1+exp(X-5)).^-0.022;
RSE2=(sum((y-(52+47*(1+exp(x-8)).^-0.15)).^2))^.5
R2_2=1-[(sum((y-(47+52*(1+exp(x-5)).^-0.022)).^2))/(sum((y-
mean(y)).^2))]
plot(X,Y,'K'); xlabel('Solute concentartion (%)');ylabel('Relative
humidity (%)'); title('b. Curve fitting on SC-RH data')
```

VI.2.3. Stress-Relaxation, Maxwell Model and Slope of Stress Curves

```
% -----NATIVE------1.4---------0% PEG
time=time_native_0_spec01; area=97.81; force=force_native_0_spec01;
a=5.10; b=-0.03; c=50; d=-6.72e-5;   %RMSE=0.21%<-- 2 Maxwell models
in parallel

% -----MATRIX------1.4----------0% PEG
time=time_matrix_0_spec01; area=68.55; force=force_matrix_0_spec01;
a=5.24; b=-0.03; c=30.18; d=-4.95e-5; %RMSE=0.25 %<-- 2 Maxwell
models in parallel
```

```
% -----ELASTIN-----1.4----------0% PEG
time=time_elastin_0_spec02(1:6000); area=84.62;
force=force_elastin_0_spec02(1:6000);
a=5.25; b=-0.05; c=33.17; d=-2.67e-6;   %RMSE=0.15 %<-- 2 Maxwell
models in parallel

% -----NATIVE------2.0---------0% PEG
time=time_native_0_spec04(1:6000); area=85.88;
force=force_native_0_spec04(1:6000);
a=15.58; b=-0.01; c=79.45; d=-3.06e-5; %RMSE=0.76; %<-- 2 Maxwell
models in parallel

% -----NATIVE------2.0---------20% PEG
time=time_native_20_spec01(1:6000); area=54.17;
force=force_native_20_spec01(1:6000);
a=62.2; b=-0.022; c=125.5; d=-0.15e-03; %RMSE=2.58 %<-- 2 Maxwell
models in parallel

% % -----NATIVE------2.0---------40% PEG
time=time_native_40_spec01(1:6000); area=39.81;
force=force_native_40_spec01(1:6000);
a=69.32; b=-0.02; c=189.5; d=-0.24e-03; %<-- 2 Maxwell models in
parallel

%------------------------------------ raw stress data--------------
stress=force/area*1000; size1=size(stress);
% plot(time,stress); hold

%------------------------------------ raw stress data- impulse part
removed--------------
[M,I]=max(stress); size1=size(stress); stress=stress(I:size1(2)-1);
time=time(I:size1(2)-1);
plot(time,stress); plot(time, a*exp(b*time)+c*exp(d*time));

%------------------------------------ slope of stress--------------
time_aug=[time(2),time,time(size1(2)-1)];
stress_aug=[stress(2),stress,stress(size1(2)-1)];
slope_stress=[];
for i=1:(size1(2))
    slope_stress(i)=0.5*([stress_aug(i+1)-
stress_aug(i)]/[time_aug(i+1)-time_aug(i)]+[stress_aug(i+2)-
stress_aug(i+1)]/[time_aug(i+2)-time_aug(i+1)]);
end
% plot(time,slope_stress);

%------------------------------------ smoothed slope of stress---
---
slope_stress_ave2(1)=slope_stress(1);
slope_stress_aug2=[slope_stress(1),slope_stress(1),slope_stress,slop
e_stress(size1(2)),slope_stress(size1(2))]; %<----augmenting data to
account for two pairs of endpoints data
for i=2:size1(2)-1
    slope_stress_ave2_temp=mean(slope_stress_aug2(i-1:i+5));
    slope_stress_ave2(i)=slope_stress_ave2_temp;
end
```

```
% plot(time(1:size1(2)-1),slope_stress_ave2);
% plot(stress(1:size1(2)-1),slope_stress_ave2)

%------------------------------------ normalized & smoothed stress-
-------------
[M,I]=max(stress);
stress_norm=[stress(I:size1(2))-stress(size1(2))];
stress_norm=stress_norm/max(stress_norm);
size2=size(stress_norm);

stress_norm_ave2(1)=stress_norm(1);
stress_norm_aug2=[stress_norm(1),stress_norm(1),stress_norm,stress_n
orm(size2(2)),stress_norm(size2(2))]; %<----augmenting data to
account for two pairs of endpoints data
for i=2:size2(2)-1
    stress_norm_ave2_temp=mean(stress_norm_aug2(i-1:i+5));
    stress_norm_ave2(i)=stress_norm_ave2_temp;
end
time_norm_ave2=time(I:size1(2)-1);
plot(time_norm_ave2,stress_norm_ave2)
hold;
plot(time_norm_ave2,a*exp(b*time_norm_ave2)+c*exp(d*time_norm_ave2))
%<-- 2 Maxwell models in parallel
```

Glossary

This section furnishes descriptions to any abbreviation, uncommon terminology or notations that have been used throughout this dissertation. The notation adopted in this dissertation is to indicate a *scalar* simply by the proper character, a *vector* by placing the "$\rightarrow$" sign above the character and a *tensor* by placing the "$\sim$" sign underneath the character. The "$'$" sign at the top of the character shows the differentiation of the character with respect to the variable under consideration. The differentiation with respect to time is specifically shown by the "." sign above the character. Depending on the context, some characters are used to describe multiple parameters, which are separated by the ";" sign.

c	Dashpot component constant	F_k	Force within spring component
$\underset{\sim}{C}$	Right Cauchy-Green strain tensor	GAG	Glycosaminoglycan
d	Diameter	J	Determinant of the deformation gradient tensor
$\underset{\sim}{E}$	Green-Lagrange strain tensor	k	Spring component constant; Boltzman's constant
ECM	Extracellular Matrix	l	Length
$\underset{\sim}{F}$	Deformation gradient tensor	$\tilde{l}$	Lagrange multiplier
F	Force	LPM	Liquid Phase Method
F_c	Force within dashpot component	LSE	Least Squares Error

LVM	Liquid vapor method	u	Displacement
m	Mass	$\underset{\sim}{\vec{u}}$	Displacement vector in spatial coordinate
m_d	Sample's Dried Mass	VPM	Vapor Phase Method
m_h	Sample's Hydrated Mass	VSM	Vascular Smooth Muscle
m_w	Water Mass	w	Width
n	Number of required samples	W	Strain energy function
p	Pressure	WC	Water Content
$\underset{\sim}{P}$	1st Piola-Kirchhoff stress tensor	WC_g	Gravitational water content
PEG	Polyethylene Glycol	x	Location along the aorta
Q	Function of Green strain tensor	z	Axial direction
r	Radius; Radial direction	α	Significance level
RH	Relative humidity	$\underset{\sim}{\varepsilon}$	Engineering strain tensor
RMSE	Root mean squared error	δ	Smallest difference to be detected
$\underset{\sim}{S}$	2nd Piola-Kirchhoff stress tensor	$\underset{\sim}{\lambda}$	Stretch tensor
SC	Solute Concentration	λ_u	Ultimate stretch
SMC	Smooth Muscle Cell	ν	Degrees of freedom
t	Time; Thickness	θ	Angle; Angular direction
T	Temperature	$\underset{\sim}{\sigma}$	Cauchy stress tensor
T_d	Denaturation Temperature	σ_c	Circumferential stress

σ Stress; true standard deviation

$I_{\underset{\sim}{A}}$ First invariant of tensor $\underset{\sim}{A}$

$II_{\underset{\sim}{A}}$ Second invariant of tensor $\underset{\sim}{A}$

$III_{\underset{\sim}{A}}$ Third invariant of tensor $\underset{\sim}{A}$

Bibliography

[1] Adams MA, McNally DS, Dolan P. “Stress distributions inside intervertebral discs. The effects of age and degeneration,” J Bone Joint Surg Br 78: 965–972, 1996.

[2] Alberts B, et al., “Essential Cell Biology: An Introduction to the Molecular Biology of Cell”, Garland Publishing Inc., New York, 1998.

[3] Alberts B, et al., Molecular Biology of the Cell, 4th edition, New York: Garland Science, 2002.

[4] Amenabar JM, Hugo FN, Fossati AMC, Padilha, DMP. The use of stereology as a method in histological research. Rev Fac Odontol Porto Alegre, 44, 62-65, 2003.

[5] Amenabar JM, Martins GB, Cherubini K, Figueiredo MA. Comparison between semi-automated segmentation and manual point-counting methods for quantitative analysis of histological sections. J Oral Sci. 2006 Sep;48(3):139-43.

[6] Apter JT, “Mathematical Development of a Physical Model of Visco-Elastic Properties of the Aorta”, Bulletin of Math Biophys, Vol. 26, pp. 267-288, 1964.

[7] Apter JT, M. Rabinowitz, D. H. Cummings, “Correlation of Visco-Elastic Properties of Large Arteries with Microscopic Structure, I., II., III.”, Journal of Circulation Research, Vol. 19, pp. 104-121, 1966.

[8] Apter JT, “Correlation of Visco-Elastic Properties with Microscopic Structure of Large Arteries: IV. Thermal Responses of Collagen, Elastin, Smooth Muscle, and Intact Arteries”, Journal of Circulation Research, Vol. 21, pp. 901-918, 1967.

[9] Apter JT, E. Marquez, “Correlation of Visco-Elastic Properties of Large Arteries with Microscopic Structure: V. Effects of Sinusoidal Forcings at Low and at Resonance Frequencies”, Journal of Circulation Research, Vol. 22, pp. 393-404, 1968.

[10] Avolio A, Jones D, Tafazzoli-Shadpour M Quantification of alterations in structure and function of elastin in the arterial media. Hypertension. 32(1):170-5, 1998.

[11] Ayad S, R. Boot-Handford, M. J. Humphries, K. E. Kadler, A. Shuttleworth, “The Extracellular Matrix Facts Book”, Academic Press., New York, 1994.

[12] Ballard D, C. Brown, Computer Vision, Prentice-Hall, pp 24 – 30, 1982.

[13] Banerjee B, Roy D, Vasu RM, A pseudo-dynamic sub-optimal filter for elastography under static loading and measurements, Phys Med Biol, 21;54(2):285-305, 2009.

[14] Basciano CA, Kleinstreuer C, Invariant-based anisotropic constitutive models of the healthy and aneurysmal abdominal aortic wall, J Biomech Eng;131(2), 2009.

[15] Basser PJ, Schneiderman R, Bank RA, Wachtel E, Maroudas A, “Mechanical properties of the collagen network in human articular cartilage as measured by osmotic stress technique,” Arch Biochem Biophys 351: 207-19, 1998.

[16] Bayliss MT, Urban JP, Johnstone B, and Holm S. In vitro method for measuring synthesis rates in the intervertebral disc. J Orthop Res, 4: 10-17, 1986.

[17] Bedossa P, et al. Intraobserver and interobserver variations in liver biopsy interpretation in patients with chronic hepatitis C: The French METAVIR Cooperative Study Group. J Hepatol 20, 15–20, 1994.

[18] Berenson GS, B. Radhakrishnamurthy, E. R. Dalferes, S. R. Srinivasan, "---", Journal of Human Pathology, Vol. 2, pp. 57-79, 1971.

[19] Bischoff JE, "Static Indentation of Anisotropic Biomaterials Using Axially Asymmetric Indenters- A Computational Study", ASME Journal of Biomechanical Engineering, Vol. 126(4), pp. 498-505, 2004.

[20] Bolender RP, Biological stereology: history, present state, future directions. Microsc Res Tech, 21, 255-261, 1992.

[21] Bonet J, "Large Strain Viscoelastic Constitutive Models", International Journal of Solids and Structures, Vol. 38, pp. 2953-2968, 2001.

[22] Bracewell RN, The Fourier Transformation and its Applications, McGraw-Hill Book Company, New York, pp. 640, 1965.

[23] Brown E, T. McKee, E. diTomaso, A. Pluen, B. Seed, Y. Boucher, and R. K. Jain, "Dynamic imaging of collagen and its modulation in tumors in vivo using second-harmonic generation," Nat. Med. 9, 796–800, 2003.

[24] Bru A, Pastor, JM, "Experimental characterization of hydration and pinning in bentonite clay, a swelling, heterogeneous, porous medium", Geoderma 134: 295-305, 2006.

[25] Bruck HA, S. R. McNeill, M. A. Sutton and W. H. Peters III, Digital image correlation using Newton-Raphson method of partial differential correction. 29(3), pp. 261-267, 1989.

[26] Brunt EM, "Grading and staging the histopathological lesions of chronic hepatitis: The Knodell histology activity index and beyond," J. Hepatol 31, pp.241–246, 2000.

[27] Brzezinski J, G. Oszkinis, E. Marzec, "Dielectric Relaxation of a Protein-Water System in Atherosclerotic Artery Wall", Journal of Medical and Biological Engineering and Computing, Vol. 45(6), pp. 525-529, 2007.

[28] Buckwalter JA "Aging and degeneration of the human intervertebral disc," Spine Update 20: 1307–1314, 1995.

[29] Burnstock G, Structure of Smooth Muscle Cell and Its Innervation", Smooth Muscle, Arnold Publication, London, 1970.

[30] Buttafoco L, N. G. Kolkman, P. Engbers-Buijtenhuijs, A. A. Poot, P. J. Dijkstra, I. Vermes, J. Feijen, "Electrospinning of Collagen and Elastin for Tissue Engineering Applications", Journal of Biomaterials, Vol. 27, pp. 724-734, 2006.

[31] Caracciolo G, Petruccetti M, Caminiti R, "A new experimental setup for the study of lipid hydration by energy dispersive X-ray diffraction, Chemical Physics Letters 414, 456–460, 2005.

[32] Castleman KR, Digital image processing, Prentice-Hall, New Jersey, 15-72, 1996.

[33] Chan RW, Tayama N, “Biomechanical effects of hydration in vocal fold tissues,” Otolaryngol Head Neck Surg 126: 528-537, 2002.

[34] Chu SW, Chen IH, Liu TM, Chen PC, Sun CK, Lin BL, “Multimodal nonlinear spectral microscopy based on a femtosecond Cr: Forsterite laser,” Opt. Lett. 26, 1909–1911, 2001.

[35] Chuong CJ, Y. C. Fung, “Three-Dimensional Stress Distribution in Arteries”, Journal of Biomechanical Engineering, Vol. 105, pp. 268-274, 1983.

[36] Cieplak M, Robbins, M.O., “Influence of contact angle on quasistatic fluid invasion of porous media”, Phys. Rev. B 41: 11508–11521, 1990.

[37] Costi JJ, Hearn TC, Fazzalari NL, “The effect of hydration on the stiffness of intervertebral discs in an ovine model,” Clin Biomech 17: 446-455, 2002.

[38] Cox MAJ, N. J. B. Driessen, C. V. C. Bouten, F. P. T. Baaijens, "Mechanical Characterization of Anisotropic Planar Biological Soft Tissues Using Large Identation: A Computational Feasibility Study", Journal of Biomechanical Engineering, Vol. 128(3), pp. 428-436, 2006.

[39] Dahab GM, M. M. Kheriza, H. M. El-Beltagi, A. M. Fouda, and O. A. El-Din, “Digital quantification of fibrosis in liver biopsy sections: description of a new method by Photoshop software,” J. Gastroenterol. Hepatol 19, 78–85, 2004.

[40] Daniels F, B. M. Ter Haar Romeny, M. P. Rubbens, and H. van Assen. Quantification of collagen orientation in 3D engineered tissue. In: IFMBE Proceedings, 3rd Kuala Lumpur International Conference on Biomedical Engineering 2006, Vol. 15, pp. 282–285, 2006.

[41] Decraemer WF, M. A. Maes, V. J. Vanhuyse, P. Vanpeperstraete, “A Non-linear Viscoelastic Constitutive Equation for Soft Biological Tissues, Based Upon A Structural Model”, Journal of Biomechanics, Vol. 13, pp. 559-564, 1980.

[42] Demjancukova L, E. Rohan, R. Cimrman, J. Polansky, Z. Tonar, O. Boiron, “Composite Model of Healthy Arterial Wall: Material Identification based on Uniaxial Traction Tests and Morphometric Analysis”, Journal of Biomechanics, Vol. 39, Suppl. 1, pp. S622, 2006.

[43] Denk W, J. H. Stricjler, and W. W. Webb, “Two-photon laser scanning fluorescence microscopy,” Science 248, 73–76, 1990.

[44] Dickson JM, et al., Choice of cross size in stereology- A cautionary note, Neuroradiology, 45, 896-899, 2003.

[45] Dougherty A, Carle, N., “Distribution of avalanches in interfacial motion in a porous medium”, Phys. Rev. E 58: 2889–2893, 1998.

[46] Duda RO, PE Hart, "Use of the Hough Transformation to Detect Lines and Curves in Pictures," Comm. ACM, Vol. 15, pp. 11–15, 1972.

[47] Elsheikh A, Alhasso D, Rama P., “Assessment of the epithelium's contribution to corneal biomechanics.” Exp Eye Res. 86: 445-451, 2008.

[48] Erikson A, Ortegren J, Hompland T, de Lange Davies C, Lindgren M. Quantification of the second-order nonlinear susceptibility of collagen I using a laser scanning microscope. J Biomed Opt. 12(4), 2007.

[49] Ferrans VJ, et al. “Structural changes in glutaraldehyde-treated porcine heterografts used as substitute cardiac valves,” Am J Cardiol 48: 1159–1184, 1978.

[50] Flahiff CM, Kraus VB, Huebner JL, Setton LA. Cartilage mechanics in the guinea pig model of osteoarthritis studied with an osmotic loading method. Osteoarthritis Cartilage;12:383-388, 2004.

[51] Fonck E, G. Prod’Hom, S. Roy, L. Augsburger, D. Rufenacht, N. Stergiopulos, “Mechanical Properties of Elastase Treated Arteries”, Journal of Biomechanics, Vol. 39, Suppl. 1, pp. S319, 2006.

[52] Fox SI, Human Physiology, 4th Edition, Brown Publishers, 2008.

[53] Freund I, M. Deutsch, and A. Sprecher, “Connective tissue polarity,” Biophys. J. 50, 693–712, 1986.

[54] Fung YC, “Elasticity of Soft Tissues in Simple Elongation”, American Journal of Physiology, Vol. 28, pp. 1532-1544, 1967.

[55] Fung YC, “Biomechanics: Its Foundation and Objectives”, Prentice Hall, Englewood Cliff, NJ, pp. 181-208, 1972(a).

[56] Fung YC, “Stress-Strain History Relations of Soft Tissues in Simple Elongations”, In: Fung, Y. C., N. Perrone, M. Anliker (eds), Biomechanics: Its Foundations and Objectives, Prentice-Hall, Englewood Cliffs, pp. 181-208, 1972(b).

[57] Fung YC, “Biomechanics: Mechanical Properties of Living Tissues”, Second Edition, Springer-Verlag, New York, 1993.

[58] Gainaru C, Fillmer A., and Bohmer R., Dielectric Response of Deeply Supercooled Hydration Water in the Connective Tissue Proteins Collagen and Elastin, J. Phys. Chem. B 113:12628-12631, 2009.

[59] Gosline JM, C. J. French, "Dynamic Mechanical Propeties of Elastin", Journal of Biopolymers, Vol. 18, pp. 2091-2103, 1979.

[60] Gow BS, M. S. Taylor, "Measurement of Viscoelastic Properties of Arteries in the Living Dog", Journal of Circulation Research, Vol. XXIII, pp. 111-122, 1968.

[61] Gravey W, et al., A Modified Verhoeff Elastic Van Geieson Stain, The Journal of Histotechnology, 14(2), 113-114, 1991.

[62] Grigera JR, and H.J.C. Berendsen, "The molecular details of collagen hydration," Biopolymers 18: 47–57, 1979.

[63] Grodzinsky AJ, Roth V, Myers E, Grossman WD, Mow VC. The significance of electromechanical and osmotic forces in the nonequilibrium swelling behavior of articular cartilage in tension. J Biomech Eng; 103:221-231, 1981.

[64] Gundiah N, M. B. Ratcliffe, L. A. Pruitt, "Determination of Strain Energy Function for Arterial Elastin: Experiments Using Histology and Mechanical Tests", Journal of Biomechanics, Vol. 40(3), pp. 586-594, 2007.

[65] Hamilton PW, Allen DC, Quantitative clinical pathology, Blackwell Science, Oxford, 11-22, 1995.

[66] Han SM, Lee SY, Cho MH, Lee JK., "Disc hydration measured by magnetic resonance imaging in relation to its compressive stiffness in rat models," Proc Inst Mech Eng H 215: 497-501, 2001.

[67] Harley BA, Leung JH, Silva EC, Gibson LJ. “Mechanical characterization of collagen-glycosaminoglycan scaffolds,” Acta Biomater 3: 463-74, 2007.

[68] Hart-Smith LJ, J. D. C. Crisp, “Large Elastic Deformations of Thin Rubber Membranes”, International Journal of Engineering Science, Vol. 5, pp. 1-24, 1967.

[69] Haslach HW, “Nonlinear Viscoelastic, Thermodynamically Consistent, Models for Biological Soft Tissue”, Biomechanics and Modeling in Mechanobiology., Vol. 3, pp. 172-189, 2005.

[70] Hayashi K, “Experimental Approaches on Measuring the Mechanical Properties and Constitutional Laws of Arterial Walls”, Journal of Biomechanical Engineering, Vol. 115, pp. 481-488, 1993.

[71] He S, Kahanda, G.L.M.K.S., Wong, P., “Roughness of wetting fluid invasion fronts in porous media,” Phys. Rev. Lett. 69: 3731–3734, 1992.

[72] He CM, M. R. Roach, “The Composition and Mechanical Properties of Abdominal Aortic Aneurysms”, Journal of Vascular Surgeries, Vol. 20, pp. 6-13, 1994.

[73] Hertzberg RW and Manson, JA, Fatigue of Engineering Plastics, Academic Press, New York, p. 61, 1980.

[74] Hoeve CAJ, P. J. Flory, “The Elastic Properties of Elastin”, Journal of Applied Physics, Vol. 80, pp. 6523-6526, 1958.

[75] Holzapfel GA, T. C. Gasser, R. W. Ogden, “A New Constitutive Framework for Arterial Wall Mechanics and a Comparative Study of Material Models”, Journal of Elasticity, Vol. 61, pp. 1-48, 2000(a).

[76] Holzapfel GA, C. A. J. Schulze-Bauer, M. Stadler, "Mechanics of Angioplasty: Wall, Balloon and Stent", In: Casey, J., G. Bao, editors, Mechanics in Biology, American Society of Mechanical Engineers, AMD-Vol. 242/BED-Vol. 46, New York, pp. 141-156, 2000(b).

[77] Holzapfel GA, "Nonlinear Solid Mechanics: A Continuum Approach for Engineering", Wiley, New York, 2000(c).

[78] Holzapfel GA, T. C. Gasser, "Computational Stress-Deformation Analysis of Arterial Walls Including High-Pressure Response", International Journal of Cardiology, Vol. 116, pp. 78-85, 2007.

[79] Hopwood D, Some Aspects of Fixation with Glutaraldehyde, J. Anat., 101, 83-92, 1967.

[80] Hopwood D, "Cell and tissue fixation," Histochem J 17: 389–442, 1985.

[81] Horowitz A, C. B. Menice, R. Laporte, K. G. Morgan, "Mechanisms of Smooth Muscle Contraction", Physiol. Rev., Vol. 76(4), pp. 967-1003, 1996.

[82] Horvath I, "A Noninvasive Viscoelastic Pressure-Flow Measurement of Human Carotid Artery to Follow the Progression of Arteriosclerosis", PhD Dissertation, Rutgers, The State University of New Jersey, NJ, 2003.

[83] Huber G, Morlock MM, Ito K. Consistent hydration of intervertebral discs during in vitro testing. Med Eng Phys;29:808-813, 2007.

[84] Huijing PA, Muscle as a collagen fiber reinforced composite: a review of force transmission in muscle and whole limb. J Biomech.;32(4):329-45, 1999.

[85] Humphrey JD, "An Evaluation of Pseudoelastic Descriptors Used in Arterial Mechanics", Journal Biomech. Eng., Vol. 121, pp. 259-262, 1999.

[86] Humphrey JD, “Cardiovascular Solid Mechanics: Cells, Tissues and Organs”, Springer, Berlin, 2002.

[87] Ishak K, et al., “Histological grading and staging of chronic hepatitis,” J. Hepatol 22, 696–699, 1995.

[88] Ivancevic VG, New mechanics of traumatic brain injury, Cogn Neurodyn 3(3):281-293, 2009.

[89] Jeffrey JE, Gregory DW, Aspden RM. Matrix damage and chondrocyte viability following a single impact load on articular cartilage. Arch Biochem Biophys;32287-32296, 1995.

[90] Johnstone B, Urban JP, Roberts S, and Menage J. The fluid content of the human intervertebral disc. Comparison between fluid content and swelling pressure profiles of discs removed at surgery and those taken postmortem. Spine (Phila Pa 1976); 17: 412-416, 1992.

[91] Kage M, et al. Long-term evolution of fibrosis from chronic hepatitis to cirrhosis in patients with hepatitis C: Morphometric analysis of repeated biopsies. J Hepatol 25, 1028–1031, 1997.

[92] Karami G, Grundman N, Abolfathi N, Naik A, Ziejewski M, A micromechanical hyperelastic modeling of brain white matter under large deformation, J Mech Behav Biomed Mater. Jul;2(3):243-54, 2009.

[93] Kardar M, Parisi G, Zhang Y-C. “Dynamic scaling of growing interfaces,” Phys. Rev. Lett. 56: 889–892, 1986.

[94] Kausch HH, Polymer Fracture, Springer-Verlag, Berlin, p. 223, 1976.

[95] Kerin AJ, Wisnom MR, Adams MA, " The compressive strength of articular cartilage," Proc Inst Mech Eng H 212: 273-80, 1998.

[96] Kessler DA, Levine, H., Tu, Y., "Interface fluctuations in random media," Phys. Rev. A 43: 4551–4554, 1991.

[97] Knodell RG, K. G. Ishak, W. C. Black, T. S. Chen, R. Craig, N. Kaplowitz, T. W. Kiernan, and J. Wollman, "Formulation and application of a numerical scoring system for assessing histological activity in asymptomatic chronic active hepatitis," J. Hepatol 1, 431–435, 1981.

[98] Koplik J, Levine, H., "Interface moving through a random background," Phys. Rev. B 32: 280–292, 1985.

[99] Kunzelman KS, Cochran RP, Stress/strain characteristics of porcine mitral valve tissue: parallel versus perpendicular collagen orientation, J Card Surg. 7(1):71-78, 1992.

[100] Lakes RS, Nakamura S, Behiri JC, Bonfield W, Fracture mechanics of bone with short cracks, J Biomech, 23(10):967-975, 1990.

[101] Lanir Y, "Constitutive Equations for Fibrous Connective Tissues", Journal of Biomechanics, Vol. 16, pp. 1-12, 1983.

[102] Lehner KB, et al. Structure, function, and degeneration of bovine hyaline cartilage: assessment with MR imaging in vitro. Radiology;170:495-499, 1989.

[103] Li H, Leow WK, Chiu IS, Predictive simulation of bidirectional Glenn shunt using a hybrid blood vessel model, Med Image Comput Assist Interv, 12(Pt 2):266-274, 2009.

[104] Lillie MA, "---", PhD Dissertation, University of Western Ontario, London, Canada, 1986.

[105] Lillie MA, J. M. Gosline, "The Effects of Hydration on the Dynamic Mechanical Properties of Elastin", Biopolymers, Vol. 29, pp. 1147-1160, 1990.

[106] Lillie MA, G. W. G. Chalmers, J. M. Gosline, "The Effects of Heating on the Mechanical Properties of Arterial Elastin", Connect. Tissue Res., Vol. 31, pp. 23-35, 1994.

[107] Lillie MA, G. W. G. Chalmers, J. M. Gosline, "Elastin Dehydration Through the Liquid and the Vapor Phase: A Comparison of Osmotic Stress Models", Biopolymers, Vol. 39, pp. 627-639, 1996.

[108] Lillie MA, G. David, J. M. Gosline, "Mechanical Role of Elastin-Associated Microfibrils in Pig Aortic Elastic Tissue", Connective Tissue Res., Vol. 37, pp. 121-141, 1998.

[109] Lord JD, Penn D, Whitehead P. The Application of Digital Image Correlation for Measuring Residual Stress by Incremental Hole Drilling. Applied Mechanics and Materials. Vol.3-14, 65-73, 2008.

[110] Lovekamp JJ, et al., "Stability and function of glycosaminoglycans in porcine bioprosthetic heart valves", Biomaterials 27:1507-1518, 2006.

[111] MacDougall AJ, at al., "Swelling Behavior of the Tomato Cell Wall Network," Biomacromolecules 2: 450–455, 2001.

[112] Maiti S, R. M. Williams, J. B. Shear, W. R. Zipfel, and W. W. Webb, "Measuring serotonin distribution in live cells with three-photon excitation," Science 275, 530–532, 1997.

[113] Manderim-de-lacerda C, Quantitative methods in morphology, EDUERJ, Rio de Janeiro, 60-69, 1995.

[114] Maroudas A, Adult Articular Cartilage: Physico-chemical Properties of Articular cartilage Freeman, M. A. R., Ed., Pitman Medical, London, 1973.

[115] Maroudas A, and Bannon C. Measurement of swelling pressure in cartilage and comparison with the osmotic pressure of constituent proteoglycans. Biorheology; 18: 619-632, 1981.

[116] Maroudas A, Ziv I, Weisman N, Venn M. Studies of hydration and swelling pressure in normal and osteoarthritic cartilage. Biorheology;22:159-169, 1985.

[117] Masseroli M, T. Caballero, F. O'Valle, R. M. Del Moral, A. Perez-Milena, and R. G. Del Moral, "Automatic quantification of liver fibrosis: design and validation of a new image analysis method: Comparison with semi-quantitative indexes of fibrosis," J. Hepatol 32,453–464, 2000.

[118] Maton A, et al., "Human Biology and Health", Prentice Hall, Englewood Cliffs, NJ, 1993.

[119] Mathews MB, "---", Biochem. Journal, Vol. 96, pp. 710-716, 1965.

[120] Matsumoto T, T. Goto, M. Sato, "Microscopic Residual Stress Caused by the Mechanical Heterogeneity in the Lamellar Unit of the Porcine Thoracic Aortic Wall", JSME International Journal, Series A, Vol. 47(3), pp. 341-348, 2004.

[121] Mayne R, “Collagenous Proteins of Blood Vessels”, Arteriosclerosis, Vol. 6, pp. 585-593, 1986.

[122] Milnor WR, “Cardiovascular Physiology”, Oxford University Press, Oxford, UK, 1990.

[123] Minns RJ, F. S. Steven, “---”, Br. J. Exp. Pathol., Vol. 58, pp. 572-579, 1978.

[124] Moerman KM, Holt CA, Evans SL, Simms CK. Digital image correlation and finite element modelling as a method to determine mechanical properties of human soft tissue in vivo. J Biomech. 42(8):1150-3, 2009.

[125] Mogilner IG, Ruderman G, Grigera JR, “Collagen stability, hydration and native state,” J Mol Graph Model 21: 209-13, 2002.

[126] Mooney M, “A Theory of Large Elastic Deformations”, Journal of Applied Physics, Vol. 11, pp. 582-592, 1940.

[127] Naka MH, Morita Y, Ikeuchi K. Influence of proteoglycan contents and of tissue hydration on the frictional characteristics of articular cartilage. Proc Inst Mech Eng H;219:175-182, 2005.

[128] Narmoneva DA, Wang JY, Setton LA. Nonuniform swelling-induced residual strains in articular cartilage. J Biomech;32:401-408, 1999.

[129] Ogden RW, “Non-Linear Elastic Deformations”, John Wiley & Sons, New York, 1984.

[130] Orecchini A, Paciaroni A, et al. Collective dynamics of protein hydration water by brillouin neutron spectroscopy. J Am Chem Soc 131:4664-4669, 2009.

[131] Park HC, Lakes RS, Cosserat micromechanics of human bone: strain redistribution by a hydration sensitive constituent, J Biomech, 19(5):385-397, 1986.

[132] Patel DJ, D. L. Fry, "The Elastic Symmetry of Arterial Segments in Dogs", Journal of Circulation Research, Vol. 24, pp. 1-8, 1969.

[133] Pezzin G, M. Scandola, L. Gotte, "The Low-Temperature Mechanical Relaxation of Elastin: I. The Dry Protein", Biopolymers, Vol. 15, pp. 283-292, 1976.

[134] Pflaster DS, Krag MH, Johnson CC, Haugh LD, Pope MH. "Effect of test environment on intervertebral disc hydration," Spine 22: 133–139, 1997.

[135] Png GM, Choi JW, Ng BW-H, Mickan SP, Abbott D, and Zhang X-C, The impact of hydration changes in fresh bio-tissue on THz spectroscopic measurements, Phys. Med. Biol. 53: 3501–3517, 2008.

[136] Radhakrishnamurthy B, H. A. Ruiz, G. S. Beresson, "Isolation and Characterization of Proteoglycans from Bovine Aorta", Journal of Biological Chemistry, Vol. 252(14), pp. 4831-4841, 1977.

[137] Rand RP & Parsegian, V. A., "Hydration forces between phospholipids bilayers" Biochem. Biophys. Acta 988, 351-376, 1989.

[138] Ravikumar KM, Hwang W. Region-specific role of water in collagen unwinding and assembly. Proteins 72:1320-1332, 2008.

[139] Rivlin RS, D. W. Saunders, "Large Elastic Deformations of Isotropic Materials. VII. Experiments on the Deformation of Rubber", Philos. Trans. R. Soc. Lond., A243, pp. 251-288, 1951.

[140] Robert L, et al, Estimation of Digital Image Correlation (DIC) Performances. Experimental Analysis of Nano and Engineering Materials and Structures Proceedings of the 13th International Conference on Experimental Mechanics, Alexandroupolis, Greece, July 1–6, 2007.

[141] Roberts N, Puddephat MJ, McNulty V, The benefit of stereology for quantitative radiology, Br J Radiol, 73, 679-697, 2000.

[142] Rochette LM, Patterson SM, Hydration status and cardiovascular function: effects of hydration enhancement on cardiovascular function at rest and during psychological stress, Int J Psychophysiol. 56:81-91, 2005.

[143] Rodbard S, Ikeda, K, and Montes, M, "An analysis of mechanisms of poststenotic dilatation," Angiology 18: 349-367, 1967.

[144] Roy CS, "The Elastic Properties of the Arterial Wall", Philo. Trans. R. Soc. Lond. (Biol.), Vol. 99, pp.1-31, 1880.

[145] Rubbens MP, et al, Quantification of the temporal evolution of collagen orientation in mechanically conditioned engineered cardiovascular tissues. Ann Biomed Eng. 2009 Jul;37(7):1263-72, 2009.

[146] Rubio MA, et al., "Self affine fractal interfaces from immiscible displacement in porous media," Phys. Rev. Lett. 63: 1685–1688, 1989.

[147] Sacks MS, D. A. Vorp, M. L. Raghavan, M. P. Federle, M. W. Webster, "In Vivo Three-Dimensional Surface Geometry of Abdominal Aortic Aneurisms", Annals of Biomedical Engineering, Vol. 27, pp. 469-479, 1999.

[148] Sajdera SW, V. C. Hascall, "---", Journal of Biol. Chem., Vol. 244, pp. 77-87, 1969.

[149] Samouillan V, A. Lamure, E. Maurel, J. Dandurand, C. Lacabanne, F. Ballarin, M. Spina, “Characterization of Elastin and Collagen in Aortic Bioprostheses”, Journal of Medical and Biological Engineering and Computing, Vol. 38(2), pp. 226-231, 2000.

[150] Sarraf CE, A. B. Harris, A. D. McCulloch, M. Eastwood, “Heart Valve and Arterial Tissue Engineering”, Journal of Cell Proliferation, Vol. 36(5), pp. 241-254, 2003.

[151] Scandola M, G. Pezzin, “Water in Polymers”, American Chemical Society, Washington, DC., pp. 225-234, 1980.

[152] Scharnagl C, Reif M, Friedrich J. Local compressibilities of proteins: comparison of optical experiments and simulations for horse heart cytochrome-c. Biophys J 89:64-75, 2005.

[153] Setton LA, Mow VC, Muller FJ, Pita JC, Howell DS. Mechanical properties of canine articular cartilage are significantly altered following transection of the anterior cruciate ligament. J Orthop Res ;12:451-463, 1994.

[154] Shadwick RE, “Elasticity in Arteries”, American Scientist, Vol. 86(6), pp. 535-541, 1998.

[155] Shapiro L, and G Stockman. "Computer Vision", Prentice-Hall, Inc. 2001.

[156] Sheehan DC, and Hrapchak BB, Theory and Practice of Histotechnology, St Louis, The Moxby Company, 190-191, 1980.

[157] Silver FH, Christiansen DL, Bunrin CM, “Mechanical Properties of the Aorta: A Review”, Crit Rev Biomed Eng, 17: 323-358, 1989.

[158] Sims AJ, Bennett MK,Murray A, Comparison of semi-automated image analysis and manual methods for tissue quantification in pancreatic carcinoma, Phys Med Biol, 47, 1255-1266, 2002.

[159] Skalak R, A. Rachev, A. Tozeren, "Stress-Strain Relations for Membranes under Finite Deformations", Bulg. Acad. Sci.: Biomech., Vol. 2, pp. 24-29, 1975.

[160] Sobolewski K, M. Wolanska, E. Bankowski, M. Cacko, S. Glowinski, "Collagen, Elastin and Glycosaminoglycans in Aortic Aneurysms", Acta Biochimica Polonica, Vol. 42, pp. 301-308, 1995.

[161] Soloway RD, A. H. Baggenstoss, L. J. Schoenfield, and W. H. Summerskill, "Observer error and sampling variability tested in evaluation of hepatitis and cirrhosis by liver biopsy," Am. J. Dig. Dis. 16, 1082–1086, 1971.

[162] Somlyo AP, A. V. Somlyo, "Smooth Muscle Structure and Function", The Heart and Cardiovascular System, 2nd Edition, Raven Press, New York, 1992.

[163] Spillmann J, Teschner M, Cosserat nets, IEEE Trans Vis Comput Graph. 15(2):325-338, 2009.

[164] Staverman AJ, F. R. Schwarzl, "Linear Deformation Behavior of High Polymers", In Die Physik der Hochpolymeren, Vol. IV, edited by H. A. Stuart, Berlin, Springer-Verlag, pp. 1-95, 1956.

[165] Stjin AI, Anatomy of overview of human artery, PhD Dissertation, Maastricht, 2005.

[166] Strupler M, A. M. Pena, M. Hernest, P. L. Tharaux, J. L. Martin, E. Beaurepaire, and M. C. Schanne-Klein, "Second harmonic imaging and scoring of collagen in fibrotic tissues," Opt. Express 15, 4054–4065, 2007.

[167] Sun W, Chang S, Tai DC, Tan N, Xiao G, Tang H, Yu H. Nonlinear optical microscopy: use of second harmonic generation and two-photon microscopy for automated quantitative liver fibrosis studies. J Biomed Opt 13, 2008.

[168] Sutton MA, Ke X, Lessner SM, Goldbach M, Yost M, Zhao F, Schreier, HW. Strain field measurements on mouse carotid arteries using microscopic three-dimensional digital image correlation. Journal of Biomedical Materials Research Part A 84A (1), 178–190, 2008.

[169] Talman EA, Boughner DR, " Effect of altered hydration on the internal shear properties of porcine aortic valve cusps," Ann Thorac Surg 71: S375-378, 2001.

[170] Tang H, Buehler MJ, Moran B, A constitutive model of soft tissue: from nanoscale collagen to tissue continuum, Ann Biomed Eng. 37(6):1117-1130, 2009.

[171] Taylor AM, Bonser RHC, Farrent JW, The influence of hydration on the tensile and compressive properties of avian keratinous tissues, J Materials Science 39: 939– 942, 2004.

[172] Theodossiou TA, C. Thrasivoulou, C. Ekwobi, and D. L. Becker, "Second harmonic generation confocal microscopy of collagen type I from rat tendon cryosections," Biophys. J. 91, 4665–4677, 2006.

[173] Timoshenko S, “Strength of Materials”, Part II, 3rd edn., Van Nostrand, New York, 1956.

[174] Tonar Z, et al, Microscopic image analysis of elastin network in samples of normal, atherosclerotic and aneurysmatic abdominal aorta and its biomechanical implications, Journal of Applied Biomedicine, 1: 149-159, 2003.

[175] Torzilli PA, Grigiene R, Borrelli J, Helfet DL. Effect of impact load on articular cartilage: cell metabolism and viability, and matrix water content. J Biomech Eng;121:433-441, 1999.

[176] Treloar LRG, “The Physics of Rubber Elasticity”, Clarendon Press, Oxford, UK, 1975.

[177] Trillo A, and Huast, MD, “Arterial elastic tissue and collagen in experimental poststenotic dilatation in dogs,” Exp. Mol. Pathol. 23: 473-490, 1975.

[178] Tsai BM, M. Wang, J. M. Pitcher, K. K. Meldrum, D. R. Meldrum, “Hypoxic Pulmonary Vasoconstriction and Pulmonary Artery Tissue Cytokine Expression are Mediated by Protein Kinase C”, American Journal of Physiology: Lung Cellular and Molecular Physiology, Vol. 287, pp. L1215-L1219, 2004.

[179] Urban JP, Maroudas A, “Swelling of the intervertebral disc in vitro,” Connect Tissue Res 9: 1–10, 1981.

[180] Valanis KC, R. F. Landel, “The Strain-Energy Function of a Hyperelastic Material in Terms of the Extension Ratios”, Journal of Applied Physics, Vol. 38, pp. 2997-3002, 1967.

[181] Viidik A, “A Rheological Model for Uncalcified Parallel-Fibered Collogeneous Tissue”, Journal of Biomechanics, Vol. 1, pp. 3-11, 1968.

[182] Wang DM, J. M. Tarbell, “Modeling Interstitial Flow in an Artery Wall Allows Estimation of Wall Shear Stress on Smooth Muscle Cells”, Journal of Biomech. Eng., Vol. 117, pp. 358-363, 1995.

[183] Wasano K & Yamamoto, T., Tridimensional Architecture of Elastic Tissue in the Rat Aorta and Femoral Artery—A Scanning Electron Microscope Study,Journal of Electron Microscopy. 32, pp, 33-44, 1983.

[184] Weibel ER, Measuring through the microscope: development and evolution of stereological methods. J Microsc 155, 393-403, 1989.

[185] Weinberg PD, C. P. Winlove, K. H. Parker, “The Distribution of Water in Arterial Elastin: Effects of Mechanical Stress, Osmotic Pressure, and Temperature”, Biopolymers, Vol. 35(2), pp. 161-169, 1995.

[186] Weinberg EJ, Shahmirzadi D, Mofrad MRK. On the Multiscale Modeling of Heart Valve in health and Disease. J Biomechanics and Modeling in Mechanobiology. In press.

[187] Wexler HR, et al. “Quantitation of lung water by nuclear magnetic resonance imaging,” Investigative Radiology 20: 583–590, 1985.

[188] Wright NT, J. D. Humphrey, “Denaturation of Collagen via Heating: An Irreversible Rate Process”, Annual Review of Biomedical Engineering, Vol. 4, pp. 109-128, 2002.

[189] Wu JZ, Herzog W, Elastic anisotropy of articular cartilage is associated with the microstructures of collagen fibers and chondrocytes, J Biomech.;35(7):931-42, 2002.

[190] Young JT, R. N. Vaishnav, D. J. Patel, "Nonlinear Anisotropic Viscoelastic Properties of Canine Arterial Segments", Journal of Biomechanics, Vol. 10, pp. 549-559, 1977.

[191] Zhou J, Y. C. Fung, "The Degree of Nonlinearity and Anisotropy of Blood Vessel Elasticity", Proceedings of the National Academy of Sciences of the USA, Vol. 94, pp. 14255-14260, 1997.

[192] Zipfel WR, R. M. Williams, and W. W. Webb, "Nonlinear magic: multiphoton microscopy in the biosciences," Nat. Biotechnol. 21, 1368–1376, 2003.

[193] Zsivanovits G, MacDougall AJ, Smith AC, Ring SG., "Material properties of concentrated pectin networks" Carbohydr Res. 339: 1317-22, 2004.

[194] Zulliger MA, A. Rachev, N. Stergiopulos, "A Constitutive Formulation of Arterial Mechanics Including Vascular Smooth Muscle Tone", American Journal of Physiology: Heart and Circulation Physiology, Vol. 287, pp. 1335-1343, 2004.

Vita

Danial Shahmirzadi studied at the national organization for developing exceptional talents (NODET), Allame Helli Tehran, his guidance and secondary school, in Tehran, Iran (1990-1997). He attended the mechanical engineering department at the University of Tehran in 1997-2002 where he received his BSc, while being a researcher in several institutes the IKCO Industrial Group (2000), the School of Intelligent Systems (2001-2002). In summer 2003, he started his graduate studies at the mechanical engineering department of Texas A&M University as a graduate research assistant and received his MSc in 2005. He joined the mechanical engineering department at the University of Maryland on January 2006 as a PhD student and has been conducting his dissertation research in Orthopaedic Mechanobiology Lab in Fischell department of bioengineering. He has been a recipient of many prestigious awards from the University of Maryland, such as Ann G Wylie dissertation fellowship, future faculty fellowship, distinguished teaching assistant certification, George R Irwin centennial travel award and multiple certifications of excellence from mechanical engineering department.

Prior to starting his PhD program, his research background has mainly been in the areas of biologically-inspired and intelligent control systems, and soft computing, where he has contributed more than 20 articles to several journals and conferences in the field. His current research interests are mainly focused on Soft tissue biomechanics and modeling of biological systems.

He is planning to obtain few years of postdoc research experience before establishing his career in academia.